

Studies on Conducting Polymer-based Nanocomposites for Pesticide Detection

**Thesis submitted to the Delhi Technological University
for the award of the Degree of**

DOCTOR OF PHILOSOPHY

by

Saroj Paneru

(2K18/Ph.D./AC/04)



**Department of Applied Chemistry,
Delhi Technological University,
Main Bawana Road,
Delhi-110042
India
July 2023**

Declaration

I state that this Ph.D thesis titled “**Studies on Conducting Polymer-based Nanocomposites for Pesticide Detection**” was completed by me for the award of degree of Doctor of Philosophy under the supervision of Prof. D. Kumar, Department of Applied Chemistry, Delhi Technological University, New Delhi, India.

This thesis presents the results of my original research work. The research work reported in this thesis is original and has not been submitted either in part or full to any university or institution for the award of any degree or diploma.

Saroj Paneru

(Research Scholar)

2k18/PhD/AC/04

Certificate

This is to certify that the thesis entitled “**Studies on Conducting Polymer-based Nanocomposites for Pesticide Detection**” submitted by **Saroj Paneru** to **Delhi Technological University, New Delhi, India** for the award of the degree of “Doctor of Philosophy” in **Chemistry** is a record of the work carried out by her. Saroj Paneru has worked under my guidance and fulfilled the requirements for the submission of this thesis.

The results contained in the thesis have not been submitted either in part or full or in any other form to any university or institution for the award of any degree or diploma.

Prof. D. Kumar

Professor

Department of Applied Chemistry

Delhi Technological University

Bawana Road, Delhi-110042

Prof. Anil Kumar

Head, Department of Applied Chemistry

Delhi Technological University

Bawana Road, Delhi-110042

*Dedicated
To
My Parents
Husband, Mother-in
-law & Son*

Acknowledgments

This work will never be possible without God's grace and compassion, who continues to look after me despite my flaws.

Completion of my thesis involved a lot of hardships and challenges. Fortunately, many people contributed to this endeavour. I take this opportunity to express my sincere gratitude to the people who have been instrumental in the successful completion of the thesis for their guidance, help and constant motivation.

*First and foremost, I would like to extend my sincere gratitude to my learned research supervisor **Prof. D. Kumar**, Department of Applied Chemistry, Delhi Technological University, New Delhi for his dedicated help, advice, inspiration, encouragement and continuous support throughout my Ph.D. tenure. His enthusiasm, integral view on research and expedition for providing high-quality work has made a deep impression on me. During our course of interaction of the last five years, I have learnt enormously from him and really glad to be associated with him in my research journey.*

I wish to express my warm and sincere thanks to the Department of Applied Chemistry, Delhi Technological University for providing the research facilities during my Ph.D. tenure. Many thanks to all academic and administrative staffs of Delhi Technological University for their kind co-operation and support.

*I am extremely grateful to **UGC** for the necessary financial support.*

*I would like to convey my thanks to **Dr. C.M. Pandey** for his constant support and inspiration.*

*To my friends, and labmates (**Dr. Owais Jalil, Sakshi Verma, Deeksha Thakur, Sweety, Divya and Tanushee**) many thank you for listening, offering me advice and supporting me through the entire process.*

*I would like to extend my deepest gratitude to my parents **Mr. Suresh Chandra Paneru** and **Smt. Bhawana Paneru**, for their sacrifice throughout my life and for providing unconditional*

*love, trust and care. I would not have made this achievement without them. I am grateful to my dearest Mother in law (**Smt. Bimla Joshi**), brothers (**Neeraj & Dheeraj Paneru**) and sister (**Dr. Meenakshi Paneru**) for being my pillar of strength in my life. I owe thanks to a very special person in my life, my beloved husband, **Dr. Susheel Joshi** whose dedication, enduring love and constant support have nurtured me to gain confidence and strength to excel in my research journey. Words would never say how grateful I am to my son **Siddharth** for bringing joy and happiness in my life.*

Finally, I would like to recognize everyone whose contribution make the successful completion of the thesis.

Abstract

The research work reported in the thesis speaks about the development of biosensors that provides quantitative information about pesticide detection by utilizing a bio-component (enzyme) in a direct contact with a transducer. Pesticides are extensively used to enhance productivity in the agriculture field due to their high insecticidal property and potency for pest control. However, their careless use on a large scale can lead to severe health issues, making it a global concern. Pesticides leave behind residues in agricultural resources, soil, and water which can enter the human body and lead to serious health problems, such as Alzheimer's, Parkinson's, cognitive disorders, thyroid problems, etc. Thus, there is an urgent need to develop a sensitive and effective technique for monitoring the concentration of these harmful substances to protect living beings from their injurious effects. Among the various pesticides, organophosphate pesticides (OPs) are commonly used because of their unique characteristics, including high insecticidal activity, low persistence, low bioaccumulation, and rapid degradation in the environment.

In the literature, various chromatographic methods are available for detecting the presence of OPs. High-performance liquid chromatography (HPLC) and gas chromatography (GC) are the most popular methods in this domain. Although these methods are reliable, few shortcomings are still there. These methods are time-consuming and usually very rigid to implement. Therefore, we require a new technique that is authentic, possesses a low detection limit, cost-effective, rapid and easy to use. In this context, biosensors can be an attractive alternative to these conventional techniques for the detection of pesticides. Biosensors are analytical devices having biological sensing elements that are attached to a transducer and produce an electronic signal. The acetylcholinesterase (AChE)-based electrochemical

biosensors have become increasingly popular for detecting OPs due to their on-site convenience, low-cost instrumentation, excellent selectivity, and rapid analysis. Their sensitivity significantly depends on the efficiency of enzyme immobilization and the electron transfer rate between the enzyme and electrode surface. To address these critical factors, researchers have explored various transducers in their studies.

In recent years, conducting polymers (CPs) have been widely used as a supporting material for fabricating effective transducers. CPs contain π -electron backbone responsible for their unusual electronic properties such as electrical conductivity, low energy optical transitions, low ionization potential and high electron affinity. CPs based biosensors are cost-effective, easy to fabricate and offer a direct electrical readout for the detection of biological analytes with high sensitivity and selectivity. Various CPs such as polypyrrole, polythiophene, polyaniline, etc. have been widely used in biosensor fabrication. Apart from the merits, pure CPs have a few shortcomings like low sensitivity and poor selectivity. Nanomaterials based CPs nanocomposites overcome these issues. Nanomaterials have their own characteristics like high conductivity, large surface area, biocompatibility and excellent catalytic activity. Metal oxides (CuO, TiO₂, MnO₂, ZnO), graphene, carbon nanotube, etc. are some widely used nanomaterials. The incorporation of these nanomaterials effectively enhances the effective specific surface area, density, and catalytic power of nanocomposite. CPs nanocomposites increase electron transfer in an electrochemical reaction which further improves the sensitivity and selectivity of the biosensor.

Contents

| | |
|----------------------|------|
| Declaration..... | I |
| Certificate..... | II |
| Acknowledgement..... | III |
| Abstract..... | IV |
| Contents..... | V |
| List of Figures..... | VI |
| List of Tables..... | VII |
| Abbreviations..... | VIII |

1. Introduction and Literature Review

| | |
|---|----|
| 1.1. Introduction to Pesticides..... | 1 |
| 1.2. Classification of Pesticides..... | 1 |
| 1.2.1. Bio-Pesticides..... | 2 |
| 1.2.2. Chemical Pesticides..... | 3 |
| 1.3. Benefits of Pesticides to Mankind and the Environment..... | 5 |
| 1.4. Consequences of Pesticides on human health and Environment..... | 6 |
| 1.4.1. Acute Illnesses..... | 6 |
| 1.4.2. Chronic Illnesses..... | 6 |
| 1.5. Detection Techniques of Pesticides..... | 7 |
| 1.5.1. Traditional Analytical Methods..... | 7 |
| 1.5.2. Advanced Detection Techniques..... | 7 |
| 1.5.2.1. Biosensors..... | 7 |
| 1.6. Electrochemical Biosensors for OPs detection..... | 11 |
| 1.7. Enzyme-based Electrochemical Biosensors for OPs detection..... | 13 |
| 1.7.1. Acetylcholinesterase-based Biosensors for OPs detection..... | 14 |
| 1.8. Conducting Polymers..... | 17 |
| 1.8.1. Evolution of Conducting Polymers..... | 17 |
| 1.8.2. Conducting Polymer-based Composites..... | 19 |
| 1.8.3. Synthesis Techniques of Conducting Polymer-based Composite..... | 20 |
| 1.8.4. Applications of Conducting Polymer-based Composites for OPs detection..... | 20 |
| 1.9. Research gaps and Objectives..... | 22 |
| 1.9.1. Research gaps..... | 22 |
| 1.9.2. Objective..... | 23 |
| 1.10. Research Contribution..... | 24 |
| 1.11. Thesis Organization..... | 27 |
| 1.12. References..... | 30 |

2. Materials and Experimental Methods

| | |
|------------------------|----|
| 2.1. Introduction..... | 40 |
| 2.2. Materials..... | 40 |

| | |
|---|----|
| 2.2.1. Chemicals..... | 40 |
| 2.2.2. Solutions and Buffers..... | 41 |
| 2.3. Characterization Methods..... | 41 |
| 2.3.1. X-Ray Diffraction (XRD)..... | 42 |
| 2.3.2. Fourier Transform Infrared (FT-IR) Spectroscopy..... | 43 |
| 2.3.3. Ultraviolet-Visible (UV-Vis) Spectroscopy..... | 44 |
| 2.3.4. Scanning Electron Microscopy (SEM)..... | 45 |
| 2.3.5. Transmission Electron Microscopy (TEM)..... | 47 |
| 2.3.6. Energy Dispersive X-Ray Spectroscopy (EDAX)..... | 48 |
| 2.3.7. Electrochemical Techniques..... | 49 |
| 2.3.7.1 Cyclic Voltammetry (CV)..... | 50 |
| 2.3.7.2 Differential Pulse Voltammetry (DPV)..... | 50 |
| 2.3.7.3. Chronoamperometry..... | 51 |
| 2.4. Methods to Immobilize Enzyme onto Conducting Polymer-based Matrix..... | 51 |
| 2.4.1. Covalent Immobilization..... | 51 |
| 2.4.2. Physical Adsorption..... | 52 |
| 2.5. Protocols used for the determination of different Parameters pertaining to the Performance of Conducting Polymer-based Biosensors for Pesticide Detection..... | 52 |
| 2.5.1. Diffusion Coefficient and Effective Surface Area..... | 52 |
| 2.5.2. Sensitivity, linear range and detection limit..... | 52 |
| 2.5.3. Stability and Reproducibility parameters of the fabricated electrodes..... | 53 |
| 2.6. References..... | 54 |

3. Nanostructured CuO-embedded Polyaniline-modified Electrochemical Biosensor for Paraoxon-Ethyl Detection

| | |
|---|----|
| 3.1 Introduction..... | 56 |
| 3.2. Experimental Section..... | 56 |
| 3.2.1. Synthesis of CuO Nanoparticles..... | 56 |
| 3.2.2. Synthesis of CuO@PANI-based Composite..... | 57 |
| 3.2.3. Electrophoretic Deposition of CuO@PANI-based Composite and Fabrication of Biosensor..... | 57 |
| 3.3. Results and Discussion..... | 58 |
| 3.3.1. Structural, Morphological and Elemental Analysis..... | 58 |
| 3.3.2. Electrochemical Characterization..... | 62 |
| 3.3.3. Optimization Studies..... | 64 |
| 3.3.4. Electrochemical Biosensing Studies..... | 64 |
| 3.3.5. Selectivity and Real Sample Analysis..... | 66 |
| 3.3.6. Reproducibility and Stability Studies..... | 67 |
| 3.4. Conclusion..... | 68 |
| 3.5. References..... | 69 |

4. Ag@CuO embedded Polyaniline modified Electrochemical Biosensor for Paraoxon-Ethyl Detection

| | |
|--|----|
| 4.1. Introduction..... | 71 |
| 4.2. Experimental Section..... | 71 |
| 4.2.1. Synthesis of CuO and Ag@CuO Nanoparticles..... | 71 |
| 4.2.2. Synthesis of Ag@CuO/PANI-based Composite..... | 72 |
| 4.2.3. Electrophoretic Deposition of Ag-doped-CuO/PANI-based Composite and | |

| | |
|--|-----|
| Biosensor Fabrication | 72 |
| 4.3. Results and Discussion..... | 73 |
| 4.3.1. Design of Sensor..... | 73 |
| 4.3.2. Structural, Morphological and Elemental Studies..... | 74 |
| 4.3.3. Electrochemical Characterization..... | 76 |
| 4.3.4. Optimization Studies..... | 79 |
| 4.3.5. Electrochemical Biosensing Studies..... | 80 |
| 4.3.6. Selectivity and Real Sample Analysis..... | 82 |
| 4.3.7. Reproducibility and Stability Studies..... | 83 |
| 4.4. Conclusion..... | 83 |
| 4.5. References..... | 85 |
| 5. CeO₂ embedded Polyaniline modified Electrochemical Biosensor for Paraoxon-Ethyl Detection | |
| 5.1 Introduction..... | 86 |
| 5.2. Experimental Section..... | 86 |
| 5.2.1. Synthesis of CeO ₂ Nanocrystals..... | 86 |
| 5.2.2. Synthesis of CeO ₂ /PANI-based Composite..... | 87 |
| 5.2.3. Electrophoretic Deposition of CeO ₂ @PANI Composite and Fabrication of Biosensor..... | 87 |
| 5.3. Results and Discussion..... | 88 |
| 5.3.1. Design of Sensor..... | 88 |
| 5.3.2. Structural, Morphological and Elemental Studies..... | 89 |
| 5.3.3. Electrochemical Characterization..... | 92 |
| 5.3.4. Optimization Studies..... | 95 |
| 5.3.5. Electrochemical Biosensing Studies..... | 96 |
| 5.3.6. Selectivity and Real Sample Studies..... | 96 |
| 5.3.7. Reproducibility and Stability Studies..... | 98 |
| 5.4. Conclusion..... | 99 |
| 5.5. References..... | 100 |
| 6. CuO and PEDOT:PSS grafted Whatman paper-based Biosensor for PE Detection | |
| 6.1 | |
| Introduction..... | 102 |
| 6.2. Experimental Section..... | 102 |
| 6.2.1. Synthesis of CuO Nanoparticles..... | 102 |
| 6.2.2. Fabrication of PEDOT:PSS/WP and CuO@PEDOT:PSS/WP and EG-treated CuO@PEDOT:PSS/WP Conducting Papers..... | 103 |
| 6.2.3 Biosensor Fabrication..... | 103 |
| 6.3. Results and Discussion..... | 104 |
| 6.3.1. Design of Sensor..... | 104 |
| 6.3.2. Structural and Morphological Characterization of Prepared Materials and Fabricated Electrodes..... | 105 |
| 6.3.3. Electrical Conductivity Study of all Fabricated Electrodes..... | 107 |
| 6.3.4. Electrochemical Characterization..... | 108 |
| 6.3.5. Electrochemical Biosensing Studies..... | 108 |
| 6.3.6. Selectivity and Real Sample Analysis..... | 110 |
| 6.3.7. Reproducibility and Stability Studies..... | 111 |
| 6.4. Conclusion..... | 111 |

| | |
|---|-----|
| 6.5. References..... | 113 |
| 7. CeO₂ and PEDOT:PSS grafted Whatman paper-based Biosensor for PE Detection | |
| 7.1 Introduction..... | 115 |
| 7.2. Experimental Section..... | 115 |
| 7.2.1. Biosynthesis of CeO ₂ Nanocrystals..... | 115 |
| 7.2.2. Fabrication of PEDOT:PSS/WP, CeO ₂ @PEDOT:PSS/WP, and ethylene glycol-treated CeO ₂ @PEDOT:PSS/WP Conducting Papers..... | 116 |
| 7.2.3. Biosensor Fabrication..... | 117 |
| 7.3. Results and Discussion..... | 118 |
| 7.3.1. Design of Sensor..... | 118 |
| 7.3.2. Structural, Morphological and Elemental Characterization of Prepared Materials and Fabricated Electrodes..... | 118 |
| 7.3.3. Electrical Conductivity Study of all Fabricated Electrodes..... | 122 |
| 7.3.4. Electrochemical Characterization..... | 123 |
| 7.3.5. Optimization Studies..... | 124 |
| 7.3.6. Electrochemical Biosensing Studies..... | 125 |
| 7.3.7. Selectivity and Real Sample Studies..... | 126 |
| 7.3.8. Reproducibility and Stability Studies..... | 127 |
| 7.4. Conclusion..... | 128 |
| 7.5. References..... | 129 |
| 8. Summary and Future Prospects | |
| 8.1. Summary..... | 131 |
| 8.2. Future Scope..... | 132 |

List of Figures

Fig. 1.1. Classification of pesticides

Fig. 1.2. A Schematic view of biosensor

Fig. 1.3. Components of biosensor

Fig. 1.4. The mechanism of AChE enzyme inhibition in the presence of OPs

Fig. 1.5. Working mechanism of AChE-based biosensor for OPs detection

Fig. 1.6. Research methodology

Fig. 2.1. (A) A pictorial view of XRD, (B) X-ray diffraction patterns of CuO, CuO@PANI and PANI

Fig. 2.2. (A) Schematic diagram of Michelson interferometer, (B) FTIR of CeO₂, PANI and CeO₂@PANI

Fig. 2.3. (A) A pictorial diagram of UV-Vis spectrophotometer and (B) UV-Vis spectra of PANI and CuO@PANI

Fig. 2.4. (A) A pictorial view of Scanning electron microscope and (B) SEM micrograph of CuO@PEDOT:PSS/WP electrode

Fig. 2.5. (A) Schematic representation of Transmission electron microscope, (B) TEM image of CeO₂ nanocrystals

Fig. 2.6. (A) Schematic diagram of Potentiostat, (B) CV curve of Ag@CuO/PANI/ITO electrode with different scan rates (10 - 300 mV/sec)

Fig. 3.1. Schematic illustration of (A) Synthesis of nanocomposite and fabrication of transducer, (B) Working mechanism of fabricated biosensor for PE detection.

Fig. 3.2. (A) X-ray diffraction pattern of (a) CuO, (b) CuO@PANI and (c) PANI. (B) FTIR of (a) CuO, (b) PANI and (c) CuO@PANI. (C) UV-Visible spectra of (a) PANI and (b) CuO@PANI

Fig. 3.3. (A) SEM micrograph of PANI, (B) SEM micrograph of CuO nanoparticles, (C) TEM micrograph of CuO nanoparticles, (D) SEM micrograph of CuO@PANI

Fig. 3.4. EDAX spectra of CuO@PANI-based composite

Fig. 3.5. (A) cyclic voltammogram of CuO@PANI/ITO (a), PANI/ITO (b), AChE/CuO@PANI/ITO (c) and ITO (d) at a scan rate 30 mV/sec (B) Cyclic voltammogram of (A) PANI/ITO, (B) CuO@PANI/ITO electrode with varying scan rate (10–300 mV/sec), (C) Plots of current vs. square root of scan rate in case of CuO@PANI (a) and PANI (b), (D) Plots of potential vs. log (scan rate) in case of CuO@PANI (a) and PANI (b)

Fig. 3.6. Optimization of (A) effect of pH, (B) incubation time of PE

Fig. 3.7. (A) DPV response data of the fabricated electrode after incubation at various conc (1-200 nM) of PE (B) Calibration curve between log of PE conc with change in current (C) Specificity of AChE/CuO@PANI/ITO biosensor in the presence of 1 μ M paraoxon-ethyl, uric acid, ascorbic acid, CaCl₂, NaCl and ferrous sulphate

Fig. 3.8. (A) Reproducibility study of AChE/CuO@PANI/ITO electrode for PE detection (B) Stability study of AChE/CuO@PANI/ITO electrode over a period of 40 days

Fig. 4.1. A Schematic view of (A) biosensor fabrication and (B) working mechanism of fabricated biosensor for PE detection

Fig. 4.2. (A) XRD spectra of (a) CuO (b) Ag@CuO (c) Ag@CuO/PANI (c) and PANI (B) FTIR spectra of CuO (a), Ag@CuO (b) and Ag@CuO/PANI (c)

Fig. 4.3. SEM images of (A) PANI (B) CuO nanoparticles (C) Ag@CuO nanoparticles (D) Ag@CuO/PANI nanocomposite and (E) Ag@CuO/PANI/ITO

Fig. 4.4. SEM-EDAX data of (A) CuO, (B) Ag@CuO, and (C) Ag@CuO/PANI

Fig. 4.5. (A) Cyclic voltammogram of Ag@CuO/PANI/ITO (a), Ag@CuO/ITO (b), CuO/ITO (c), AChE/Ag@CuO/PANI/ITO (d) and ITO (e) at a scan rate of 50 mV/sec. cyclic voltammogram of curves of (B) Ag@CuO/PANI/ITO (C) Ag@CuO/ITO and (D) CuO/ITO

electrodes with different scan rates (10 - 300 mV/sec) (E) Graphs of potential vs. log (scan rate) in case of CuO (a), Ag@CuO (b) and Ag@CuO/PANI nanocomposite (c). (F) Graphs of current vs. square root of scan rate in case of CuO (a), Ag@CuO (b) and Ag@CuO/PANI nanocomposite (c)

Fig. 4.6. Optimization of (A) effect of pH (6-8 pH), (B) incubation time (0-20 min) of PE (C) concentration of enzyme (0.025 to 0.125 mg/mL)

Fig. 4.7. (A) DPV response study of AChE/Ag@CuO/PANI/ITO developed electrode after incubation of various conc of PE (5-100 pM). (B) Calibration curve between current vs PE conc (C) Interference data in presence of 1 μM Na^+ , K^+ , SO_4^{2-} ions, malathion, and uric acid with the coexistence of 5 pM PE

Fig. 4.8. (A) Reproducibility study of PE using different electrodes, (B) Stability study of the fabricated electrodes (AChE/Ag@CuO/PANI/ITO) over a period of 25 days

Fig. 5.1. Schematic diagram of biosensor fabrication and working mechanism for PE detection

Fig. 5.2 (A) XRD curves of (a) PANI (b) CeO_2 (c) CeO_2 @PANI (B) FTIR spectra of (a) CeO_2 (b) PANI and (c) CeO_2 @PANI

Fig. 5.3. (A) SEM micrograph of CeO_2 nanocrystals (B) TEM micrograph of CeO_2 nanocrystals (C) SEM micrograph of CeO_2 @PANI composite (D) TEM micrograph of CeO_2 @PANI composite

Fig. 5.4. SEM-EDAX analysis of (A) CeO_2 and (B) CeO_2 @PANI-based composite

Fig. 5.5. (A) Cyclic voltammogram of CeO_2 @PANI/ITO (a), AChE/ CeO_2 @PANI/ITO (b), PANI/ITO (c) and ITO (d) at scan rate 50 mV/sec. CV curves of (B) PANI/ITO (C) CeO_2 @PANI/ITO at different scan rates (10 - 300 mV/sec). (D) Plots of current vs. square root of scan rate for PANI (a) and CeO_2 @PANI (b). (E) Plots of potential vs. log (scan rate) for CeO_2 @PANI/ITO (a) and PANI/ITO (b)

Fig. 5.6. Optimization of (A) pH effect (6-8 pH), (B) incubation time (0-10 min) of PE

Fig. 5.7. (A) DPV response study of AChE/CeO₂@PANI/ITO developed electrode after incubation of various conc (1-100 pM) of PE (B) Calibration graph of current vs. conc (C) Interference data in presence of 10 pM glucose, ascorbic acid, uric acid, K⁺, SO₄²⁻ ions, Na⁺, Cu²⁺ with the coexistence of 10 pM PE

Fig. 5.8. (A) Reproducibility study of PE using different electrodes (B) Stability study of the fabricated electrodes (AChE/CeO₂@PANI/ITO) over a period of 40 days

Fig. 6.1. Fabrication and mechanism of CuO@PEDOT:PSS-grafted paper based biosensor for OPs detection

Fig. 6.2. (A) XRD pattern of PEDOT: PSS/ITO (a) CuO (b) and CuO@PEDOT: PSS/WP (c) (B) FTIR spectra of PEDOT: PSS/WP (a) and CuO@PEDOT: PSS/WP (b)

Fig. 6.3. SEM micrographs of (A) WP, (B) PEDOT: PSS/WP, (C) CuO@PEDOT: PSS/WP (D) Ethylene glycol treated CuO@PEDOT: PSS/WP electrodes

Fig. 6.4. (A) Chronoamperometry curves of (a) CuO@PEDOT: PSS/WP, (b) PEDOT: PSS/WP and (c) AChE/CuO@PEDOT:PSS/WP electrodes (B) An electrochemical response study of AChE/CuO@PEDOT: PSS/WP electrode after incubation of various conc (10-80 nM) of PE (C) Calibration graph of current vs. PE conc (D) Interference data of AChE/CuO@PEDOT: PSS/WP electrode in 10 nM uric acid, CaCl₂, FeSO₄, ascorbic acid and glucose.

Fig. 6.5. (A) Reproducibility studies of the developed biosensor for PE detection using different electrodes (B) Stability studies of AChE/CuO@PEDOT: PSS/WP biosensor over a period of 28 days

Fig. 7.1. A Schematic view of biosensor fabrication and working mechanism for PE detection

Fig. 7.2. (A) XRD pattern of (a) PEDOT:PSS/WP, (b) CeO₂ and (c) CeO₂@PEDOT:PSS/WP. (B) FTIR plots of (a) CeO₂, (b) PEDOT:PSS/WP and (c) CeO₂@PEDOT:PSS/WP

Fig. 7.3 (A) SEM micrograph of CeO₂ nanocrystals (B) TEM micrograph of CeO₂

nanocrystals (C) SEM micrograph of WP (D) SEM micrograph of PEDOT:PSS/WP electrode (E) SEM micrograph of CeO₂@PEDOT:PSS/WP electrode (F) SEM micrograph of EG-treated CeO₂@PEDOT:PSS/WP electrode

Fig. 7.4. SEM-EDAX analysis of (A) CeO₂ and (B) CeO₂@PEDOT:PSS/WP electrode

Fig. 7.5. (A) Chronoamperometry plot obtained for (a) PEDOT: PSS/WP, (b) CeO₂@PEDOT: PSS/WP, (c) AChE/EG-treated- CeO₂@PEDOT: PSS/WP and (d) EG-treated- CeO₂@PEDOT: PSS/WP (B) Chronoamperometry response study of AChE/EG-treated- CeO₂@PEDOT: PSS/WP electrode after incubation of various concentrations (0, 0.1, 0.5, 1, 5, 10, 20, 30, 40, 50, 100, 150, and 200 nM) of PE. (C) Calibration graph of inhibition (ΔI) vs. PE concentration (C_{PE}). Inset of 6(C) shows a linear curve of ΔI vs. $\log(C_{PE})$ (D) Interference study of AChE/EG-treated-CeO₂@PEDOT: PSS/WP electrode in the presence of Na⁺, K⁺, uric acid (UA), glucose, and ascorbic acid (AA).

Fig. 7.6. Optimization of (A) incubation time (0-6 min) of PE (B) pH effect (6-8 pH)

Fig. 7.7. (A) Reproducibility studies of the developed biosensor for PE detection using different electrodes (B) Stability studies of the developed electrode (AChE/CeO₂@PEDOT: PSS/WP) over a period of 28 days

List of Tables

Table 1.1. Different type of electrochemical biosensors used to determine the concentration of OPs.

Table 3.1. Detection of PE in spiked Rice and Pulse samples using AChE/CuO@PANI/ITO Electrode.

Table 4.1. Kinetic parameters of all the modified electrodes

Table 4.2. PE detection in spiked soil, banana and tomato samples using AChE/Ag@CuO/PANI/ITO electrode

Table 5.1. Kinetic parameters of PANI/ITO and CeO₂@PANI /ITO electrodes

Table 5.2. Detection of PE in spiked Soil and Carrot Samples using AChE/CeO₂@PANI/ITO Electrode.

Table 6.1. Electrical conductivities of various electrodes

Table 6.2. Detection of PE in Spiked Rice and Pulse samples by using the AChE/CuO@PEDOT: PSS/WP biosensor

Table 7.1. Electrical conductivity studies of all modified electrodes

Table 7.2. Detection of PE in Spiked Soil and Carrot Samples using AChE/CeO₂@PEDOT: PSS/WP Electrode

Abbreviations

| | |
|-------|--------------------------------------|
| PANI | Polyaniline |
| ATCl | Acetyl thiocholine chloride |
| AChE | Acetylcholinesterase |
| CV | Cyclic Voltammetry |
| PE | Paraoxon-ethyl |
| CP | Conducting Polymer |
| DPV | Differential Pulse Voltammetry |
| EDAX | Energy Dispersive X-ray Spectroscopy |
| PBS | Phosphate Buffer Saline |
| ITO | Indium Tin Oxide |
| EPD | Electrophoretic Deposition |
| XRD | X-ray Diffraction |
| FT-IR | Fourier Transforms Infrared |
| TEM | Transmission Electron Microscopy |
| SEM | Scanning Electron Microscopy |
| RSD | Relative Standard Deviation |
| LOD | Limit of Detection |

CHAPTER 1

Introduction & Literature Review

1.1. Introduction to Pesticides

Pesticides are chemical or biological substances extensively used to control, prevent or eliminate pests [1]. They are commonly used in agriculture, horticulture fields to protect crops, plants, and stored products from pests such as insects, weeds, fungi, and disease-causing organisms. Pesticides can be categorized into different types based on the target pest and the method of application [2]. Some common types of pesticides include:

1. Insecticides: These are pesticides designed to kill or control insects. They can target specific types of insects or have a broader spectrum of activity.
2. Herbicides: They are used to control or eliminate unwanted plants or weeds. They can be selective, targeting specific types of plants.
3. Fungicides: Fungicides are used to prevent or treat fungal diseases in plants. They can be applied to seeds, soil plant foliage to protect against fungal infections.
4. Rodenticides: These pesticides are used to control rodents such as rats and mice. They are typically designed as poisons to attract and kill rodents.
5. Bactericides: They are used to control bacteria that can cause diseases in plants or animals. They are often used in agricultural and medical fields.

1.2. Classification of Pesticides

Pesticides are categorized into different classes depending on their chemical and physical properties. The classification of pesticides depends on their source, chemical structure and the target of the pests they kill. Depending on their source, they are majorly classified into two classes:

1.2.1. Bio-Pesticides

Bio-pesticides are naturally occurring compounds obtained from some natural sources like plants, animals, minerals and bacteria. They use non-toxic mechanisms for pest control [3]. These are more environment friendly alternative to conventional synthetic pesticides due to their lower toxicity. The properties of bio-pesticides are summarized below:

- Compare to conventional pesticides, biopesticides are very low toxic.
- Bio-pesticides are very effective in less quantity.
- They show biodegradable nature and break down more quickly, reducing their persistence in the environment.
- They only affect the specific pests, such as certain insects, pathogens or weeds, while leaving the beneficial organisms unharmed. The selective targeting minimizes the impact on non-target organisms and reduces the risk of developing resistance in pest populations.

Biopesticides are categorized into three categories:

1. Biochemical - They are manufactured from various natural sources like animals, certain minerals, plants, etc. They are made up of insect sex pheromones [3]. They disrupt the specific biochemical processes in pests, often affecting their behaviour or growth.
2. Microbial – They are comprised of microorganisms like fungi, yeast, bacteria, etc. and are widely used in agriculture to control plant diseases [4]. They can control pests by infecting them with diseases or producing toxins, which are harmful to the pests.
3. Plant-based – They are biological microorganisms like antimicrobials, bacteria viruses, etc. that are made up of plant extracts or oils that repel or disrupt the feeding and reproduction of pests [3].

1.2.2. Chemical Pesticides

Chemical pesticides are not found in nature. They are synthesized in laboratories and highly toxic when compared to natural pesticides. They are synthesized through various chemical processes and are designed to control or eliminate pests. Their common properties are as follows:

- They are formulated to have a broad spectrum of activity. They can target and control a variety of pests, such as insects, weeds, fungi and other organisms. Their versatility makes them effective against multiple types of pest but also increase the risk of impacting non-target organisms.
- Many chemical pesticides have the property of persistence. They can remain in the environment for an extent period. This allows for long-lasting pest control but they can also lead to the accumulation of their residues in soil, water and agricultural resources, which further affect the health of leaving beings.
- They can contaminate water, affect beneficial organisms, such as bees, birds, fish and disrupt the ecosystem [5].

They are categorized into four categories:

1. Carbamate - These synthetic pesticides are esters of carbamic acid. They are applicable as insecticides and herbicides. Some carbamate pesticides are propoxur, bendiocarb and carbaryl [6, 7] .
2. Organochlorine - These are chlorinated hydrocarbons. Hexachlorocyclohexane (HCH) and dichlorodiphenyltrichloroethane (DDT) are commonly used organochlorines [8].
3. Pyrethroid - These are the synthetic version of natural pesticide pyrethrins. They have less level of toxicity and fast rate of degradation. Deltamethrin, cyfluthrin, lambda-cyhalothrin and Premehrin are pyrethroid pesticides [9].
4. Organophosphate pesticides (OPs) – OPs are a class of chemical pesticides that are

widely used for the control of insects in agriculture, public health and veterinary applications. They are composed of two moieties (a) phosphate moiety and (b) organic moiety. Their properties are as follows:

(a) Mode of action: Their work is based on inhibition of acetylcholinesterase (AChE) enzyme. A breakdown of the neurotransmitter acetylcholine in the nervous system is attributed to the AChE enzyme. By inhibiting AChE enzyme, OPs accumulate the acetylcholine, resulting in the overstimulation and dysfunction of nervous system in pests [10].

(b) Broad spectrum of activity: They are effective against the wide range of insects, pests, including mosquitoes, mites, agricultural pests, etc. Their broad-spectrum activity makes them versatile for pest control in various fields.

(c) Persistence: Some OPs have moderate to high persistence in the environment. They can remain active for an extended period, which leads to their accumulation in soil, water and agricultural resources. Their accumulation causes environmental contamination and affects the non-target organisms [11].

(d) Toxicity: They are highly toxic for insects but they can cause the risks to humans, wildlife and other non-target organisms.

(e) Health effects: OPs can affect the human nervous system and are considered neurotoxic. They can covalently bind with the serine hydroxyl group of the acetylcholinesterase (AChE) enzyme which prevents neurotransmission function. The acetylthiocholine chloride (ATCI) undergoes hydrolysis through the catalytic action of AChE enzyme, which is responsible for transmitting nerve impulses. OPs are paraoxon-ethyl, malathion, fenitrothion, chlorpyrifos, trichlorfon, etc. [12].

The classification of pesticides is represented in Fig. 1.1.

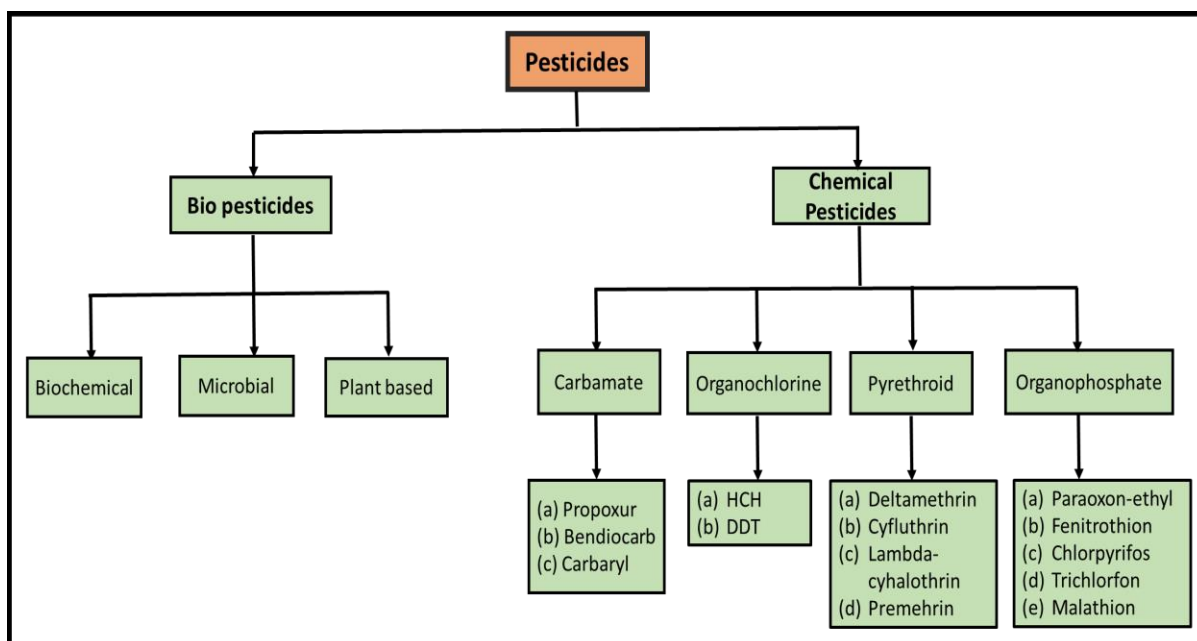


Fig. 1.1. Classification of pesticides

1.3. Benefits of Pesticides to Mankind and the Environment

The careful use of pesticides provides various positive outcomes to mankind. The main advantages of pesticides are as follows:

1. **Increased Agricultural Productivity:** Pesticides play an indispensable role in contemporary agriculture by safeguarding crops against the perils of pests, diseases and weeds. They control plant and pest diseases that help to increase the agricultural productivity and quality of crops. Increasing crop production enhances food availability at a reasonable price and improves national agricultural economics.
2. **Disease Prevention:** Pesticides are used in public health programs to control disease vectors, such as mosquitoes, ticks, etc. They can control various unwanted organisms and prevents the spreading of diseases caused by vector or insects, such as malaria, dengue, etc. [13].
3. They play a vital role in preserving the environment. Their limited use helps to reduce air pollution.

4. Herbicides are extensively used in various transport sectors. They also used to maintain sports and cricket grounds.
5. Insecticides are used to protect wooden products from woodworms [14].

1.4. Consequences of Pesticides on human health and Environment

The working of all pesticides is not specific for all species. Their careless and extensive use causes severe health issues that can be divided into two categories:

1.4.1. Acute illnesses – The symptoms of acute illness caused by pesticides are headache, nausea, body ache, panic attacks, excessive sweating, etc. Intake of pesticides in large amounts causes death [15].

1.4.2. Chronic illnesses – The intake of pesticides for a long period (even if the pesticide is in significantly less amounts) can affect the immune system and causes various chronic diseases. Some pesticides (organochlorines, DDT, etc.) are tumor promoters and carcinogenic for humans [16, 17].

OPs are also very toxic pesticides and are widely used as warfare agents. The degradability of OPs is also very slow, which causes their bioaccumulation in agricultural resources, soil and water. They can enter into the living body through intake of contaminated food, water, etc. and cause various health issues [18]. They can cause phosphorylation of the AChE enzyme (the enzyme responsible for the nervous system functioning) which further results the neurotoxic effects in living beings. The regular intake of OPs (even in small amounts) can cause very serious diseases like Alzheimer's, Parkinson's, bone marrow and nerve disorders, etc. [19]. According to EPA, they belong to high and moderately toxic pesticides [20]. By considering the poisonous effects of OPs, it is highly required to control their limits in food, water, agricultural resources, etc. For this reason, an effective technique is highly needed for quantification, fast and effective detection of OPs.

1.5. Detection Techniques of Pesticides

For achieving the benefits of pesticides and reducing related health issues, a technique is highly required for their optimal detection in various real samples. In the course of the past few decades, a diverse range of detection techniques has been developed.

1.5.1. Traditional Analytical Methods

In the literature, well-known traditional methods such as gas chromatography [21], liquid chromatography coupled mass spectroscopy [22], fluorimetric [23], colorimetry [24], immunoassay [25], capillary electrophoresis [26] , spectrophotometry [27], etc. have been proposed so far. These methods are reliable and selective but require professional operators, time taking, cheap and off-site procedures. Due to these flaws, such methods can be replaced by other methods which can provide a fast, simple, highly sensitive channel for OPs detection.

1.5.2. Advanced Detection Techniques

To overcome the flaws of traditional methods, biosensors are the majorly used advanced detection technique reported in the literature. This advanced technique provides various advantages like fast on-site operation, low-cost, simple for handling, high sensitivity, and selectivity.

1.5.2.1. Biosensors

Biosensor, an analytical device, is used to detect a specific target molecule or any chemical substance. It is composed of the biological sensing element connected with a transducer, which produces an electronic signal. It detects the physiological change of the whole process followed by the transmission of information, which finally produces the signal. Prof. Leland C. Clark is called the father of biosensors. He first demonstrated the term biosensor in 1962 by developing the first enzyme electrode using glucose oxidase for glucose analysis. In 1975, the first biosensor (Yellow Springs, OH, USA) was commercially placed in the market for fast glucose detection in the blood sample [28]. At present, various biosensing

techniques have been explored by various research groups which are applied in various fields. Biosensors are highly sensitive, selective, portable, and fast analytical devices. They require minimal analyte concentration and simple procedures. They are extensively applied in the field of environmental monitoring, food & soil quality monitoring, disease detection, veterinary, etc. [29]. A pictorial view of biosensor is given in the Fig. 1.2.

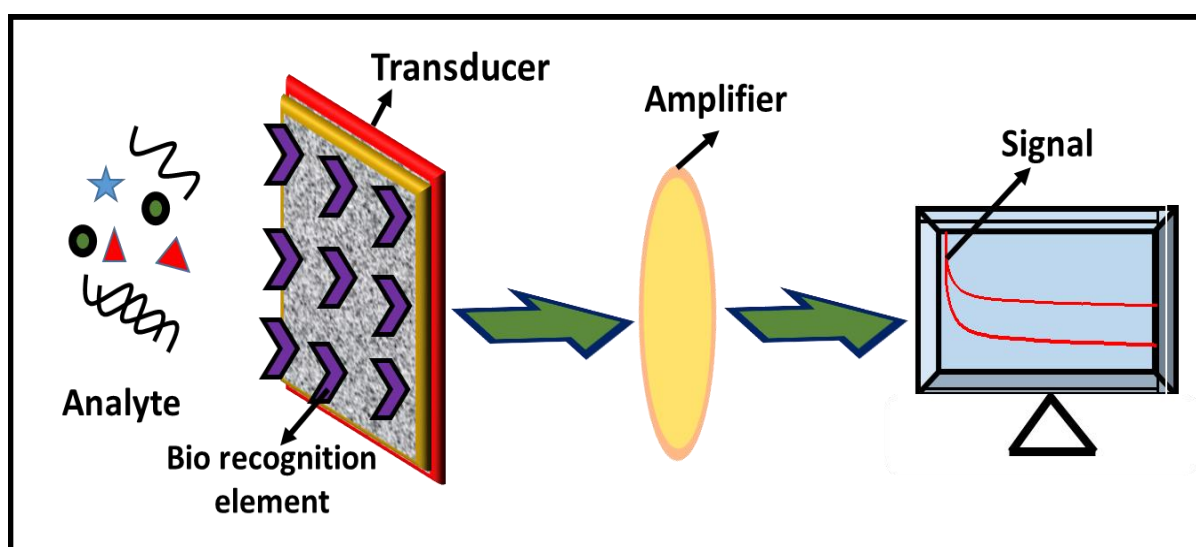


Fig. 1.2. A schematic view of biosensor

Biosensors are majorly composed of three components. These components of biosensor are represented in the Fig. 1.3.

1. **Bio-receptor or bio-recognition element** - Bio-receptors are the molecules, such as an enzyme, antibody, cell, DNA, etc., that specifically interacts with the analyte. The prerequisite of bio receptors is the high selectivity towards specific analyte molecules.
2. **Immobilization matrix** - A matrix is used to integrate bio-recognition elements at the surface of the transducer. It can help to maintain the biomolecule's functionality and further provide accessibility for the analyte molecule. Ideal solid support should have the properties like inert nature, good bioaffinity, hydrophilicity, availability at a cheap

rate, etc. which enhances the electron kinetics and performance of biosensors [30]. The type of immobilization (covalent bonding, adsorption, entrapment, cross-linking, etc.) totally depends upon the chemical properties of bio-receptors and desired solid surface. Various immobilization matrices have been proposed so far. Conducting polymers are attracted much attention worldwide for the application of biosensors due to their high conductivity, good bioaffinity, thermal and chemical stability, easy and cheap preparation [31]. They are frequently used to fabricate the electrochemical biosensors owing to their high charge transfer ability and biocompatibility. The sensing ability and properties of conducting polymers are enhanced by incorporating nanomaterials like metal oxides (CuO, CeO₂, TiO₂, ZnO, NiO, etc.) metal sulfides [32] carbon nanotubes, etc. [33].

- 3. Transducer** - The transducer detects the interaction of the analyte and biological sensing element and finally converts it into a measurable signal. In other words, it can be used as an energy converter from one form to another. This process is called signalization. Depending upon the transducing element, biosensors are divided into optical, thermoelectrical, piezoelectric, and electrochemical biosensors. All electrical and optical signals are directly proportional to the biorecognition element and analyte interactions.

Electrochemical biosensors, a subcategory of chemical sensors, are getting popularity because of their good sensitivity, high selectivity, simple instrumentation and high reproducibility. The principle of electrochemical sensors is based on the production of electrons which results from the enzyme catalysis in a reaction. They contain three electrode systems; a working electrode (fabricated electrode), counter electrode (Pt electrode), and reference electrode (Ag/AgCl). They monitor the change in electrical current distributions and can be classified into three types:

- Conductometric - They measure the electrical conductivity resulting from the biochemical reaction between two electrodes in a solution. They consist of two and more electrodes separated by an insulating layer. When the target analyte interacts with the bioreceptors (e.g., enzymes and antibodies), it induces a change in the conductivity of the solution surrounding the electrodes. The measurement and correlation of this change can be attributed to the concentration of analyte.
- Potentiometric – The potential difference between two electrodes resulting from the redox reaction between the analyte and bioreceptor is measured by potentiometric biosensors. They are used in the applications including pH sensing, gas sensing and ion sensing.
- Amperometric – The electric current or potential obtained on the transducer by the chemical reaction of electroactive materials is measured by amperometric biosensor. These biosensors consist of a working electrode and a reference electrode immersed in the sample solution. The bioreceptors or enzyme immobilized on the working electrode play a crucial role to catalyze a reaction with analyte. This reaction generates an electrochemical current. This current is directly proportional to the analyte conc. Amperometric biosensors are often used for detecting various analytes such as neurotransmitters, environmental pollutants and biomarkers.

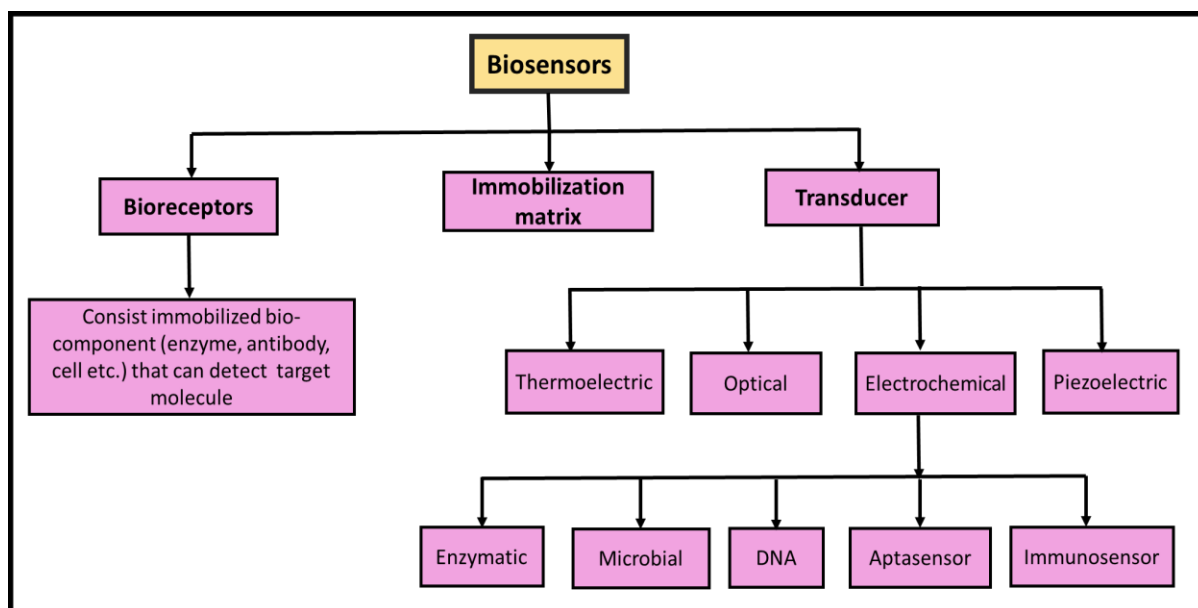


Fig. 1.3. Components of biosensor

1.6. Electrochemical Biosensors for OPs detection

Recently, various studies have been proposed for OPs detection by upgrading the biological components like microbial cells, aptamer, antibody, DNA and enzyme. Based on the biological component, electrochemical biosensors for OPs detection are also classified into the following categories:



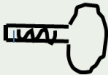



1. **Microbial Biosensors** – They involve the immobilization of microbial cells onto a conducting platform. The microbial cell contains organophosphorus hydrolase (OPH) enzyme which hydrolyzes bonds like P-F, P-O, P-CN, and P-S. The hydrolysis of these bonds results in the formation of para-nitrophenols and two protons which further produce the signal. They are highly specific because these can be engineered to respond only to specific OPs. However, their sensitivity may be limited and they require complex sample preparation steps.
2. **Aptasensor** - Deoxyribonucleic acid or ribonucleic acid (single-stranded oligonucleotides) are used in these biosensors as biorecognition elements. They can bind to specific molecules including OPs. They provide sensitive and selective results but

aptamers are expensive and require optimization to improve their stability and selectivity.

3. **Immunosensor** - The basic principle of immunosensor is based on the interaction of antigen (specific target molecule) and antibody. They possess high sensitivity and selectivity due to the specific binding of antibody-antigen. Except of having various benefits of immunosensor, they show some shortcomings like complex procedure, large analysis time involved in the monoclonal antibody generation, etc. Although, immunosensors are sensitive and selective but their limited shelf life and high cost make them less applicable for OPs detection.
4. **DNA-based biosensor** - These biosensors consist of the DNA immobilized working electrode. In this biosensor, the interaction of analyte and DNA causes a change in redox properties (change in guanine base oxidation) of DNA. These biosensors are also sensitive but they require complex sample preparation and can be vulnerable to degradation.
5. **Enzyme-based biosensor** - These biosensors are very popular for OPs detection. They consist an enzyme immobilized into the surface of conducting platform. In the current technology of biosensors, the enzyme was first exploited as a biorecognition element. Enzyme-based electrochemical biosensors are analytical devices in which the combination of enzyme and transducer provides the signal. The resulting signal is directly proportional to the concentrations of substrate and analyte. Their working principle is commonly based on inhibiting enzymes in the presence of the analyte (OPs).

Table 1.1 presents the different types of electrochemical biosensors used to determine the concentration of target OPs. Among all these electrochemical biosensors, enzyme-based biosensors are most significant for OPs detection owing to their high specificity, bio-catalytic signal amplification property, fast and straightforward detection process [34].

Table 1.1. Different type of electrochemical biosensors used to determine the concentration of OPs.

| Analyte | Bio recognition element | Mechanism | Type of Biosensor |
|---|--|--|-------------------|
| Organophosphate Pesticides  | Microbial cells  | Microbial cells express the enzyme OPH, which hydrolyse P-O bond and forms p-nitrophenol and two protons | Microbial |
| | Aptamers  | Conformation change | Aptasensor |
| | Antibody  | Interaction of Antigen and Antibody | Immunosensor |
| | DNA  | Oxidation of guanine base | DNA |
| | Enzyme  | Inhibition of enzyme, no substrate (ATCL) hydrolysis | Enzymatic |

1.7. Enzyme-based Electrochemical Biosensors for OPs detection

The enzymes such as butyrylcholinesterase (BChE), acetylcholinesterase (AChE), organophosphorus hydrolase (OPH), and organophosphorus acid anhydrolase (OPAA) are being used most commonly for OPs detection. Among all, AChE-based biosensors are widely explored for OPs detection due to the following reasons [35].

1. High sensitivity: AChE enzyme exhibits high sensitivity to a wide range of OPs compounds. It can detect low concentrations of OPs, making it suitable for applications requiring high sensitivity.
2. Broad spectrum of detection: AChE can interact and detect a variety of OPs, providing a broad spectrum of detection capability. It can be used to detect and monitor different

types of OPs.

3. Commercial availability: AChE is commercially available and obtained from various sources, making it more accessible for researchers and developers for OPs detection.
4. Well-studied and established: AChE has been extensively studied and characterized, both structurally and functionally. This knowledge provides a solid foundation for design and optimization of biosensors based on AChE.

1.7.1. Acetylcholinesterase-based Biosensors for OPs detection

AChE is a very important enzyme composed of mainly three amino acids: serine, histidine, and glutamate. They belong to the hydrolases family and are mostly present in vertebrates and insects. They catalyze the hydrolysis of the neurotransmitter acetyl-thiocholine chloride (ATCl) into two electrocatalytic products, namely, acetic acid and thiocholine. The inhibition of the AChE enzyme is caused by organophosphate pesticides [36]. The phosphorus atom of OPs binds covalently with the hydroxyl groups of serine (HO-Ser) present in the AChE enzyme. The phosphorylation of AChE causes the blocking of active serine groups of AChE [37]. The mechanism of AChE enzyme inhibition in the presence of OPs is illustrated in Fig. 1.4. The AChE inhibition-based biosensors were first reported during the 1980s.

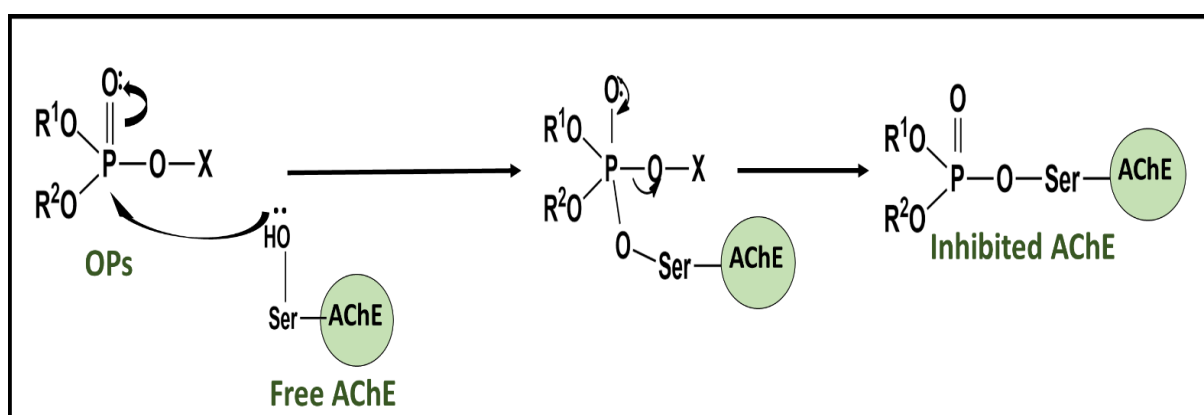


Fig. 1.4. The mechanism of AChE enzyme inhibition in the presence of OPs

The principle of OPs detection using an AChE-based electrochemical biosensor depends on the inhibition of AChE enzyme. A working mechanism of this biosensor is illustrated in Fig. 1.5. In this figure, acetyl thiocholine chloride (ATCl) hydrolysis is catalyzed by an immobilized AChE enzyme. This reaction results in the formation of acetic acid (CH_3COOH) and thiocholine ($\text{N}^+(\text{CH}_3)_3\text{-CH}_2\text{-CH}_2\text{-SH}$), which generates an irreversible oxidation peak. In contrast, the presence of the analyte (OPs) blocks the catalytic activity of the AChE enzyme, which prevents the ATCl hydrolysis resulting a decrease in oxidation peak. Therefore, by monitoring the peak current in the presence and absence of an analyte, the concentration of OPs can be determined. They also have their inherent drawback. The main drawback is sensitivity. It is affected by the oxidation potential of electroactive product (thiocholine) and the immobilization efficiency of AChE on the electrode surface. The oxidation potential of thiocholine chloride has a relatively high value which can results in poor sensitivity [33, 38].

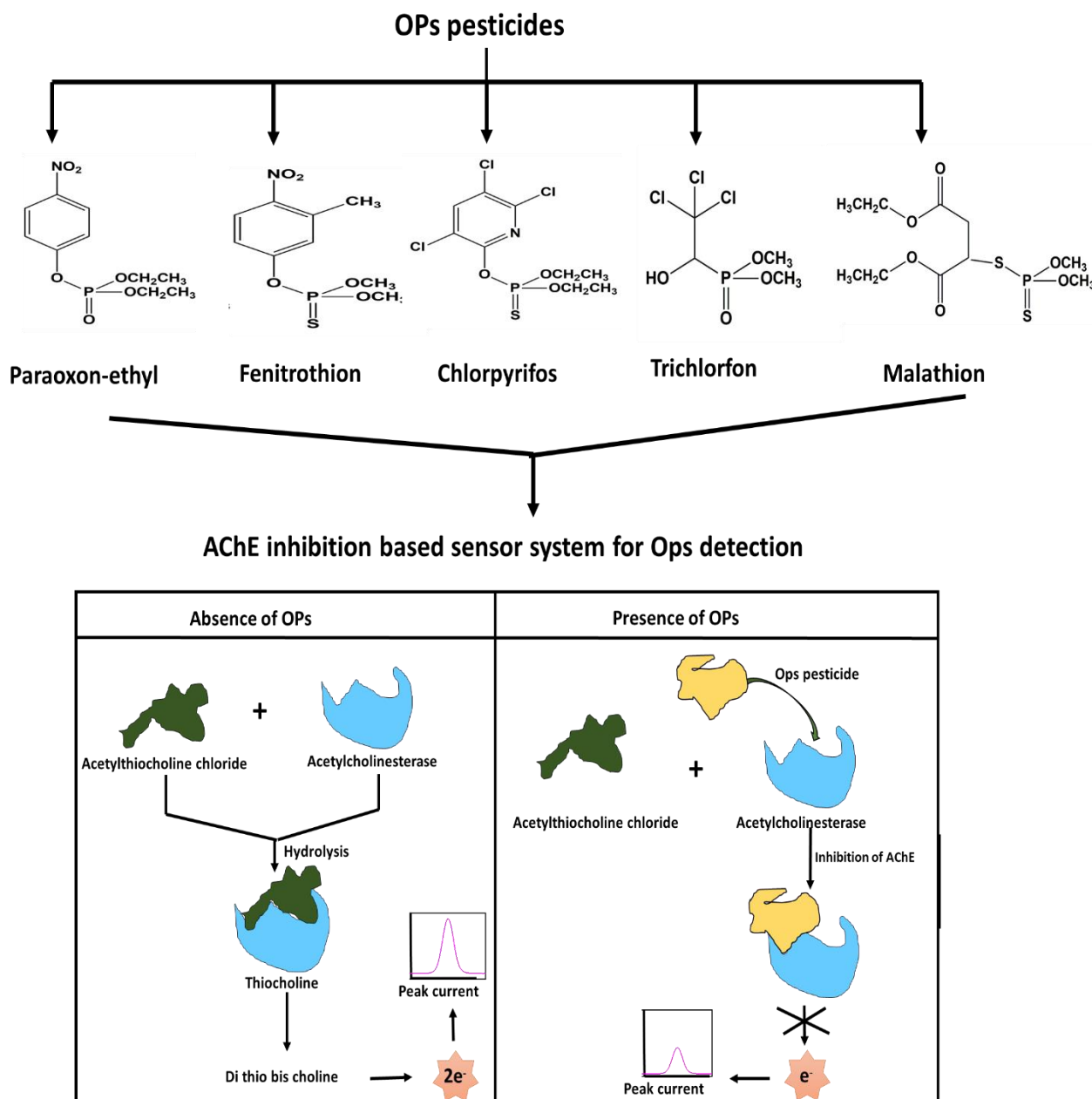


Fig. 1.5. Working mechanism of AChE-based biosensor for OPs detection

The performance of AChE-based biosensors is highly affected by two factors:

1. Degree of enzyme immobilization onto the electrode surface and
2. Electron transfer rate between electrode surface and enzyme.

An effective immobilization of enzymes drastically enhances biosensors' sensitivity, reproducibility, stability and response time. For the immobilization of enzymes, various

techniques such as physical entrapment, covalent immobilization and cross-linking have been reported [39].

Considering the factors mentioned above, different studies have been conducted to explore the materials like conducting polymers [40], graphene [41], carbon nanotubes [42], metal oxides [43, 44] etc. Among them, the conducting polymer has attracted high attention for the development of AChE-based biosensors.

1.8. Conducting Polymers

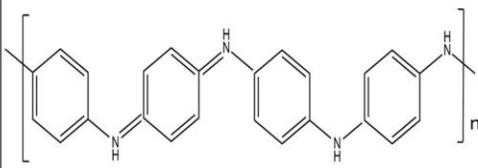
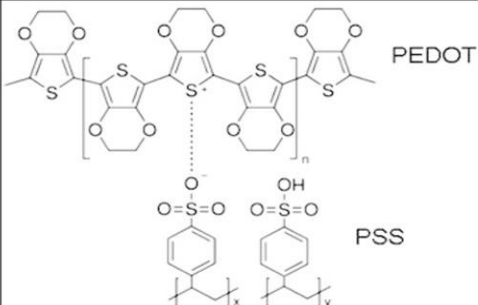
Conducting polymers also called as synthetic metals are the organic polymers that conduct electricity. They contain conjugated π -electrons in their structure which is responsible for their conducting property. These are extensively used owing to their high conductivity, easy preparation method and availability, good thermal, mechanical, optical and environmental stability, etc. [45]. They make a favorable immobilization platform by tuning the electronic and structural properties. Additionally, they can provide a sensitive microenvironment for analyte [46]. Conducting polymers are now highly useful in numerous applications like environmental monitoring devices [47], chip-based sensors [48], optical sensors [49, 50], electrochemical biosensors [51], etc. Apart from these applications, their applicative progress is still going on till date.

1.8.1. Evolution of Conducting Polymers

The conducting polymers were first reported in the early 1900s by synthesizing aniline black and pyrrole black [52, 53]. The discovery of poly(sulfur nitride) in 1975 further explored the research based on conducting polymer [54]. The electrically conducting polymer polyacetylene was later synthesized by Shirakawa et al. in 1977 using Ziegler Natta catalyst [55]. MacDiarmid and Heeger modified the polyacetylene by doping with oxidizing and reducing agents. In this study, they increased the conductivity (106 fold) of polyacetylene

[55]. Despite its metal-like conductivity, it shows poor thermal stability. Therefore, the scientific community further discovered various new conducting polymers for better properties. In 1979, poly(p-phenylene) was synthesized by Ivory et al. It was doped by n- and p-type dopants and formed a highly-conducting charge transfer complex [56]. In 1980 Rabolt et al. discovered poly(p-phenylene sulfide). This polymer was highly conducting compared to previously discovered conducting polymers. Further, other conducting polymers, namely, polyindole, polycarbazole, polyfuran, poly(3,4-ethylene dioxythiophene) (PEDOT), polypyrrole (PPy), polyaniline (PANI), etc. were also discovered. Among all these, PANI, PEDOT are highly applicable in biosensing field due to their remarkable properties [57, 58].

The structure, properties and applicability of PANI and PEDOT are summarized as below:

| S. No. | Conducting Polymer | Structure | Properties | Applications |
|--------|--|---|--|---|
| 1. | Polyaniline (PANI) |  | Highly conducting nature, biocompatible in nature due to large amino groups, flexible structure, redox behavior, high surface area, easy synthesis procedure, environmental, thermal and electrochemical stability | Highly applicable in gas sensors, glucose biosensors, solar batteries, supercapacitors, storage fibers, etc. |
| 2. | Poly(3,4-ethylenedioxythiophene):polystyrene sulfonate (PEDOT:PSS) |  | Possess moderate band gap, low redox potential, shows biocompatible nature, excellent thermoelectric performance | It is highly used in electrochemical application, such as sensing, solar cells, photovoltaics, electroluminescent devices, etc. |

1.8.2. Conducting Polymer-based Composites

The direct use of conducting polymers as a sensing platform is not providing the effective results because the presence of both ionic and redox species in the system can interfere with the recorded potential. Therefore, the composites of solid contact phase (conducting polymer) and ions (nanomaterials) are advised to use as a sensing platform for better efficiency of biosensors [59]. Composites are hybrid materials that contain two or more components. The special combination of these components improves the properties of the resultant composite which makes it highly applicable in different fields of biosensor. The properties of conducting polymer-based composites are tuned by special combination of appropriate matrix (polymers) and a filler (nanomaterials). The combination of matrix and filler develop an organic-inorganic conducting platform with improved sensing ability due to the following reasons:

- The strength of electrical break down is increased during the formation of composites.
- The increase in magnetization property, melting point and charge capacity is significantly increased with the formation of composite.
- The electrical conductivity, dielectric behaviour and corrosion resistance are also improved.

To achieve better results in the biosensing and electrochemical applications, the composites of conducting polymers are taken into consideration. Their integration with nanomaterials such as metal oxide nanoparticles (CuO [60, 61], TiO₂ [61], CeO₂ [62], ZnO [63], etc.), graphene [64], carbon nanotubes [65], etc. enhances the properties which further improve the sensitivity, selectivity and stability performance of biosensor.

1.8.3. Synthesis Techniques of Conducting Polymer-based Composites

They are synthesized by following methods:

1. Electrochemical Polymerization - This technique involves the use of electric current for initiating the polymerization reaction. In this process, the monomer and nanomaterials are dissolved into the solvent and the electrodes are also inserted into the solution. Then, the monomer undergo oxidation and reduction at the electrode surface after applying electric current which results in the formation of composite. The properties of electrochemical polymerization are as follows:

- Expensive and complicated technique. It provides low yield of product.
- It requires more time for completion of reaction.

2. Chemical Polymerization - Chemical polymerization is a process which involves a chemical reaction for synthesizing conducting polymers and their composites without a cell assembly. This method exhibits the following properties:

- Chemical initiators, such as ammonium per sulfate, potassium per sulfate etc. are used to initiate the polymerization.
- For controlling the structure and properties of resulting composite, templates like cetyltrimethylammonium bromide, sodium dodecyl sulfate, etc. are used.
- Simple, cost effective and less time-consuming technique. It provides high yield of product in comparison to electrochemical polymerization.

1.8.4. Applications of Conducting Polymer-based Composites for OPs detection

The reviews of existing literature reveal that various conducting polymers based nanocomposites have been used as a sensing platform for OPs detection. An electrochemical biosensor has been developed by Ivanov et al. [66] by anchoring the AChE enzyme onto the polyaniline (PANI) modified glassy carbon electrode (GCE) for OPs (trichlorfon) and

carbamate pesticides (coumaphos, methiocarb, aldicarb) detection. Further, Somerset et al. [67] developed an AChE-based organic-phase biosensor using gold electrode modified by mercaptobenzothiazole and PANI for fenitrothion and diazinon detection. The gold nanoparticles and polypyrrole-based composite was further used by Gong et al. [68] for methyl parathion detection. A gold electrode was modified by Viswanathan et al. [69] using the vertically aligned DNA, single walled carbon nanotubes and PANI. The fabricated electrode was further used for methyl parathion and chlorpyrifos detection in vegetable crops. An amperometric biosensor was developed by Marinov et al. [70] by immobilizing AChE enzyme onto gold modified poly(acrylonitrile-methyl methacrylate-sodium vinyl sulfonate) electrode surface. The biosensor was further used for paraoxon-ethyl detection. Jha et al. [71] established an AChE-based electrochemical biosensor using polypyrrole and carbon nanotube (CNT)-based composite for paraoxon-ethyl detection. A green and low-cost method for paraoxon-ethyl detection was developed by Ivanov et al. [72] using poly-(acrylonitrile-methyl methacrylate-sodium vinyl sulfonate) integrated multiwalled carbon nanotubes modified electrode surface. Further, carbon nanotubes and copolymer of polyaniline and polypyrrole based composite was used by Du et al. [73] for malathion detection. Chauhan et al. [74] have developed an amperometric biosensor for OPs (malathion and chlorpyrifos) detection using ZnS nanoparticles doped poly(indole-5-carboxylic acid) deposited on Au electrode as a sensing platform. Kanik et al. [75] developed an AChE inhibition based amperometric biosensor for the detection of paraoxon-ethyl. They immobilized AChE enzyme onto graphite modified poly(4-(2,5-di(thiophene-2-yl)-1H-pyrrole-1-yl) benzenamine) surface by covalent bonding. Further, Yang et al. [76] developed an electrochemical biosensor using gold nanoparticles, reduced graphene oxide and polypyrrole based modified electrode for paraoxon-ethyl detection. Kesik and co-workers [46] used poly(SNS-NH₂) and multiwalled carbon nanotube modified graphite electrode for paraoxon-ethyl, methyl parathion and chlorfenvinphos

detection. Li et al. [77] electrochemically deposited the graphene and polyaniline based nanocomposite onto glassy carbon electrode for sensitive detection of carbaryl. He et al. [33] reported the fabrication of an electrochemical biosensor for malathion detection using hollow carbon sphere and polyaniline as a sensing platform. A sensitive AChE based amperometric sensor has been developed by Zhang P et.al. [78] for malathion and trichlorfon detection. A conjugated polymer, poly(FBThF) and Ag-rGO-NH₂-based composite was used as a sensing platform in this work. An AChE-based electrochemical biosensor was developed by Itsoponpan et al. [79] using CuInS₂ (CIS)-linked reduced graphene oxide (rGO) microsphere for chlorpyrifos detection. Jia et al. [80] proposed an AChE-based electrochemical biosensor using AuNPs-MoS₂-reduced graphene oxide and polyimide flexible film (rGO/PI).

1.9. Research gaps and Objective

The main aim of this thesis is focused on the study for applications of conducting polymer-based composites for pesticides, specifically organophosphate pesticide detection in real samples like soil, water, vegetables, fruits, etc. Based on the intensive study and literature survey, the following research gaps are being identified:

1.9.1. Research gaps

1. Selection of effective approach for OPs detection

The traditional methods available for pesticide detection so far provide relatively accurate results but these are very time-consuming, costly, difficult to handle, and need specialized equipment and chemicals. They also require the use of hazardous chemicals which can have negative environmental impacts. In these circumstances, the applicability and efficiency of traditional techniques are questionable. The enzyme inhibition-based electrochemical biosensors are very simple, robust, and highly selective making them more attractive alternatives to all detection methods. However,

they also have their inherent drawback. Their drawback is mainly related to their sensitivity which can be affected by the immobilization efficiency of AChE enzyme on the electrode surface and electron transfer rate. Therefore, further research is required to investigate more effective transducers to construct cholinesterase-based electrochemical biosensors which can improve the biosensor's analytical performance as high sensitivity, broad linear range, low detection limit, fast response, and high selectivity.

2. Selection of transducer

The sensitivity of enzyme-based biosensors highly depends on the efficient immobilization of enzymes and high electron transfer rate. Considering these two factors, the selection of a biocompatible and highly conducting transducer is required. So far, nanostructured metal oxides incorporated conducting polymer based sensing platform is not explored for OPs detection as they provide high surface area for effective immobilization of the desired biomolecule. These materials have demonstrates intriguing nano-morphological characteristics, functional biocompatibility, non-toxicity and catalytic properties, which can provide effective results in the AChE-based biosensors for OPs detection.

- 3.** Different fabricated biosensors require costly materials and electrodes which inspires researchers to develop the cost-effective sensing techniques for OPs detection.

1.9.2. Objective

The objective of the thesis is being achieved with the following steps:

1. To study and develop more efficient and robust biosensing techniques which are suitable for high sensitive OPs detection in real samples like soil, water, milk, vegetables, fruits, etc.
2. To enhance the efficiency and performance of biosensor for OPs detection, the

following steps are considered:

- Selection of novel, biocompatible materials, which enhance the electron kinetics and improve the performance of biosensor in terms of sensitivity and selectivity.
 - Fabrication of working electrode using different techniques to improve the biosensor's performance.
 - Optimization of experimental parameters using electrochemical techniques.
3. Electrochemical studies of pesticides using the modified bioelectrodes.
 4. Validation of fabricated biosensor for real samples taken from fruits, vegetables, soil, milk, water, etc.

1.10. Research Contribution

Keeping in view the above objective, the thesis presents the conducting polymer-based composites for pesticide detection application. The research contributions made in this thesis are listed as below:

1. An enzymatic electrochemical biosensor using acetylcholinesterase (AChE) was fabricated.
2. The conjugated polymers, including polyaniline (PANI) and poly(3,4-ethylene dioxy thiophene)-poly(styrene sulfonate) (PEDOT: PSS) along with their composites with metal oxides like copper oxide (CuO), Ag-doped-CuO (Ag@CuO) and CeO₂ are being used for making the efficient transducers. The reinforcement of metal oxide nanomaterials into the considered conducting polymers has acquired much interest due to the improvement of properties of end-use material for the following reasons:
 - The synergistic effect of conducting polymers and metal oxides tune the biosensor's performance which results to an enhanced sensitivity and selectivity.

- The integration of metal oxides into conducting polymer enhances the surface area and density of the resultant composite.
- Conducting polymers (PANI and PEDOT:PSS) show the strong bio-affinity toward the AChE enzyme, improving the efficiency of immobilization. Additionally, metal oxides (CuO and CeO₂) enhance the rate of hydrolysis of substrate (ATCI) which improve the electron kinetics.

For the fabrication of working electrodes, an electrophoretic deposition and dipping process are being used. To achieve the more robust performance of biosensors, the optimization of experimental parameters (concentration of AChE enzyme, pH of the electrolytic solution and incubation time) was also considered.

3. The fabricated biosensor was applied for paraoxon-ethyl detection.
4. To assess the practicality of the constructed biosensor in real-world situations, its usability was evaluated in various samples, including soil, fruit samples, vegetable samples, rice and pulse.

The process of research that has been used to carry out the present research work illustrated in Figure 1.6.

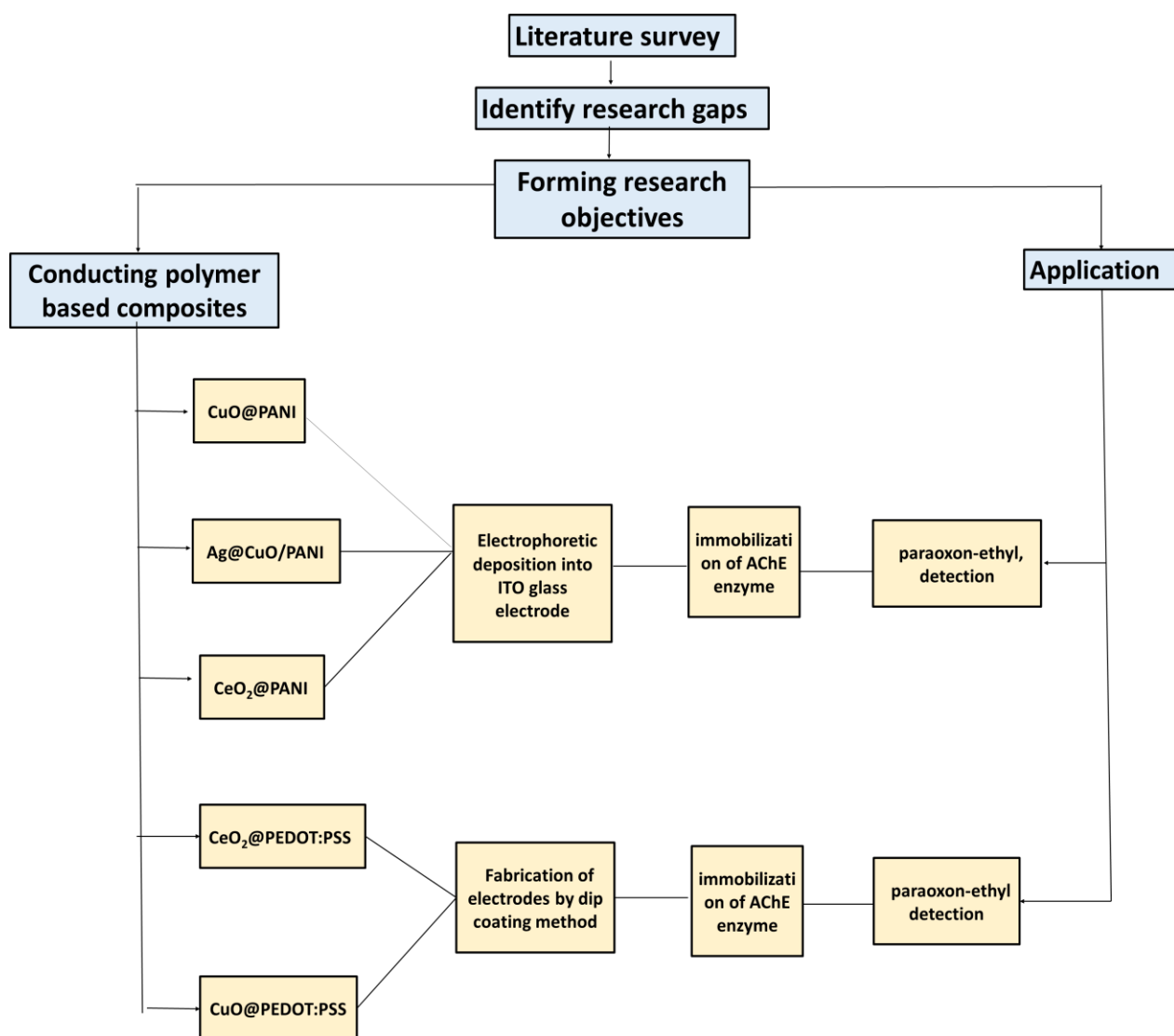


Fig. 1.6. Research methodology

1.11. Thesis Organization

The organization of present thesis is discussed as below:

Chapter 1

This chapter highlights a detailed description of pesticides, their benefits and harmful consequences on human health and environment. Further, an overview of various techniques (specifically AChE immobilized conducting polymer-based electrochemical biosensor) available for pesticide detection so far is described in this chapter.

Chapter 2

Chapter 2 deals with the details of experimental techniques such as UV-Visible spectroscopy (UV-Vis), Fourier transform infrared (FTIR) spectroscopy, X-ray diffraction (XRD), scanning electron microscopy (SEM), transmission electron spectroscopy (TEM), energy dispersive X-ray spectroscopy (EDAX), cyclic voltammetry (CV), differential pulse voltammetry (DPV) and chronoamperometry which have been used for structural, morphological and electrochemical characterization of all prepared composites and modified electrodes.

Chapter 3

This chapter reveals the data including the fabrication of an effective and novel platform using CuO-incorporated PANI-based composite for paraoxon-ethyl detection. The uniformly distributed CuO nanoparticles in PANI matrix also enhances the surface area, bio-affinity towards the AChE enzyme, and conductivity of the nanocomposite. The process of biosensor fabrication involves the electrophoretic deposition of nanocomposite onto the surface of indium-tin-oxide (ITO) coated substrate followed by an immobilization of AChE enzyme. This developed biosensor shows an excellent stability, reproducibility, and selectivity. Moreover, it

is capable of detecting paraoxon-ethyl inhibition within the range of 1 to 200 nM. Also, a low detection limit of 96 pM and the sensitivity of $49.86 \mu\text{A} (\text{nM})^{-1}$ are reported in this chapter. Additionally, this biosensor has been successfully employed to detect the paraoxon-ethyl in two real samples.

Chapter 4

This chapter reveals the fabrication of a novel and high sensitive biosensor for PE detection in real samples using Ag@CuO integrated PANI-based composite as a sensing platform. To fabricate Ag@CuO/PANI/ITO biosensor, the electrophoretic method was used to deposit the chemically synthesized nanocomposite onto the ITO electrode surface. Further, the AChE enzyme was immobilized onto the resulting electrode surface. The developed biosensor exhibits a wide linear range (5-100 pM), a low detection limit (11.35 pM) and good sensitivity of $0.59 \mu\text{A} (\text{pM})^{-1} \text{cm}^{-2}$. Additionally, it shows high selectivity, stability and reproducibility. Here, a synergistic effect of PANI and Ag@CuO gives the remarkable conductivity, biocompatibility, and catalytic activity of nanocomposite which is further responsible for an outstanding performance of biosensing platform.

Chapter 5

This chapter describes the results related to the fabrication of AChE/CeO₂@PANI/ITO biosensing platform which is utilized for paraoxon-ethyl detection. In this work, firstly the biosynthesized CeO₂ was incorporated onto the PANI matrix. Then, the prepared nanocomposite (CeO₂@PANI) was deposited onto the ITO surface using the electrophoretic technique. The AChE enzyme was further immobilized onto this electrode surface which results in the fabrication of the proposed biosensor. This biosensor is showing high stability, sensitivity ($0.64 \mu\text{A}(\text{pM})^{-1}(\text{cm})^{-2}$), a low detection limit (5.5 pM), selectivity, and reproducibility. The applicability of this developed biosensor was checked in two real samples.

An outstanding performance of the proposed biosensor is achieved by the excellent bio-affinity of PANI towards the AChE enzyme and catalyzing power of CeO₂ towards the phosphorylation of the AChE enzyme.

Chapter 6

This chapter deals with the fabrication of a novel, cost-effective and flexible biosensor for PE detection. In this study, firstly the Whatman paper was modified by CuO and PEDOT:PSS using the dip-coating method. The conductivity and stability of the paper electrode was improved by treating this CuO@PEDOT:PSS/WP electrode with ethylene glycol. Then, AChE enzyme was immobilized onto this resulting electrode surface. The biosensor exhibits a good reproducibility, stability, selectivity, high sensitivity (9.13 $\mu\text{A/nM}$), and a low detection limit (0.42 nM).

Chapter 7

In this chapter, the fabrication of a novel, cost-effective, and biodegradable AChE-based electrochemical biosensor was reported which is utilized for paraoxon-ethyl detection. In this study, CeO₂ and PESOT:PSS modified paper electrode was fabricated by a simple dip-coating method. The electrical conductivity and stability of the fabricated electrode were further improved with the treatment of ethylene glycol. All the electrochemical results infer that this biosensor shows a good selectivity ($K_{\text{selectivity}} < 1$), high sensitivity (52.10 $\mu\text{A/nM}$) and the low detection limit (0.12 nM). The accuracy and applicability of this biosensor were checked with two real samples. All these results validate that the fabricated biosensor could be a promising substitute to the conventionally available electrodes.

Chapter 8

In chapter 8, we have summarized all the key findings of this thesis work. The possible future research directions have also been highlighted here.

1.12. References

1. Poggi, S.R., *The International Code of Conduct on Pesticide Management*. Phys. Rev, 2014. p. 777-780.
2. Zamora-Sequeira, R., et al., *What are the main sensor methods for quantifying pesticides in agricultural activities? A review*. Molecules, 2019. **24**(14): p. 2659.
3. Kumar, S. and A. Singh, *Biopesticides: present status and the future prospects*. Fertil Pestic, 2015. **6**(2): p. 100-129.
4. Gill, S.S., E.A. Cowles, and P.V. Pietrantonio, *The mode of action of Bacillus thuringiensis endotoxins*. Annual Review of Entomology 1992. **37**(1): p. 615-634.
5. Hassaan, M.A. and A. El Nemr, *Pesticides pollution: Classifications, human health impact, extraction and treatment techniques*. The Egyptian Journal of Aquatic Research, 2020. **46**(3): p. 207-220.
6. Garcia, A., et al., *Antimicrobial activity of crude extracts of endophytic fungi isolated from medicinal plant Sapindus saponaria L.* Journal of Applied Pharmaceutical Science, 2012. **2**(10): p. 035-040.
7. Morais, S., F.G. Costa, and M.d.L. Pereira, *Heavy metals and human health*. Environmental Health–Emerging Issues Practice 2012. **10**(1): p. 227-245.
8. Jayaraj, R., P. Megha, and P. Sreedev, *Organochlorine pesticides, their toxic effects on living organisms and their fate in the environment*. Interdisciplinary Toxicology, 2016. **9**(3-4): p. 90-100.
9. Portney, P.R., *Public policies for environmental protection*. 2016: Routledge.
10. Kaushal, J., M. Khatri, and S.K. Arya, *A treatise on Organophosphate pesticide pollution: Current strategies and advancements in their environmental degradation and elimination*. Ecotoxicology Environmental Safety 2021. **207**: p. 111483.

11. Sidhu, G.K., et al., *Toxicity, monitoring and biodegradation of organophosphate pesticides: a review*. Critical Reviews in Environmental Science Technology 2019. **49**(13): p. 1135-1187.
12. Ghorab, M.A. and M.S. Khalil, *Toxicological effects of organophosphates pesticides*. International Journal of Environmental Monitoring Analysis 2015. **3**(4): p. 218-220.
13. Kaur, R., et al., *Pesticides classification and its impact on environment*. Int. J. Curr. Microbiol. Appl. Sci, 2019. **8**(3): p. 1889-1897.
14. Brühl, C.A., et al., *The rejection of synthetic pesticides in organic farming has multiple benefits*. Trends in Ecology, 2022. **37**(2): p. 113-114.
15. Thundiyil, J.G., et al., *Acute pesticide poisoning: a proposed classification tool*. Bulletin of the World Health Organization 2008. **86**: p. 205-209.
16. Dich, J., et al., *Pesticides and cancer*. Cancer Causes Control 1997. **8**: p. 420-443.
17. Neumeister, L., *Chemical alternatives to paraquat use in soybean*. WWF Germany, 2016. **10**.
18. Wei, M. and S. Feng, *Amperometric determination of organophosphate pesticides using a acetylcholinesterase based biosensor made from nitrogen-doped porous carbon deposited on a boron-doped diamond electrode*. Microchimica Acta, 2017. **184**: p. 3461-3468.
19. Ma, L., et al., *Nanocomposites of Pt nanoparticles anchored on UiO66-NH₂ as carriers to construct acetylcholinesterase biosensors for organophosphorus pesticide detection*. Electrochimica Acta, 2019. **318**: p. 525-533.
20. Songa, E.A. and J.O. Okonkwo, *Recent approaches to improving selectivity and sensitivity of enzyme-based biosensors for organophosphorus pesticides: A review*. Talanta, 2016. **155**: p. 289-304.

21. de Pinho, G.P., et al., *Pesticide determination in tomatoes by solid–liquid extraction with purification at low temperature and gas chromatography*. Food Chemistry, 2010. **121**(1): p. 251-256.
22. Shin, Y., et al., *Validation of a multiresidue analysis method for 379 pesticides in human serum using liquid chromatography–tandem mass spectrometry*. Journal of Agricultural Food Chemistry 2018. **66**(13): p. 3550-3560.
23. Pacioni, N.L. and A.V. Veglia, *Determination of carbaryl and carbofuran in fruits and tap water by β -cyclodextrin enhanced fluorimetric method*. Analytica Chimica Acta, 2003. **488**(2): p. 193-202.
24. Chawla, P., et al., *Organophosphorus pesticides residues in food and their colorimetric detection*. Environmental Nanotechnology, Monitoring, 2018. **10**: p. 292-307.
25. Xu, Z.-L., et al., *A simple, rapid and high-throughput fluorescence polarization immunoassay for simultaneous detection of organophosphorus pesticides in vegetable and environmental water samples*. Analytica Chimica Acta, 2011. **708**(1-2): p. 123-129.
26. Chen, Q. and Y. Fung, *Capillary electrophoresis with immobilized quantum dot fluorescence detection for rapid determination of organophosphorus pesticides in vegetables*. Electrophoresis, 2010. **31**(18): p. 3107-3114.
27. Harshit, D., K. Charmy, and P. Nrupesh, *Organophosphorus pesticides determination by novel HPLC and spectrophotometric method*. Food Chem., 2017. **230**: p. 448-453.
28. Juska, V.B. and M.E. Pemble, *A critical review of electrochemical glucose sensing: Evolution of biosensor platforms based on advanced nanosystems*. Sensors, 2020. **20**(21): p. 6013.
29. Munzar, J.D., A. Ng, and D. Juncker, *Duplexed aptamers: history, design, theory, and application to biosensing*. Chemical Society Reviews, 2019. **48**(5): p. 1390-1419.

30. Ahmad, R. and M.J.B. Sardar, *Enzyme immobilization: an overview on nanoparticles as immobilization matrix*. Biochemistry Analytical Biochemistry 2015. **4**(2): p. 1.
31. Kaur, N., H. Thakur, and N. Prabhakar, *Conducting polymer and multi-walled carbon nanotubes nanocomposites based amperometric biosensor for detection of organophosphate*. Journal of Electroanalytical Chemistry 2016. **775**: p. 121-128.
32. Itsoponpan, T., C. Thanachayanont, and P. Hasin, *Sponge-like CuInS₂ microspheres on reduced graphene oxide as an electrocatalyst to construct an immobilized acetylcholinesterase electrochemical biosensor for chlorpyrifos detection in vegetables*. Sensors & Actuators B: Chemical 2021. **337**: p. 129775.
33. He, L., et al., *Novel electrochemical biosensor based on core-shell nanostructured composite of hollow carbon spheres and polyaniline for sensitively detecting malathion*. Sensors & Actuators B: Chemical 2018. **258**: p. 813-821.
34. Campaña, A.L., et al., *Enzyme-based electrochemical biosensors for microfluidic platforms to detect pharmaceutical residues in wastewater*. Biosensors 2019. **9**(1): p. 41.
35. Wei, M. and J. Wang, *A novel acetylcholinesterase biosensor based on ionic liquids-AuNPs-porous carbon composite matrix for detection of organophosphate pesticides*. Sensors & Actuators B: Chemical 2015. **211**: p. 290-296.
36. Pundir, C.S. and N.J.A.B. Chauhan, *Acetylcholinesterase inhibition-based biosensors for pesticide determination: A review*. 2012. **429**(1): p. 19-31.
37. Kaur, N., et al., *Acetylcholinesterase immobilised eggshell membrane-based optical biosensor for organophosphate detection*. 2015. **95**(12): p. 1134-1147.

38. Bao, J., et al., *3D graphene/copper oxide nano-flowers based acetylcholinesterase biosensor for sensitive detection of organophosphate pesticides*. Sensors & Actuators B: Chemical 2019. **279**: p. 95-101.
39. Liu, Q., et al., *Effective amperometric biosensor for carbaryl detection based on covalent immobilization acetylcholinesterase on multiwall carbon nanotubes/graphene oxide nanoribbons nanostructure*. Journal of Electroanalytical Chemistry, 2015. **740**: p. 8-13.
40. Celik, H. and S. Soylemez, *An Electrochemical Acetylcholinesterase Biosensor Based on Fluorene (bisthiophene) Comprising Polymer for Paraoxon Detection*. Electroanalysis, 2022. **3** (35): p. 202200271
41. Yao, Y., et al., *The development of a novel biosensor based on gold nanocages/graphene oxide–chitosan modified acetylcholinesterase for organophosphorus pesticide detection*. New Journal of Chemistry, 2019. **43**(35): p. 13816-13826.
42. Thakkar, J.B., S. Gupta, and C.R. Prabha, *Acetylcholine esterase enzyme doped multiwalled carbon nanotubes for the detection of organophosphorus pesticide using cyclic voltammetry*. International Journal of Biological Macromolecules 2019. **137**: p. 895-903.
43. Zhao, Y., et al., *Porous hierarchical peony-like cobalt-based bimetallic oxides structured by ultrathin nanosheets for highly sensitive electrochemical pesticides detection*. Sensors & Actuators B: Chemical 2022. **352**: p. 131072.
44. Zhao, Y., et al., *Porous hollow cobalt-based oxides encapsulated with bimetallic PdAu Nanoparticles of electrochemical biosensor for highly sensitive pesticides detection*. Nanotechnology, 2022. **34** : p. 285501

45. Meng, L., A.P. Turner, and W.C. Mak, *Tunable 3D nanofibrous and bio-functionalised PEDOT network explored as a conducting polymer-based biosensor*. Biosensors and Bioelectronics 2020. **159**: p. 112181.
46. Kesik, M., et al., *An acetylcholinesterase biosensor based on a conducting polymer using multiwalled carbon nanotubes for amperometric detection of organophosphorous pesticides*. 2014. **205**: p. 39-49.
47. Partridge, A., M. Jansen, and W. Arnold, *Conducting polymer-based sensors*. Materials Science Engineering, 2000. **12**(1-2): p. 37-42.
48. Zhang, X., et al., *Development of electrorheological chip and conducting polymer-based sensor*. Frontiers of Mechanical Engineering, 2009. **4**(4): p. 393-396.
49. Chiam, Y.S., et al., *Conducting polymer coated optical microfiber sensor for alcohol detection*. Sensors & actuators A: Physical 2014. **205**: p. 58-62.
50. Ramdzan, N.S.M., et al., *Development of biopolymer and conducting polymer-based optical sensors for heavy metal ion detection*. Molecules, 2020. **25**(11): p. 2548.
51. Aydemir, N., J. Malmström, and J. Travas-Sejdic, *Conducting polymer based electrochemical biosensors*. Physical Chemistry Chemical Physics 2016. **18**(12): p. 8264-8277.
52. Chandrasekhar, P., *Conducting Polymers, Fundamentals and Applications*. 2018: Springer.
53. Zamani, F.G., et al., *Current trends in the development of conducting polymers-based biosensors*. Trends in Analytical Chemistry 2019. **118**: p. 264-276.
54. Greene, R.L., G.B. Street, and L. Suter, *Superconductivity in polysulfur nitride (SN)_x*. Physical Review Letters, 1975. **34**(10): p. 577.

55. Chiang, C.K., et al., *Electrical conductivity in doped polyacetylene*. Physical Review Letters, 1977. **39**(17): p. 1098.
56. Ivory, D., et al., *Highly conducting charge-transfer complexes of poly (p-phenylene)*. The Journal of Chemical Physics, 1979. **71**(3): p. 1506-1507.
57. Naseri, M., L. Fotouhi, and A. Ehsani, *Recent Progress in the development of conducting polymer-based nanocomposites for electrochemical biosensors applications: a mini-review*. The Chemical Record 2018. **18**(6): p. 599-618.
58. Kazemi, F., et al., *Biosensing applications of polyaniline (PANI)-based nanocomposites: a review*. Polymer Reviews, 2021. **61**(3): p. 553-597.
59. Li, M., et al., *Excellent electrochemical performance of homogeneous polypyrrole/graphene composites as electrode material for supercapacitors*. Journal of Materials Science: Materials in Electronics, 2015. **26**: p. 485-492.
60. Nafady, A., M.D. Albaqami, and A.M. Alotaibi, *CuO nanoparticles embedded in conductive PANI framework for periodic detection of alcohol from sweat*. Colloid Polymer Science 2023: p. 1-10.
61. Rashed, M.A., et al., *Surface modification of CuO nanoparticles with conducting polythiophene as a non-enzymatic amperometric sensor for sensitive and selective determination of hydrogen peroxide*. Surfaces Interfaces 2022. **31**: p. 101998.
62. Batool, R., et al., *Fabrication of polydopamine decorated carbon cloth as support material to anchor CeO₂ nanoparticles for electrochemical detection of ethanol*. Microchimica Acta, 2023. **190**(5): p. 172.
63. Kavitha, N., et al., *Polymer nanohybrid composites as conductive platform for the electrochemical sensing of pathogens*. Current Research in Green Sustainable Chemistry 2022: p. 100316.

64. Kumar, A., et al., *Ultrahigh sensitive graphene oxide/conducting polymer composite based biosensor for cholesterol and bilirubin detection*. Biosensors and Bioelectronics: 2023. **13**: p. 100290.
65. Mostafa, M.H., et al., *Recent Developments of Conductive Polymers/Carbon Nanotubes Nanocomposites for Sensor Applications*. Polymer-Plastics Technology, 2022. **61**(13): p. 1456-1480.
66. Ivanov, A., et al., *New polyaniline-based potentiometric biosensor for pesticides detection*. IEEE Sensors Journal, 2003. **3**(3): p. 333-340.
67. Somerset, V.S., et al., *Acetylcholinesterase-polyaniline biosensor investigation of organophosphate pesticides in selected organic solvents*. Journal of Environmental Science Health, Part B 2007. **42**(3): p. 297-304.
68. Gong, J., L. Wang, and L. Zhang, *Electrochemical biosensing of methyl parathion pesticide based on acetylcholinesterase immobilized onto Au-polypyrrole interlaced network-like nanocomposite*. Biosensors and Bioelectronics 2009. **24**(7): p. 2285-2288.
69. Viswanathan, S., H. Radecka, and J. Radecki, *Electrochemical biosensor for pesticides based on acetylcholinesterase immobilized on polyaniline deposited on vertically assembled carbon nanotubes wrapped with ssDNA*. Biosensors and Bioelectronics 2009. **24**(9): p. 2772-2777.
70. Marinov, I., et al., *Amperometric acetylthiocholine sensor based on acetylcholinesterase immobilized on nanostructured polymer membrane containing gold nanoparticles*. Journal of Molecular Catalysis B: Enzymatic 2010. **62**(1): p. 66-74.

71. Jha, N. and S. Ramaprabhu, *Carbon nanotube-polymer based nanocomposite as electrode material for the detection of paraoxon*. Journal of Nanoscience Nanotechnology 2010. **10**(4): p. 2798-2802.
72. Ivanov, Y., et al., *Amperometric biosensor based on a site-specific immobilization of acetylcholinesterase via affinity bonds on a nanostructured polymer membrane with integrated multiwall carbon nanotubes*. Journal of Molecular Catalysis B: Enzymatic 2010. **63**(3-4): p. 141-148.
73. Du, D., et al., *Acetylcholinesterase biosensor design based on carbon nanotube-encapsulated polypyrrole and polyaniline copolymer for amperometric detection of organophosphates*. Biosensors and Bioelectronics 2010. **25**(11): p. 2503-2508.
74. Chauhan, N., J. Narang, and C. Pundir, *Immobilization of rat brain acetylcholinesterase on ZnS and poly (indole-5-carboxylic acid) modified Au electrode for detection of organophosphorus insecticides*. Biosensors and Bioelectronics 2011. **29**(1): p. 82-88.
75. Kanik, F.E., et al., *An amperometric acetylcholine biosensor based on a conducting polymer*. International Journal of Biological Macromolecules, 2013. **59**: p. 111-118.
76. Yang, Y., et al., *Acetylcholinesterase biosensor based on a gold nanoparticle–polypyrrole–reduced graphene oxide nanocomposite modified electrode for the amperometric detection of organophosphorus pesticides*. Analyst, 2014. **139**(12): p. 3055-3060.
77. Li, Y., et al., *An acetylcholinesterase biosensor based on graphene/polyaniline composite film for detection of pesticides*. 2016. **34**(1): p. 82-88.
78. Zhang, P., et al., *A sensitive amperometric AChE-biosensor for organophosphate pesticides detection based on conjugated polymer and Ag-rGO-NH₂ nanocomposite*. Bioelectrochemistry 2019. **127**: p. 163-170.

79. Itsoponpan, T., C. Thanachayanont, and P. Hasin, *Sponge-like CuInS₂ microspheres on reduced graphene oxide as an electrocatalyst to construct an immobilized acetylcholinesterase electrochemical biosensor for chlorpyrifos detection in vegetables*. *Sensors & Actuators B: Chemical* 2021. **337**: p. 129775.
80. Jia, L., et al., *Acetylcholinesterase modified AuNPs-MoS₂-rGO/PI flexible film biosensor: Towards efficient fabrication and application in paraoxon detection*. *Bioelectrochemistry*, 2020. **131**: p. 107392.

CHAPTER 2

Materials and Experimental Methods

2.1. Introduction

A description of all materials and different characterization techniques used during the fabrication of AChE-based electrochemical biosensing platforms having conducting polymer and their composites for OPs detection is given in this chapter. The parameters, procedures and protocols related to the performance-developed biosensors are also discussed in this chapter. All the structural, morphological and electrochemical characterization techniques used for the synthesized materials and fabricated electrodes are given in section 2.3. The methods used for AChE immobilization onto the electrode surface are discussed in section 2.4. Finally, the protocols/procedures used for an estimation of different parameters related to the performance of all newly developed biosensors are summarized in section 2.5.

2.2. Materials

The detailed description of all materials are as follows:

2.2.1. Chemicals

Copper sulphate pentahydrate ($\text{CuSO}_4 \cdot 5\text{H}_2\text{O}$) ~ 98.5%, poly(3,4-ethylene dioxy thiophene)-poly(styrene sulfonate) (PEDOT: PSS), silver nitrate (AgNO_3) ~ 99%, cerium nitrate hexa hydrate ($\text{Ce}(\text{NO}_3)_3 \cdot 6\text{H}_2\text{O}$) ~ 99%, ammonium per sulphate (APS) ~ 97%, acetylcholinesterase (C3389-2KU) (AChE), paraoxon-ethyl (PE), acetyl thio choline chloride (ATCl), ethylene glycol (EG), glycerol, N,N-dimethyl acetamide (NMA), 1-methyl-2-pyrrolidone (NMP), hydrochloric acid (HCl) ~ 36.46% and hydrogen peroxide (H_2O_2) ~ 30%

have been purchased from Sigma-Aldrich, India. Aniline ~ 99% is purchased from Rankem. Sodium hydroxide (NaOH) ~ 97% and sodium lauryl sulfate (SDS) ~ 85% are being purchased from Fisher-Scientific, India. Indium-tin-oxide (ITO) is purchased from Technistro. Whatman paper grade 1 having thickness (0.18 mm) is purchased from GE healthcare, UK. All the real samples used in the present work are being procured from local market. Freshly prepared solutions in DI water (Milli-Q, 18.2 M Ω cm) have been used for the experimental analysis.

2.2.2. Solutions and Buffers

- 0.2 mM phosphate buffer saline (PBS) of pH 7.4, 6.5 and 7
- Tris buffer (7.5 pH) 0.2 mM
- PBS (6, 6.5, 7, 7.5, 8 pH) containing 5 mM [Fe(CN)₆]^{3-/4-}

2.3. Characterization Methods

The synthesis of conducting polymers such as PANI, PEDOT: PSS and their composites with metal oxide nanomaterials (CuO, Ag@CuO and CeO₂) followed by fabrication of their electrodes using both indium tin-oxide coated glass substrate and Whatman paper electrode is described in this chapter. An immobilization of AChE enzyme onto the fabricated electrode surface was also done to explore the applications of modified electrodes for OPs detection. The synthesized materials and all modified electrodes have been characterized for structural analysis by using different instruments like X-ray diffraction, Fourier transform infrared (FTIR) spectroscopy, UV-Visible spectroscopy. The morphological and elemental characterization techniques like scanning electron microscopy (SEM), transmission electron microscopy (TEM), and energy dispersive X-ray spectroscopy were used in the present work. Electrochemical characterization techniques, namely, cyclic voltammetry (CV), differential pulse voltammetry (DPV) and chronoamperometry were also used for the characterization.

2.3.1. X-ray Diffraction Study

A characterization technique, i.e., X-ray diffraction is being used for a primary study of any unknown material in respect of crystalline nature. For macromolecules, this technique determines the atomic structure within the sample while for very small sized material, it determines the crystallinity, strain, size of crystal (grain size), crystal structure and sample composition. The crystallographic structure, orientation of polycrystalline sample and crystallite size are also determined by this technique. The working of this technique is based on the Bragg's law which explains how a beam of X-ray incident on a crystal lattice of a sample is reflected at certain angles providing the informations related to the structure and sample composition. X-ray diffractometer is used to record the XRD patterns. A pictorial view of X-ray diffractometer is represented in Figure 2.1.

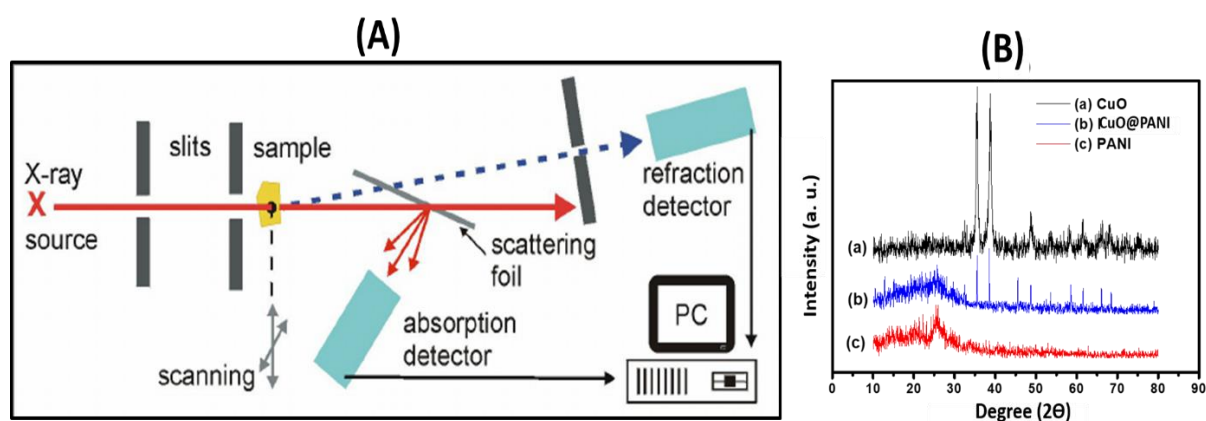


Fig. 2.1. (A) A pictorial view of XRD, (B) X-ray diffraction patterns of CuO, CuO@PANI and PANI

The average peak broadening is measured by using five most substantial diffraction peaks to obtain the peak broadening data. This data can then be used to analyze the material's structural properties. The Debye-Scherrer equation uses peak broadening in the X-ray diffraction pattern to determine any material's size. In this thesis, the average particle size of all synthesized materials is calculated using Debye-Scherrer equation (Eq. 2.1)

$$D = K\lambda / \beta \cos\Theta \quad \text{..... (2.1)}$$

In this equation, K represents the shape factor (0.9), λ represents the X-ray wave length, Θ is the Bragg's angle in degree and β represents the line broadening at full width half maxima [1, 2].

In this thesis, the structural characterization using X-ray diffraction of all prepared materials (conducting polymer-based composites and nanomaterials) have been carried out by X-ray diffractometer (Bruker D-8 Advance) having 1.5406 Å monochromatic radiation, diffraction angle ($2\Theta = 10-80^\circ$) and speed of $2^\circ/\text{min}$.

2.3.2. Fourier transform infrared (FTIR) spectroscopy

An interaction of electromagnetic radiation with material has been studied by using IR spectroscopy. Fourier transform infrared spectrometer (FTIR) is based on infrared spectroscopy. It is highly used for structural characterization due to its high accuracy, fast analysis, simple process for handling and enhanced sensitivity. This technique is non-destructive and can be employed to study samples of any nature. The fundamental principle of FTIR is based on molecule's atomic vibration, which absorb specific energies and frequencies of infrared radiation. The material or chemical substance produces various spectral lines after absorbing the electromagnetic radiations from light beam at each wavelength which further determines the chemical composition of any material or chemical substance [3].

In FTIR spectroscopy, the Michelson interferometer (Figure 2.2) has been used to study the chemical composition of any material. Its basic setup involves four components (a) source of light (filament) (b) beam splitter (c) two mirrors as arranged in Figure 2.2 (d) detector. The source emits the infrared radiation which is divided into two parts by a beam splitter. These two separate beams of light further moves along two different paths and reflecting by mirrors at the end of each path. After reflection, these separate beams recombine and create an

interference, further the interference pattern is analysed by the detector. FTIR is a powerful characterization technique which provides numerous advantages over the dispersive measurements including: wider spectral range, higher sensitivity, faster data acquisition, less sample requirement, higher spectral resolution, better signal to noise ratio, etc [4].

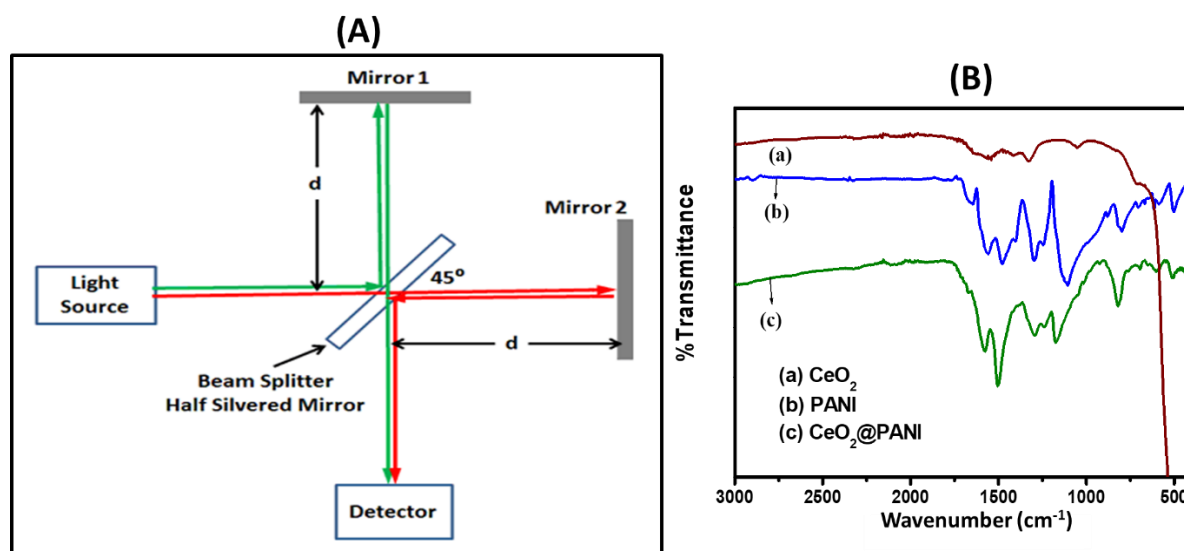


Fig. 2.2. (A) Schematic diagram of Michelson interferometer, (B) FTIR spectra of CeO₂, PANI and CeO₂@PANI

In the present thesis work, the functional groups present in all synthesized materials (conducting polymer and their composite with CuO and CeO₂) and fabricated conducting paper electrodes are investigated by attenuated total reflection (ATR) mode using FTIR Perkin Elmer Spectrum 2 at the frequency range of 400-4000 cm⁻¹.

2.3.3. Ultraviolet-Visible (UV-Vis) Spectroscopy

UV-Visible spectroscopy is a powerful analytical tool using the light in the ultraviolet and visible regions. It is very useful technique to study the electronic transitions of the ions, atoms and molecules. Once a molecule absorbs a light from UV-Vis range, it can cause a transition of electron, i.e., one energy level to the higher energy level. This transition results in the absorption of specific wavelengths of light. By measuring this specific wavelength, the

energies of these electronic transition can be determined which further provide the structure and properties of the molecules. This spectroscopic technique is widely used in various fields including chemistry, biochemistry and material science. Thus, it is a valuable tool generally used to characterize the optical properties of the materials such as polymers and nanoparticles [5]. In this thesis, UV-Vis spectroscopy is used for the characterization of PANI and CuO@PANI nanocomposite. UV-Vis analysis of PANI and CuO@PANI is described in chapter-3. The optical study was done by using UV-Vis spectrophotometer (Model 160A, Shimadzu) as depicted in Fig. 2.3.

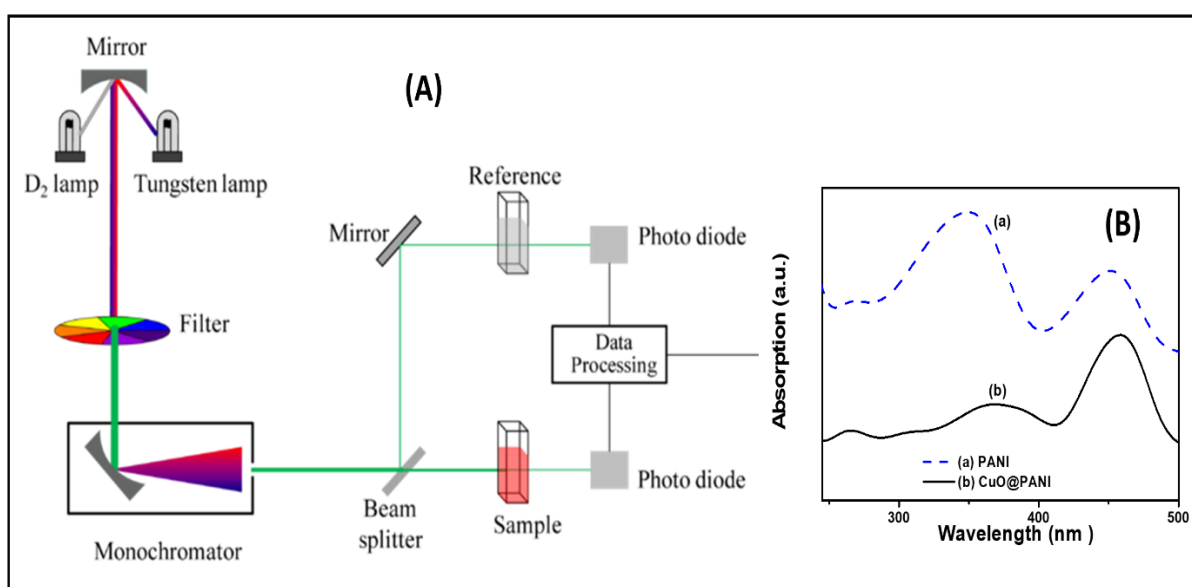


Fig. 2.3. (A) A pictorial diagram of UV-Vis spectrophotometer and (B) UV-Vis spectra of PANI and CuO@PANI

2.3.4. Scanning Electron Microscopy (SEM)

SEM is designed for analyzing the surface morphology of the sample. The SEM utilizes electrons rather than light to observe the image of a sample. SEM is advantageous with respect to other microscopes as SEM offers a comparatively larger depth of field in order to access

more specimens at one time. Also, specimens are focused to give a higher degree of magnification suggesting a higher resolution of SEM. The source of electrons, a column through which the electron beam travels via electromagnetic lenses, an electron detector, a specimen chamber and a computer along with a display unit to see the images are the main components of SEM. The SEM generates the signals at the solid object's surface by using a focused high-energy electrons beam [6, 7] as shown in the **Fig. 2.4**.

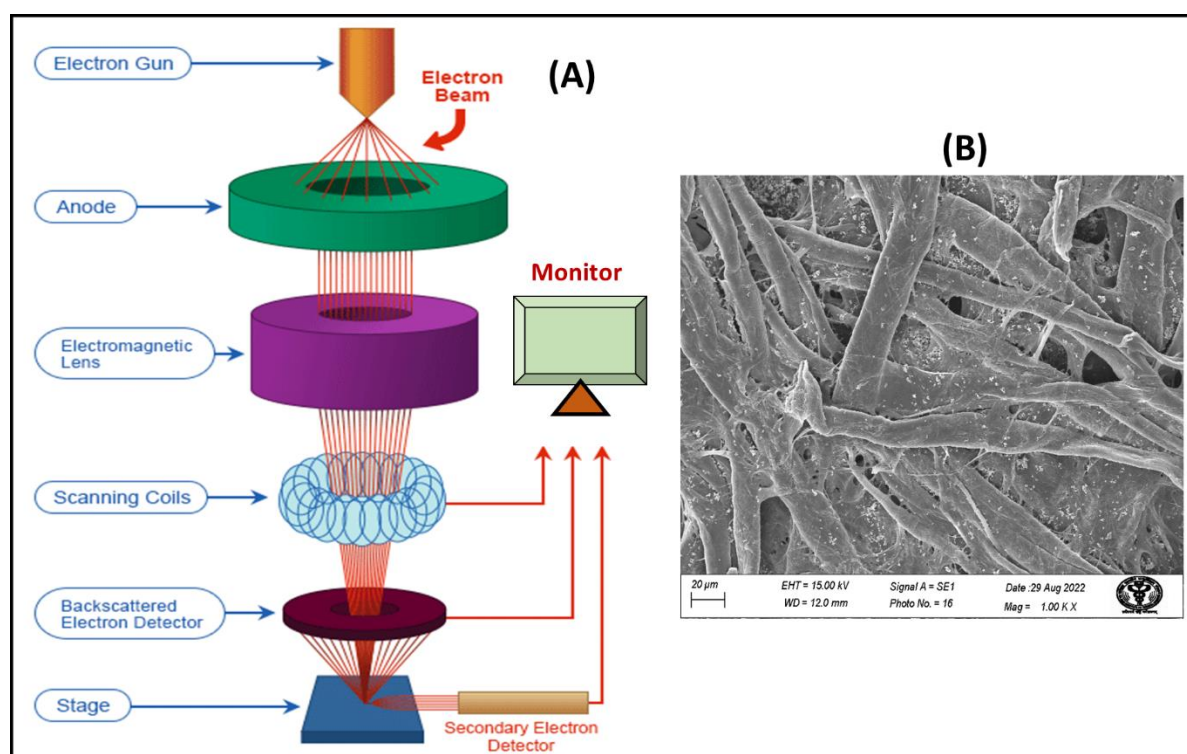


Fig. 2.4. (A) A pictorial view of scanning electron microscope and (B) SEM micrograph of the CuO@PEDOT:PSS/WP electrode

The high-energy electrons are generated at the uppermost part of the column and accelerate in a downward direction crossing through multiple lenses to result in a focused beam of electrons striking the specimen surface. In addition, SEM makes the use of vacuum conditions in the specimen chamber by the use of a combination of pumps to result in the micrographs of specimen. The interaction between the specimen and electrons produces the signals which have been identified by the detector. In this work, SEM (EVO-18, ZEISS) was

used to examine the morphology of synthesized materials as well as the fabricated electrode surface.

2.3.5. Transmission Electron Microscopy (TEM)

TEM is used to study an image of the smallest structure in a matter. Under this microscope, high-energy electrons are used to provide the morphological, compositional and crystallographic informations on the samples. TEM has the ability to visualize the detailing of the nanometer range of the specimen and also to magnify it up to the million times. Compared to other microscopes, TEM uses an electron beam of very short wavelength with respect to the wavelength of visible light which leads to an increase in the resolution of this microscope. This is the reason for the immense significance of TEM in the biological and medical fields.

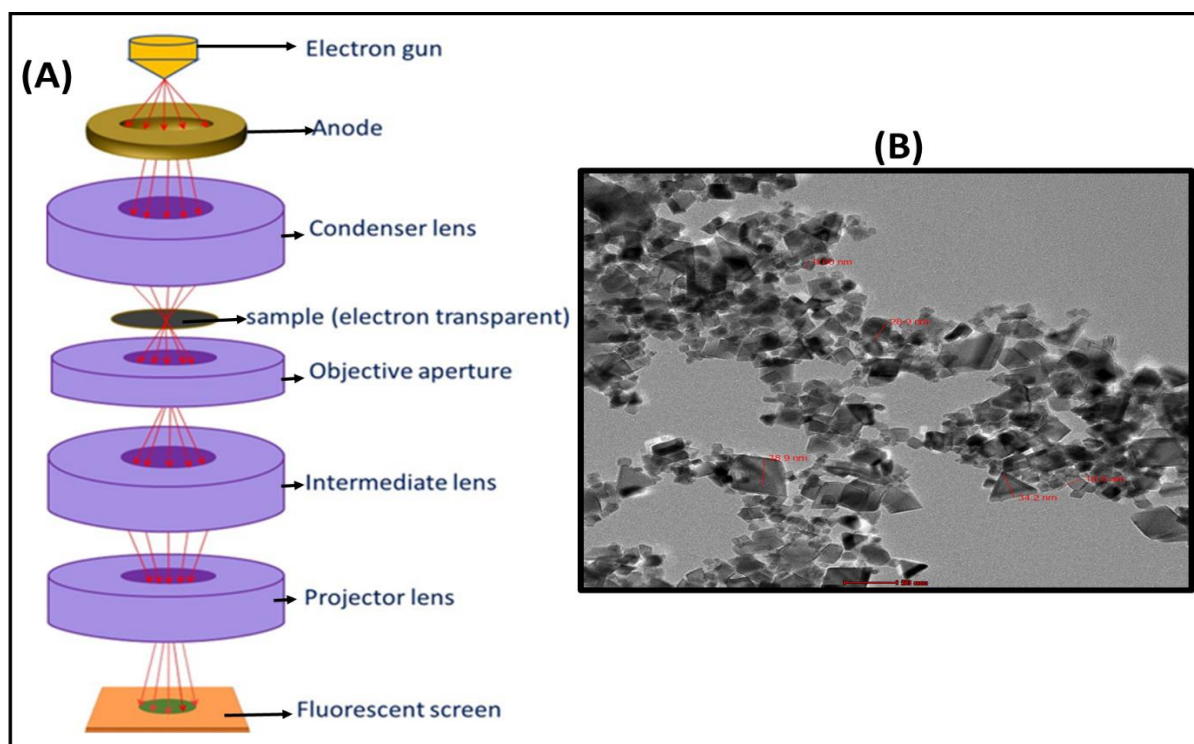


Fig.2.5. (A) Schematic representation of Transmission electron microscope, (B) TEM image of CeO₂ nanocrystals

The image visualization in TEM follows a slightly similar pathway to that of SEM. A

high-energy electron beam generated by an electron gun passes through the vacuum tube of microscope. The electromagnetic lens placed in between focuses the electrons traveling through the tube in a fine beam which then strikes at the thin specimen. This led to either scattering electrons or hitting the electrons on a fluorescent screen placed at the bottom of the microscope. Thereafter, the image of the specimen is reflected on the display unit. The image basically comprises shades of assorted parts of the specimen's depending upon the density of specimen which appears on the screen [8, 9]. In this thesis, TEM (TALOS) was used for the morphological characterization of prepared materials such as CuO (chapter 3, 4), CeO₂ (chapter 5, 7) and CeO₂@PANI (chapter 5).

2.3.6. Energy Dispersive X-ray Spectroscopy (EDAX)

This technique is very useful to analyse a sample pertaining to the near-surface elements and determines an elemental proportion at different positions. The basic principle of EDAX is used in conjunction with the SEM. Here, an electron beam of 10–20 keV energy strikes on the sample's surface which emits X-rays. This emitted X-rays energy depends on the sample material taken for investigation.

During EDAX analysis, the electron beam transports across the sample to generate the image of the elements present in the sample. In the EDAX, the composition and the quantity of the heavy metal ions of the nanoparticles can be measured easily but it is hard to be detect the elements with atomic numbers below 11. The composition of nanoparticles near or at the surface of the sample may be analysed by using the EDAX when these contain the heavy metal ions like gold, silver and palladium. In this thesis, elemental characterization of all prepared materials such as CuO, Ag@CuO, Ag@CuO/PANI, CeO₂, CeO₂@PANI (chapter 4, 5, 6, 7) and fabricated electrodes like PEDOT:PSS/WP, CeO₂@PEDOT:PSS/WP (chapter 7) are done by SEM-EDAX.

2.3.7. Electrochemical Techniques

Electrochemical techniques are a set of analytical methods that involve the use of electrochemical principles to study and analyze chemical reactions, measure concentrations and investigate the properties of substances. These techniques rely on the interaction between electricity and chemical species at the electrode-electrolyte interface. The fundamental components of electrochemical techniques include electrodes, an electrolytic solution and an external circuit. The electrolytic solution contains ions that facilitate the electrochemical reactions. Three electrodes, namely, reference electrode, working electrode and counter electrode have been used in a cell assembly. These three electrodes are well connected to the instrument, i.e., potentiostat that measures the current by controlling the potential of working electrode. This resulting current is plotted against the time. In this thesis, the electrochemical performance of all the fabricated sensors is studied by using an Autolab (EcoChemie, Netherlands) Potentiostat/Galvanostat, with respect to Ag/AgCl, a reference electrode and a counter electrode as platinum (Pt).

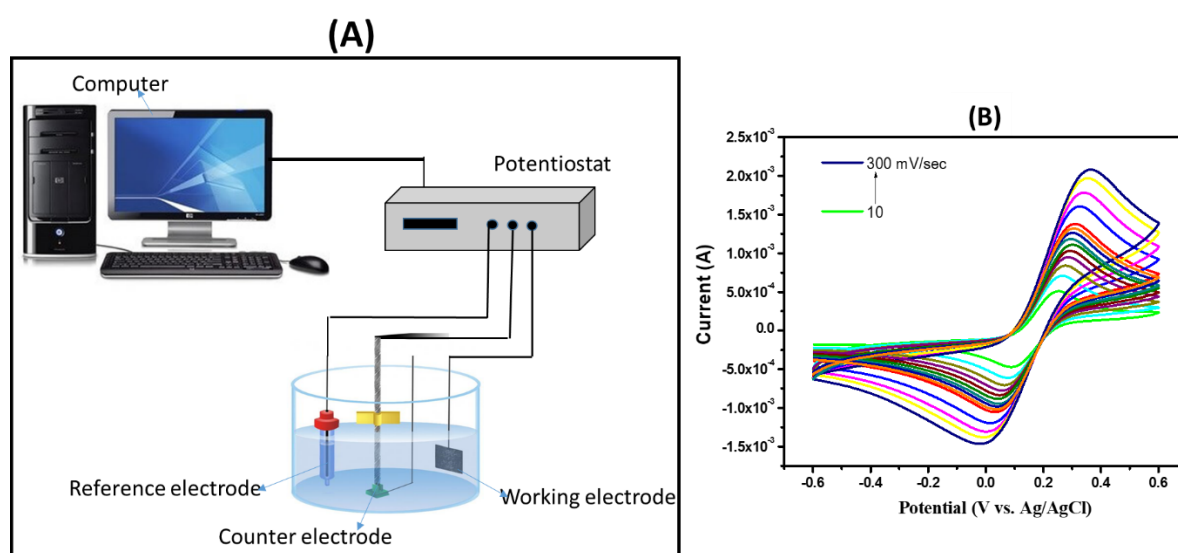


Fig. 2.6. (A) Schematic diagram of Potentiostat, (B) CV curves of Ag@CuO/PANI/ITO electrode with different scan rates (10 - 300 mV/sec)

2.3.7.1. Cyclic Voltammetry (CV)

Cyclic voltammetry is most useful electro-analytical technique for describing the electrochemical nature of organisms that are electro-chemically active. In a cyclic voltammetry study, a working electrode potential is sweeping in the opposite direction across time and brought back to its initial point after reaching the fixed point. For the purpose of creating a cyclic voltammetry graph, these potential cycles can be swept as needed. Cyclic voltammetry is used to obtain information about the electrochemical reactions involving electroactive entities having a known redox potential. Further, this counter electrode transports a current from the signal source to a working electrode. This current is checked at the working electrode during the potential scans against a fixed reference electrode potential. An electrolytic solution is used to furnish the ions to electrodes during the reduction oxidation process [10].

2.3.7.2. Differential Pulse Voltammetry (DPV)

When compared to CV, the DPV offers better detection limits and enables the resolution of electrode processes that are located closer together. Here, the electrode is subjected to the voltage versus time programme using a ramp that increases linearly. After a sequence of pulses with modest amplitudes are overlaid on a ramped voltage, the current is reported between the pulse voltage and ramped baseline voltage. The current has been measured right before the application of pulse (first point) and at the conclusion of the pulse (second point) for each and every pulse. Additionally, the sites were chosen to allow the non-faradic (charging) current to fade. Each pulse's variation in current measurements at these locations is noted for the base potential. An improved DPV detection limit over the cyclic voltammetry and other voltammetric techniques is found due to the better discrimination power against the charging current as well as impurity Faradic currents [11].

2.3.7.3. Chronoamperometry

Chronoamperometry is an electrochemical tool used to study the behaviour of an electrochemical system by recording the current response as a function of time. It is particularly useful for investigating the processes that involve electron transfer reactions, such as electrode reactions, enzymatic reactions and chemical reactions that involve redox species. Here, we apply a constant potential to the working electrode and measure the resulting current over time. This technique allows for the measurement of low currents with high sensitivity. This is particularly beneficial for paper electrodes which typically have limited conductivity and can generate lower currents compared to other electrode materials. The high sensitivity of chronoamperometry enables the detection of low analyte concentrations and enhances the overall performance of paper-based biosensors [12].

2.4. Methods to Immobilize Enzyme onto Conducting Polymer-based Matrix

The immobilization leads to improved stability and reusability of the biorecognition element. This is very important to choose an appropriate method that prevents denaturation and does not affect the chemical behaviour or reactive entities present in the antibody's binding site. Various protocols can be employed to immobilize the chosen enzyme molecule onto the conducting polymer-based matrix. These methods are as follows:

2.4.1. Covalent Immobilization

Covalent immobilization is a widely studied technique for immobilizing biomolecules and it involves the formation of covalent bonds between the support matrix and biomolecule. Such a method is typically used when the matrix possesses nucleophilic functional groups like $-NH_2$, $-SH$, $-OH$ which can form covalent bonds or be activated to create such groups for binding with the biomolecule. Covalent immobilization ensures a strong binding force between the enzyme and the matrix, preventing any leakage of enzymes. This method provides stability

and robustness to the immobilized biomolecule, making it suitable for various applications. In the present thesis, the -NH_2 groups available in polyaniline backbone covalently combine with the -COOH groups present in the AChE enzyme (Chapter 3, 4 and 5) molecule and prevent the enzyme leaching from the fabricated electrode.

2.4.2. Physical Adsorption

Physical adsorption is a common method used for immobilizing the biomolecules, such as enzymes or proteins, onto a solid support. It involves the non-covalent binding of the biomolecules to the surface of support material through the secondary forces. In this thesis, the negatively charged sulfonic acid groups and the hydroxyl groups on the PEDOT:PSS surface interact with the positively charged amino acid residues of AChE enzyme, creating a stable interface and preventing enzyme denaturation (Chapter 6 and 7).

2.5. Protocols used for the determination of different Parameters pertaining to the Performance of Conducting Polymer-based Biosensors for Pesticide Detection

2.5.1. Diffusion Coefficient and Effective Surface Area

The diffusion coefficient for a redox species and effective surface area of fabricated electrode are calculated by using following equation:

$$I_p = 2.69 \times 10^5 (n^{3/2} A C D^{1/2} \nu^{1/2}) \quad \text{.....(2.2)}$$

This equation is called as **Randles-Sevcik** equation. Here, ν is scan rate in V/sec, D is the diffusion coefficient, C is conc of redox species in mol/cm^3 , n is number of transferred electrons and A is the area of electrode.

2.5.2. Sensitivity, linear range and detection limit

A linear range of a biosensor speaks about the concentration range where the biosensor response is directly proportional to the analyte concentration. Within this range, biosensors can

provide accurate and reliable measurements. The sensitivity of all proposed biosensors is estimated using the slope of the linearity curve. The LOD for all proposed biosensors is determined by the following equation:

$$\text{LOD} = 3\sigma/S \quad \text{.....(2.3)}$$

Here, S is a sensitivity and σ is a standard deviation.

2.5.3. Stability and Reproducibility parameters of the fabricated electrodes

The stability of fabricated biosensors is depending on the parameters like shelf-life and reproducibility. The storage stability is defined as the period of time during which the sensor can maintain its effectiveness or retain the highest level of activity. The term reproducibility quantifies the variation observed in a series of measurements or outcomes conducted over a specific time frame. For all the proposed biosensors, shelf-life is checked by monitoring a current response of fabricated electrodes at a regular time interval. However, a reproducibility is checked by monitoring the current response of different bioelectrodes at constant analyte concentration.

2.6. References

1. Epp, J., *X-ray diffraction (XRD) techniques for materials characterization*, in *Materials characterization using nondestructive evaluation (NDE) methods*. 2016, Elsevier. **242** p. 81-124.
2. Rajender, G. and P.J.J.o.A. Giri, *Strain induced phase formation, microstructural evolution and bandgap narrowing in strained TiO₂ nanocrystals grown by ball milling*. 2016, Journal of Alloys Compounds. **676**: p. 591-600.
3. Segneanu, A.E., et al., *Organic compounds FT-IR spectroscopy*. 2012, Rijeka, Croatia: InTech. Vol. **145**, p.288-448.
4. Bell, R., *Introductory Fourier transform spectroscopy*. 2012, Elsevier. **41**(1), p.149-151.
5. Raghavan, R. and J.C. Joseph, *Spectroscopic Methods of Analysis: Ultraviolet and Visible Spectrophotometry*, in *Encyclopedia of Pharmaceutical Science and Technology, Six Volume Set (Print)*. 2013, CRC Press. p. 3317-3330.
6. Zhou, W., et al., *Fundamentals of scanning electron microscopy (SEM)*. Scanning Microscopy for Nanotechnology: Techniques Applications 2007: **12**(1) p. 1-40.
7. Goldstein, J.I., et al., *Scanning electron microscopy and X-ray microanalysis*. 2017: Springer. p. 93-542.
8. Shah, M. *Electron Microscopy: A versatile tool in nanoworld*. in *Materials Science Forum*. 2013. Trans Tech Publ.
9. Shi, B., *Transmission electron microscope*. Young Scientists Journal, 2016(18): p. 33.
10. Elgrishi, N., et al., *A practical beginner's guide to cyclic voltammetry*. Journal of Chemical Education, 2018. **95**(2): p. 197-206.

11. Aikens, D., *Electrochemical methods, fundamentals and applications*. 1983, ACS Publications.
12. West, B.J., et al., *Chronoamperometric study of conformational relaxation in PPy (DBS)*. The Journal of Physical Chemistry B, 2009. **113**(5): p. 1277-1293.

CHAPTER 3

Nanostructured CuO-embedded Polyaniline-modified Electrochemical Biosensor for Paraoxon-Ethyl Detection

3.1. Introduction

This chapter describes a novel approach for developing a highly sensitive biosensor for paraoxon-ethyl detection using a sensing platform made up of copper oxide (CuO) reinforced polyaniline (PANI) composite. The CuO incorporation into PANI drastically improves the surface area, catalytic power and density of nanocomposite which further enhancing the biosensor's sensitivity. The biosensor shows high sensitivity ($49.86 \mu\text{A}(\text{nM})^{-1}$), low detection limit (0.096 nM) and high selectivity. It was successfully applied for paraoxon-ethyl detection in two real samples. The details of the material's synthesis, electrophoretic deposition and biosensor fabrication are discussed in the next section 3.2. The structural, morphological and electrochemical characterization of all prepared materials, optimization studies, electrochemical biosensing studies and real sample analysis are given in section 3.3.

3.2. Experimental Section

3.2.1. Synthesis of CuO Nanoparticles

Co-precipitation method was utilized to prepare of CuO nanoparticles. In this method, firstly, 1.5 g of $\text{CuSO}_4 \cdot 5\text{H}_2\text{O}$ dissolved in water (50 mL DI) with constant stirring, for a duration of 30 min. Further, of sodium lauryl sulfate (SDS) (0.12 g) was added at a temperature of 90°C with continuous stirring and then NaOH (0.4 M) was added until the pH becomes 14. The obtained solution was further stirred for 6 h. Finally, a black-coloured precipitate was obtained. This precipitate has been centrifuged and then washed with DI water followed by ethanol,

respectively. It was dried overnight at 50°C and calcined (heated in the absence of air) at 800°C for 4 h.

3.2.2. Synthesis of CuO@PANI-based Composite

To prepare CuO@PANI nanocomposite, the 0.114 g of CuO nanoparticles was mixed in water (20 mL DI) and then ultra-sonicated which results to the Solution I. Further, in a separate step, the distilled aniline (0.36 mL) was dispersed in 50 mL of 1M hydrochloric acid by stirring for 10 min at room temperature resulting in the formation of Solution II. Both these Solution I and Solution II were then mixed, stirred for 1 h followed by a dropwise addition of 1M ammonium persulfate solution. The resultant solution has been stirred further for 4 h. Finally, this solution has been centrifuged and then washed using DI water and ethanol, respectively. The composite so obtained was dried at 80°C (Fig. 3.1, scheme A).

3.2.3 Electrophoretic Deposition of CuO@PANI-based Composite and Fabrication of Biosensor

To perform the electrophoretic deposition of the PANI and CuO@PANI nanocomposite, an indium-tin-oxide (ITO) coated glass substrate was employed as a working electrode, while platinum wire served as the counter electrode. For deposition process, firstly, the suspension of PANI and CuO@PANI was prepared by dispersing 10 g of both these materials into the water and ethanol mixture (5:1). Subsequently, for the deposition of PANI and CuO@PANI onto the ITO surface, 12 V of DC voltage has been applied for a duration of 13 and 14 sec, respectively. These deposited electrodes were further washed with water (DI) and then these were dried at room temperature which is depicted in Fig. 3.1, scheme A.

AChE/CuO@PANI/ITO biosensor was developed by immobilizing the enzyme AChE onto the CuO@PANI modified ITO electrode surface. For immobilization process, 20 µL of stock solution of AChE enzyme (0.1 mL in 1 mL PBS) was drop-casted over the developed electrode surface. After the fabrication of biosensor, it was stored in a refrigerator at 4°C

overnight to allow for optimal immobilization. Prior to conducting any electrochemical study, the above mentioned sensor electrode is being rinsed with 100 μL of PBS in order to remove any unbounded enzyme. Additionally, the enzyme concentration was used as per the previous studies [1], [2]. The schematic diagram for biosensor fabrication and working mechanism for PE detection are represented in the Fig. 3.1(A) and Fig. 3.1 (B), respectively.

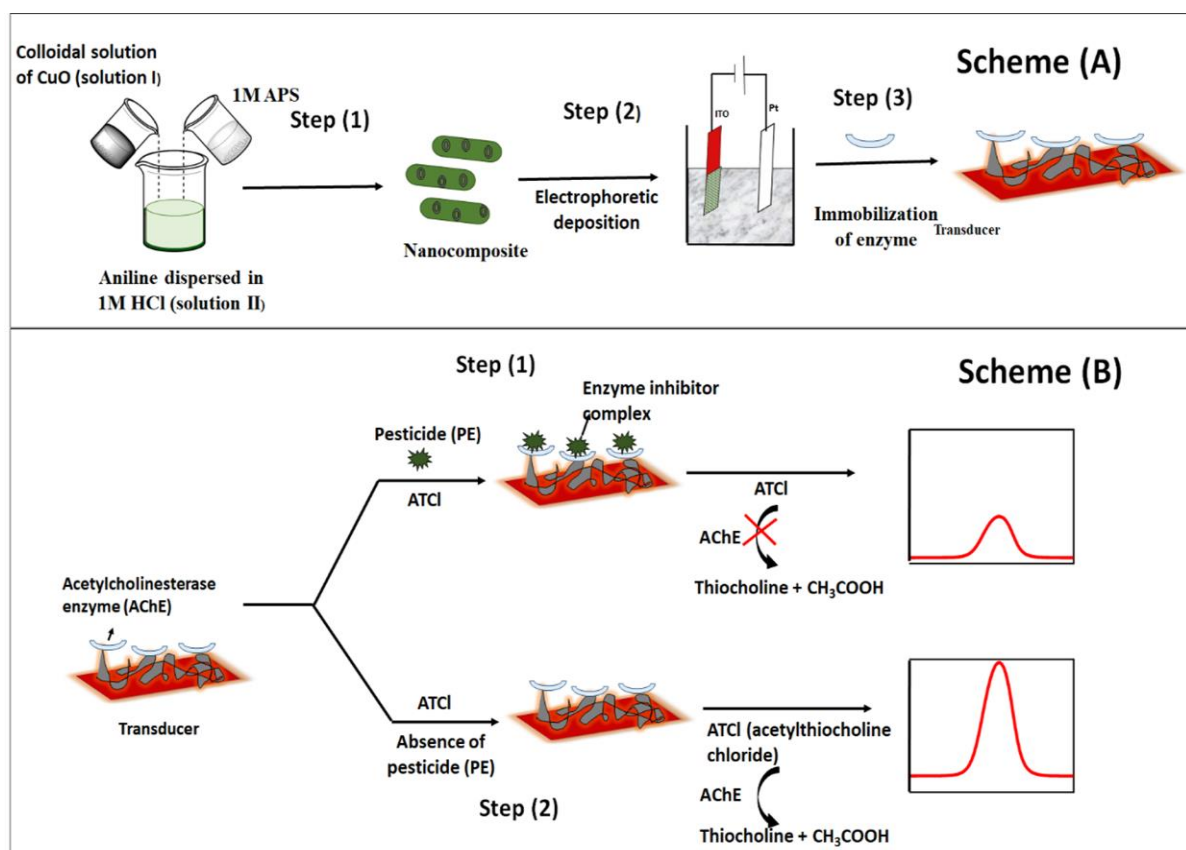


Fig. 3.1. A schematic illustration of (A) Synthesis of nanocomposite and fabrication of transducer (B) Working mechanism of fabricated biosensor for PE detection.

3.3. Results and Discussion

3.3.1. Structural, Morphological and Elemental Analysis

UV-Vis spectroscopy, FTIR and XRD techniques were utilized to conduct the structural characterization of all materials. In the XRD pattern, the peaks at $2\theta = 32.6^\circ, 35.5^\circ, 45.5^\circ, 48.4^\circ, 53.6^\circ, 58.3^\circ, 61.7^\circ$ and 68.1° represent a successful synthesis of CuO as shown in Fig. 3.2 (A), curve a [3, 4]. The diffraction pattern of PANI is showing a broad peak at $2\theta = 25^\circ$ as

shown in Fig. 3.2 (A), curve c [5]. In Fig. 3.2 (A), curve (b), on the other hand, the distinct peaks of PANI and CuO are observed. These peaks indicate that the CuO is successfully incorporated over the PANI matrix [5].

Fig. 3.2(B) represents the FTIR spectra of the CuO, PANI and CuO@PANI nanocomposite as depicted in curves (a), (b) and (c), respectively. The bands appears below 1000 cm^{-1} are due to the metal-oxygen bond vibration [4] in curve (a). While in curve (b), the band at 3330 cm^{-1} is attributed due to the stretching vibration of -N-H bond in aromatic amines. The bands at 1562 and 1485 cm^{-1} are attributed to the stretching vibrations of C=C bonds in the quinoid (Q) and benzenoid rings of PANI, respectively. The peaks at 1245 and 1294 cm^{-1} are attributed to the stretching vibrations of the C-N bond in the aromatic amine. Additionally, a strong peak at 1120 cm^{-1} is a characteristic peak of polyaniline that is attributed due to the stretching vibrations of the N-Q-N bond. In curve (c), all vibrational bands of CuO@PANI nanohybrid show a slightly higher wavenumber (red shift) with low intensity as compared to well defined peaks of polyaniline. This suggests that the introduction of CuO nanoparticles may affect the vibrational properties of the PANI nanocomposite [6].

The UV-Vis spectra of PANI show two bands located at 347 and 451 nm which are attributed to the $\pi\text{-}\pi^*$ transition in the benzenoid and quinoid rings, respectively, confirming the electronic structure of PANI as shown in Fig. 3.2(C), curve a. In curve (b) of Fig.3.2(C), the bands of PANI are shifted their peak wavelengths from 347 to 368 nm and 451 to 457 nm , respectively. An integration or incorporation of CuO in the PANI matrix is responsible for this red shift.

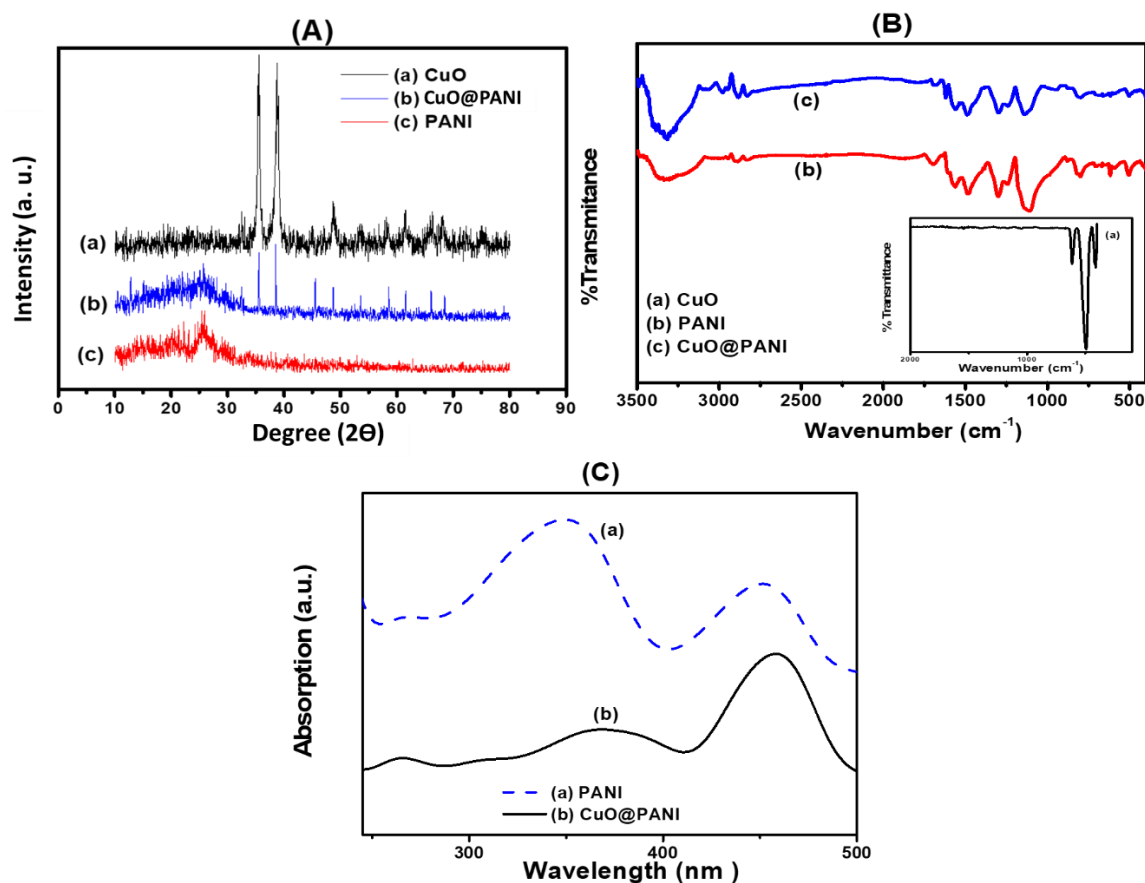


Fig. 3.2. (A) X-ray diffraction pattern of (a) CuO (b) CuO@PANI and (c) PANI (B) FTIR spectra of (a) CuO (b) PANI and (c) CuO@PANI (C) UV-Visible spectra of (a) PANI and (b) CuO@PANI

Both SEM and TEM techniques are used for the morphological characterization of all prepared materials. The SEM image of PANI is depicted in Fig. 3.3(A) and exhibits a porous network-like structure. The SEM and TEM images of CuO is depicted in Fig. 3.3(B) and 3.3(C), respectively. The TEM image confirms that the size of CuO is in nanometer range. The SEM micrograph of CuO@PANI is presented in Fig 3.3(D) where the CuO nanoparticles are observed to fill the gaps within PANI matrix in a systematic manner. The interaction between PANI and CuO resulting a smooth surface that enhances the density of composite and an effective surface area.

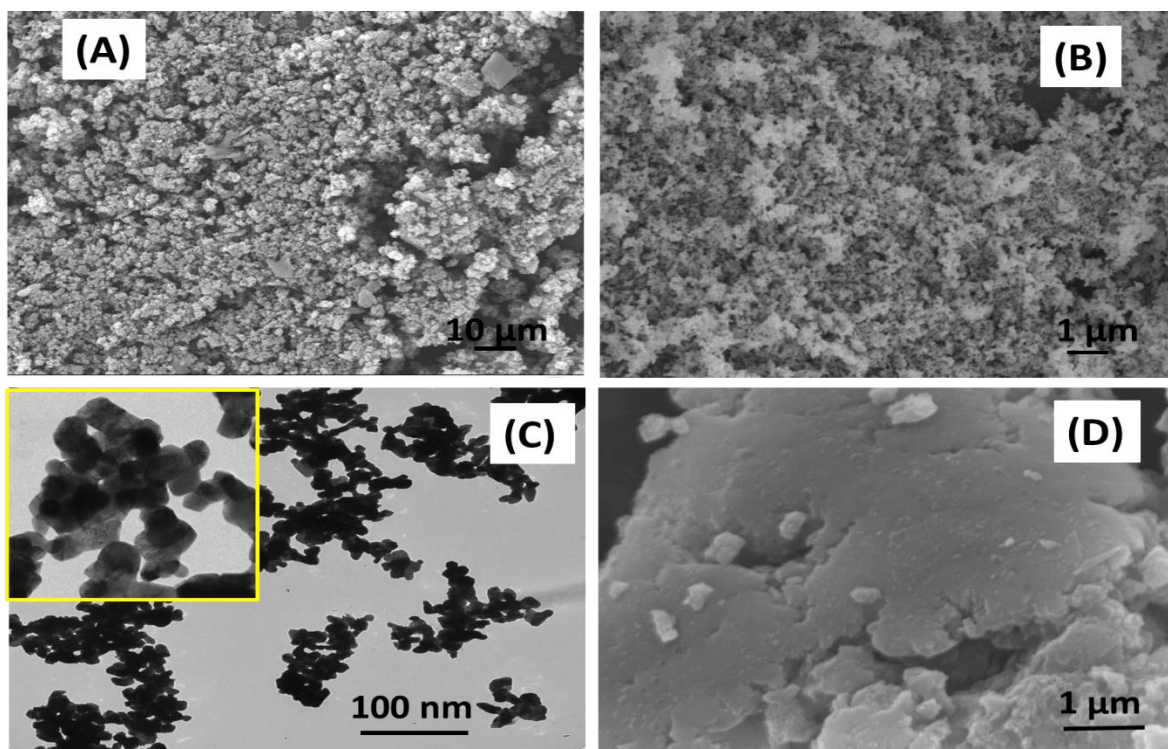


Fig. 3.3. (A) SEM micrograph of PANI (B) SEM micrograph of CuO nanoparticles (C) TEM micrograph of CuO nanoparticles (D) SEM micrograph of CuO@PANI

The elemental analysis of CuO@PANI nanocomposite has been studied by EDAX (Energy dispersive X-ray) (Fig. 3.4). This figure exhibits the peaks of C, N, O and Cu that indicates a successful synthesis of CuO@PANI composite.

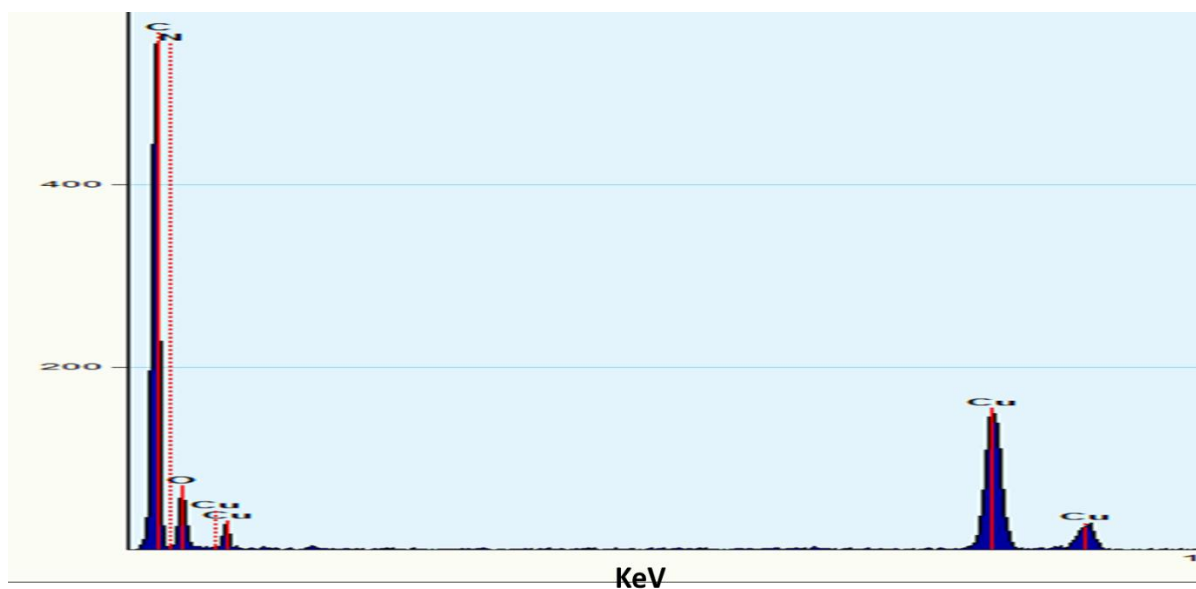


Fig. 3.4. EDAX spectra of the CuO@PANI-based composite

3.3.2. Electrochemical Characterization

CV was used for the electrochemical characterization of all the modified electrodes. This study was performed at 30 mV/sec scan rate in 7.4 pH PBS buffer containing 0.8% NaCl and 5 mM $[\text{Fe}(\text{CN})_6]^{3-/4-}$. This CV of all modified electrodes is represented in Fig. 3.5(A). This figure shows that the CuO@PANI/ITO electrode has a higher peak current which indicates its superior ability for electron transfer and conductivity compared to all other tested electrodes. On the other hand, the AChE immobilized CuO@PANI/ITO electrode exhibits a poor current due to the resistive behaviour of AChE enzyme [7].

The CV studies at scan rate of 10-300 mV/sec of PANI/ITO and CuO@PANI/ITO are depicted in Fig. 3.5(B) and Fig. 3.5(C), respectively. When the scan rate increased within the range of 10-300 mV/sec, an anodic peak current (I_{pa}) value exhibits a shifting towards a more positive value and at the same time, the cathodic peak current (I_{pc}) exhibits a shift towards a more negative value. It suggests that the peak potentials (E_{pa} and E_{pc}) and logarithmic scale of scan rate ($\log v$) are found in the linear relationship (Fig. 3.5D). This relationship is observed due to the below-mentioned equations:

$$E_{pa} [\text{CuO@PANI/ITO}] = 0.085 \text{ V } \log (v) + 0.153 \text{ V} ; R^2 = 0.9927 \quad (3.1)$$

$$E_{pc} [\text{CuO@PANI/ITO}] = - 0.065 \text{ V } \log (v) + 0.121 \text{ V} ; R^2 = 0.9915 \quad (3.2)$$

$$E_{pa} [\text{PANI/ITO}] = - 0.082 \text{ V } \log (v) + 0.129 \text{ V} ; R^2 = 0.9990 \quad (3.3)$$

$$E_{pc} [\text{PANI/ITO}] = - 0.064 \text{ V } \log (v) + 0.153 \text{ V} ; R^2 = 0.9968 \quad (3.4)$$

The slopes of above-mentioned equations (3.1 to 3.4) are further used for the calculation of electron transfer coefficient (α). The value of α is found 0.89 and 0.901 on case of PANI/ITO and CuO@PANI/ITO, respectively. The charge transfer rate constant (K_a) is calculated by utilizing the calculated values of α . The K_a values are found to be 2.33×10^{-2} and 67×10^{-2} for PANI/ITO and CuO@PANI/ITO, respectively.

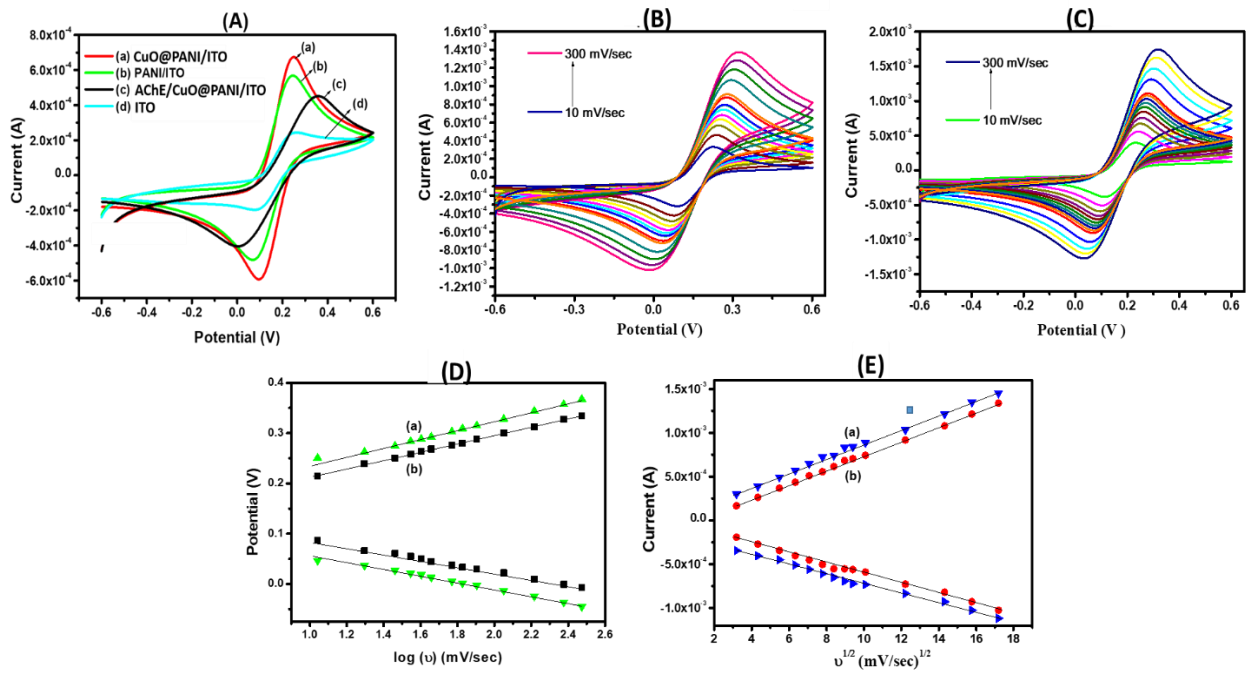


Fig. 3.5. (A) Cyclic voltammogram of CuO@PANI/ITO (a), PANI/ITO (b), AChE/CuO@PANI/ITO (c) and ITO (d) at a scan rate 30 mV/sec (B) Cyclic voltammogram of (A) PANI/ITO, (B) CuO@PANI/ITO electrode with varying scan rate (10–300 mV/sec), (C) Plots of current vs. square root of scan rate in case of CuO@PANI (a) and PANI (b), (D) Plots of potential vs. log (scan rate) in case of CuO@PANI (a) and PANI (b)

The linear relationship between peak currents (I_{pa} and I_{pc}) and $v^{1/2}$ of PANI/ITO and CuO@PANI/ITO electrodes are illustrated in Fig. 3.5(E) and obey the following equations:

$$I_{pa} [\text{CuO@PANI/ITO}] = 84.36 \mu\text{A} / (\text{mVsec}^{-1}) \times v^{1/2} + 104.36 \mu\text{A} ; R^2 = 0.9970 \quad \text{.....(3.5)}$$

$$I_{pc} [\text{CuO@PANI/ITO}] = -54.53 \mu\text{A} / (\text{mVsec}^{-1}) \times v^{1/2} - 176.21 \mu\text{A} ; R^2 = 0.9940 \quad \text{.....(3.6)}$$

$$I_{pa} [\text{PANI/ITO}] = 83.42 \mu\text{A} / (\text{mVsec}^{-1}) \times v^{1/2} + 21.25 \mu\text{A} ; R^2 = 0.9984 \quad \text{.....(3.7)}$$

$$I_{pc} [\text{PANI/ITO}] = -58.56 \mu\text{A} / (\text{mVsec}^{-1}) \times v^{1/2} - 91.87 \mu\text{A} ; R^2 = 0.9904 \quad \text{.....(3.8)}$$

Now, for calculating the effective surface area (A) for PANI/ITO and CuO@PANI/ITO, the Randles-Sevcik equation ($I_p/v^{1/2} = 2.69 \times 10^5 \text{ n}^{3/2} \text{ A D}^{1/2} \text{ C}$) is used [8].

Here, D is dissociation coefficient and C the conc of $[\text{Fe}(\text{CN})_6]^{3-/4-}$. These calculated values of A for PANI/ITO ($D = 34.81 \times 10^{-12}$) and CuO@PANI/ITO ($D = 37.44 \times 10^{-12}$) are $0.28 \times 10^{-2} \text{ cm}^2$ and $1.6 \times 10^{-2} \text{ cm}^2$, respectively.

3.3.3. Optimization Studies

The pH of electrolytic solution and incubation time are optimized by DPV technique. Fig. 3.6 (A) is presented to demonstrate the effect of pH values ranging from 6 to 8 on the sensor's performance. The maximum current was achieved at 7.4 pH as shown in this figure. Therefore, all the electrochemical studied are performed at this pH. Additionally, an incubation time is also measured by changing the time from 0 to 20 min for AChE/CuO@PANI/ITO electrode as shown in Fig. 3.6B. The observing results demonstrates a decrease in current magnitude from 0 to 10 min. Once 10 min have elapsed, the current reaches a saturation point, indicating that the maximum binding of PE with the AChE enzyme has been attained within this frame.

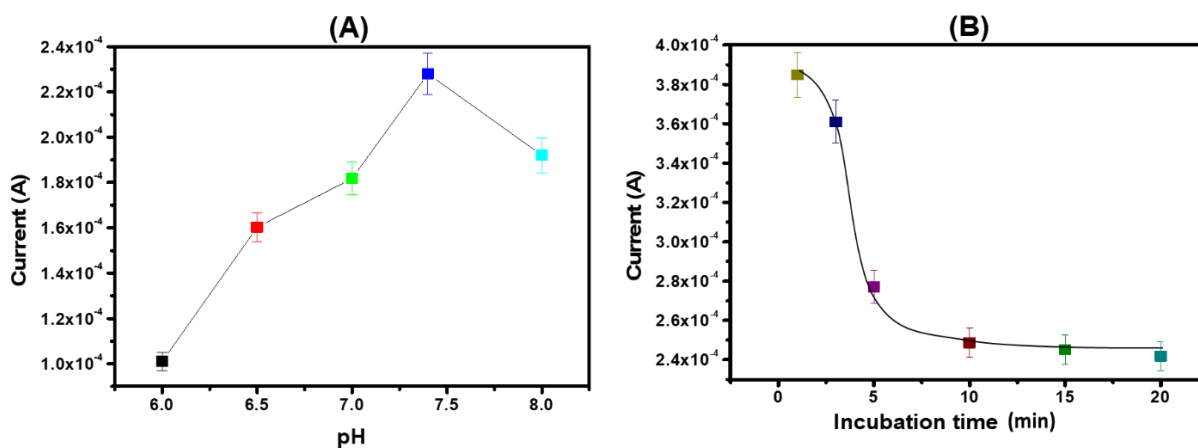


Fig. 3.6. Optimization of (A) effect of pH, (B) incubation time of PE

3.3.4. Electrochemical Biosensing Studies

Electrochemical studies of AChE/CuO@PANI/ITO was carried out as a function of PE conc (1-200 nM) in 7.4 PBS containing 5 mM $[\text{Fe}(\text{CN})_6]^{3-/4-}$ by using the DPV technique. It was observed that the anodic peak current was decreasing continuously when the developed

biosensor was treated with an increasing concentration of PE as shown in Fig. 3.7A. A decrease in current is observed due to an inhibition of AChE enzyme by PE. Fig. 3.7(B) shows the calibration curve of inhibition (ΔI) and PE concentration (C_{PE}) and follow the below-mentioned equation:

$$\Delta I = 49.86 \mu A/(nM)^{-1} \times \log C_{PE} + 33.14 \mu A ; R^2 = 0.9984 \quad \text{.....(3.9)}$$

The sensitivity calculated for AChE/CuO@PANI/ITO electrode is $49.8 \mu A (nM)^{-1}$ with a correlation coefficient value 0.9984. The limit of detection (LOD) was calculated by using a relationship $3\sigma/\text{sensitivity}$ for the developed biosensor which is found to be 0.096 nM or 96 pM, here σ is the standard deviation of the blank electrode [9].

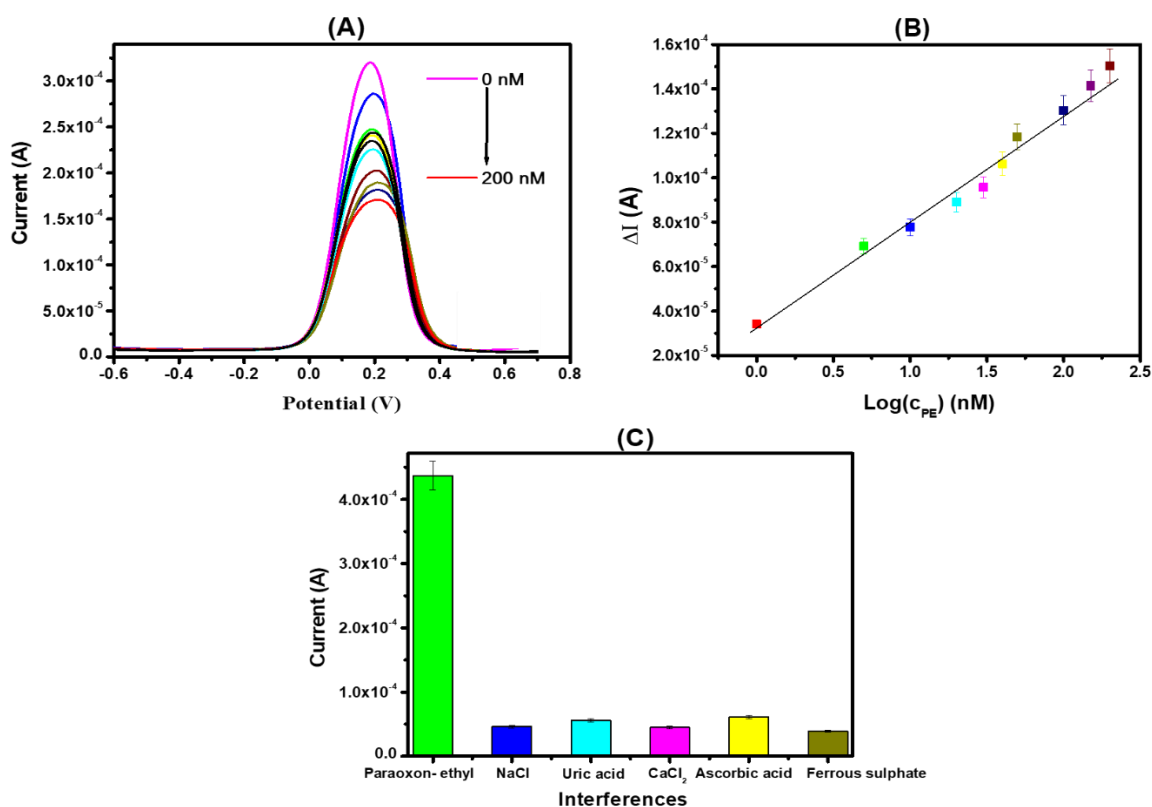


Fig. 3.7. (A) DPV response data of the fabricated electrode after incubation at various conc (1-200 nM) of PE (B) Calibration curve between log of PE conc with change in current (C) Specificity of AChE/CuO@PANI/ITO biosensor in the presence of $1 \mu M$ paraoxon-ethyl, uric acid, ascorbic acid, $CaCl_2$, NaCl and ferrous sulphate

The biosensor's performance for PE detection is further compared with the several recently developed biosensors. The developed biosensor outperforms over all the considered biosensors. The enhanced electrochemical performance of this biosensor is found because of the synergistic effect both PANI and CuO. An incorporation of CuO into PANI matrix provides the smooth surface area that improves the electron transfer. Also, $-NH_2$ groups of PANI enhance the immobilization efficiency of enzyme and the hydrolysis of ATCl is accelerated by CuO. These specific properties of CuO and PANI also drastically enhance the sensitivity of this proposed biosensor.

3.3.5. Selectivity and Real Sample Analysis

The selectivity of the biosensor fabricated in the present study was carried out by the incubation of AChE/CuO@PANI/ITO-based sensor with 1mM NaCl, $CaCl_2$, uric acid, ascorbic acid and ferrous sulfate. Fig. 3.7C shows clearly that the fabricated biosensor gives maximum current for PE in comparison to other interfering species, confirming high selectivity for PE detection.

The applicability of biosensor in real-word scenario is checked in spiked rice and pulse samples at 5, 10, 20, 30 nM. The results obtained in this study exhibit permissible recoveries of 104-111 % and the relative standard deviation (RSD) of $< 10\%$, suggesting an alternative technique for PE detection as this fabricated biosensor. The data related to the detection of PE in spiked rice and pulse samples using AChE/CuO@PANI/ITO electrode have been presented in Table 3.1.

Table 3.1. Detection of PE in Spiked Rice and Pulse samples using AChE/CuO@PANI/ITO Electrode.

| Sample | Added amount (nM) | Found amount (nM) | Recovery (%) | RSD (%) |
|--------|-------------------|-------------------|--------------|---------|
| Pulse | 5 | 5.4 | 108 | 5.97 |
| | 10 | 10.8 | 108 | 5.46 |
| | 20 | 21.4 | 107 | 5.22 |
| | 30 | 32.4 | 108 | 5.98 |
| Rice | 5 | 5.3 | 106 | 4.43 |
| | 10 | 10.4 | 104 | 5.1 |
| | 20 | 21.8 | 109 | 6.5 |
| | 30 | 33.3 | 111 | 6.6 |

3.3.6. Reproducibility and Stability Studies

Reproducibility of AChE/CuO@PANI/ITO electrode was checked by DPV in presence of 5 nM PE and 3 mM ATCl using 5 electrodes as depicted in Fig. 3.8A. The results exhibited a RSD value of 2.16 %, suggesting an excellent reproducibility of fabricated biosensor.

The storage stability of this fabricated biosensor was tested by putting the AChE/CuO@PANI/ITO electrode in a refrigerator at a temperature of 4°C and measuring its response towards PE every ten days (Fig. 3.8B). After 30 days, a very little change in current was observed (RSD = 1.37 %), confirming its high stability up to 30 days. While after 40 days, the current response remains 47.14 % of the initial value, confirming its high stability up to 30 days.

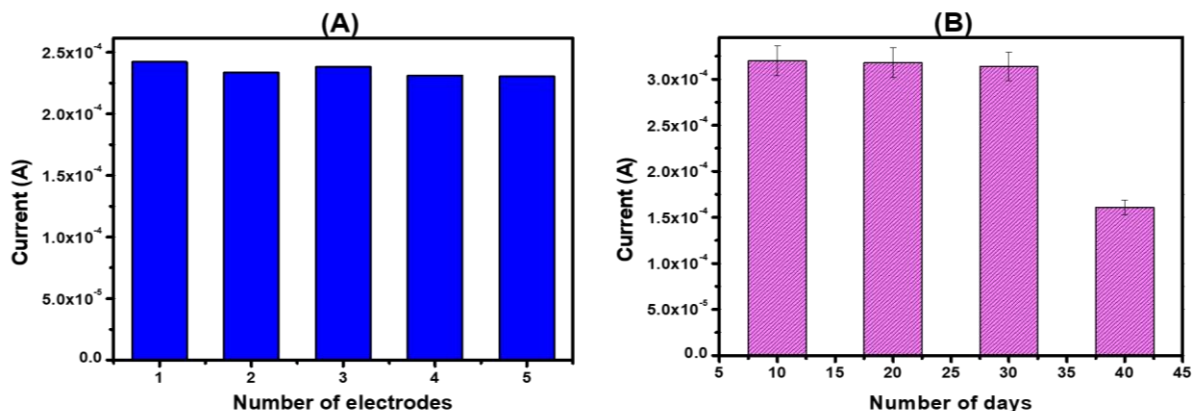


Fig. 3.8. (A) Reproducibility study of AChE/CuO@PANI/ITO electrode for PE detection (B) Stability study of AChE/CuO@PANI/ITO electrode over a period of 40 days

3.4. Conclusion

A novel and high sensitive AChE enzyme-based electrochemical biosensor is successfully developed using CuO and PANI based sensing platform and utilized for PE detection. In order to attain the best possible performance of developed biosensor, various parameters such as incubation time of PE and pH of electrolytic solution are optimized. The nanocomposite (CuO@PANI) exhibits remarkable electrochemical properties, conductivity and good catalytic power. All these collectively contribute to the outstanding performance of biosensor for PE detection. This developed biosensor shows that a high sensitivity of $49.86 \mu\text{A} (\text{nM})^{-1}$. Also, it shows a low detection limit (LOD) as 0.096 nM and a good linear range between 1 to 200 nM . The applicability of proposed biosensor in real world samples is also successfully validated in the spiked pulse and rice samples.

The results of present study have been published in Applied Biochemistry and Biotechnology 195(9) 4485-4502 (2023)

3.5. References

1. He, L., et al., *Novel electrochemical biosensor based on core-shell nanostructured composite of hollow carbon spheres and polyaniline for sensitively detecting malathion*. Sensors Actuators B: Chemical 2018. **258**: p. 813-821.
2. Loguercio, L.F., et al., *Efficient acetylcholinesterase immobilization for improved electrochemical performance in polypyrrole nanocomposite-based biosensors for carbaryl pesticide*. Sensors Actuators B: Chemical 2021. **339**: p. 129875.
3. Nagaraja, M., et al., *Polyaniline-CuO nanocomposite: Electrical, structural and sensor properties*. Materials Today: Proceedings, 2022. **49**: p. 1989-1992.
4. Iqbal, S., et al., *Controlled synthesis of Ag-doped CuO nanoparticles as a core with poly (acrylic acid) microgel shell for efficient removal of methylene blue under visible light*. Journal of Materials Science: Materials in Electronics, 2020. **31**: p. 8423-8435.
5. de Souza, V.S., H.O. da Frota, and E.A. Sanches, *Polyaniline-CuO hybrid nanocomposite with enhanced electrical conductivity*. Journal of Molecular Structure, 2018. **1153**: p. 20-27.
6. He, M., et al., *Highly sensitive and selective H₂S gas sensors based on flower-like WO₃/CuO composites operating at low/room temperature*. Journal of Alloys Compounds 2019. **788**: p. 36-43.
7. Nagabooshanam, S., et al., *Electro-deposited nano-webbed structures based on polyaniline/multi walled carbon nanotubes for enzymatic detection of organophosphates*. Food chemistry, 2020. **323**: p. 126784.
8. Jalil, O., C.M. Pandey, and D. Kumar, *Highly sensitive electrochemical detection of cancer biomarker based on anti-EpCAM conjugated molybdenum disulfide grafted reduced graphene oxide nanohybrid*. Bioelectrochemistry, 2021. **138**: p. 107733.

9. Thakur, D., C.M. Pandey, and D. Kumar, *Highly sensitive enzymatic biosensor based on polyaniline-wrapped titanium dioxide nanohybrid for fish freshness detection*. Applied Biochemistry Biotechnology 2022. **194**(8): p. 3765-3778.

CHAPTER 4

Ag@CuO embedded Polyaniline modified Electrochemical Biosensor for Paraoxon-Ethyl Detection

4.1. Introduction

This chapter describes a new method for the chemical synthesis of a composite by an integration of Ag-doped CuO nanoparticles (Ag@CuO) and a polymer, PANI matrix. This resulting composite is utilized as a sensing electrode to detect the paraoxon-ethyl. An even dispersion of Ag@CuO throughout the PANI matrix is contributing a uniform and compact surface which enhances the electron transmission. Moreover, the combined effect of Ag@CuO and PANI synergistically results in the remarkable conductivity, biocompatibility and catalytic capability. All these properties of Ag@CuO and PANI efficiently enhance the biosensor's performance for PE detection in terms of sensitivity and selectivity. This biosensor is also applicable in real-world scenarios. The specific detail of material synthesis, electrophoretic deposition and biosensor fabrication are discussed in the next section 4.2.

4.2. Experimental Section

4.2.1. Synthesis of CuO and Ag@CuO Nanoparticles

To prepare the CuO, 0.7 g of $\text{CuSO}_4 \cdot 5\text{H}_2\text{O}$ was added in 25 mL deionized (DI) water and stirred it for 15 min at 80°C . Subsequently, sodium dodecyl sulfate (SDS) (0.07 g) has been added to the solution and subsequently stirred the same for 30 min at a same temperature. Then, the dropwise addition of 1 M NaOH was continued until the pH of the solution reaches 14. This resulting solution was further stirred for another 6 h and then centrifuged (3000 rpm) until the pH reached at 7. Finally, the resulting black CuO precipitate was dried at 60°C for 8 h and then calcined by keeping it in a muffle-furnace at 800°C for 5 h.

For the preparation of Ag@CuO nanoparticles, 35 mg of AgNO₃ and 0.7 g of CuSO₄.5H₂O were dissolved in 25 mL water (DI) and then stirred at 80°C for 1 h. The subsequent steps remain same as discussed in previously paragraph.

4.2.2. Synthesis of Ag@CuO/PANI-based Composite

Firstly, 0.37 g of synthesized Ag@CuO nanoparticle was mixed in the DI water. The dispersion so obtained was added in 0.2 M aniline hydrochloride solution followed by stirring for 1 h. Then, 1 M ammonium persulfate (APS) was gradually added dropwise and this solution was stirred at room temperature for 8 h. Further, this solution was centrifuged for 15 min at 2400 rpm and then washed with water (DI) followed by ethanol for 3 to 4 times. The resulting black precipitate of Ag@CuO and PANI-based composite was dried at 60°C.

4.2.3. Electrophoretic Deposition of Ag-doped-CuO/PANI-based Composite and Biosensor Fabrication

A deposition of the prepared composite onto the indium tin oxide (ITO) coated glass substrate was carried out by electrophoretic deposition method. In this process, a colloidal suspension of Ag@CuO/PANI composite (0.1 mg) was prepared in an ethanol and water mixture (1:5 ratio). For a uniform and smooth deposition, a 20 V direct current (DC) voltage was applied for 16 sec.

The biosensor (AChE/Ag@CuO/PANI/ITO) was fabricated by drop-casting the 0.1 mg/mL AChE enzyme onto the fabricated electrode surface (Ag@CuO/PANI/ITO). Prior to the electrochemical analysis, the biosensor was incubated in a refrigerator at 4°C for 12 h. The schematic representation of biosensor fabrication is depicted in a Fig. 4.1(A).

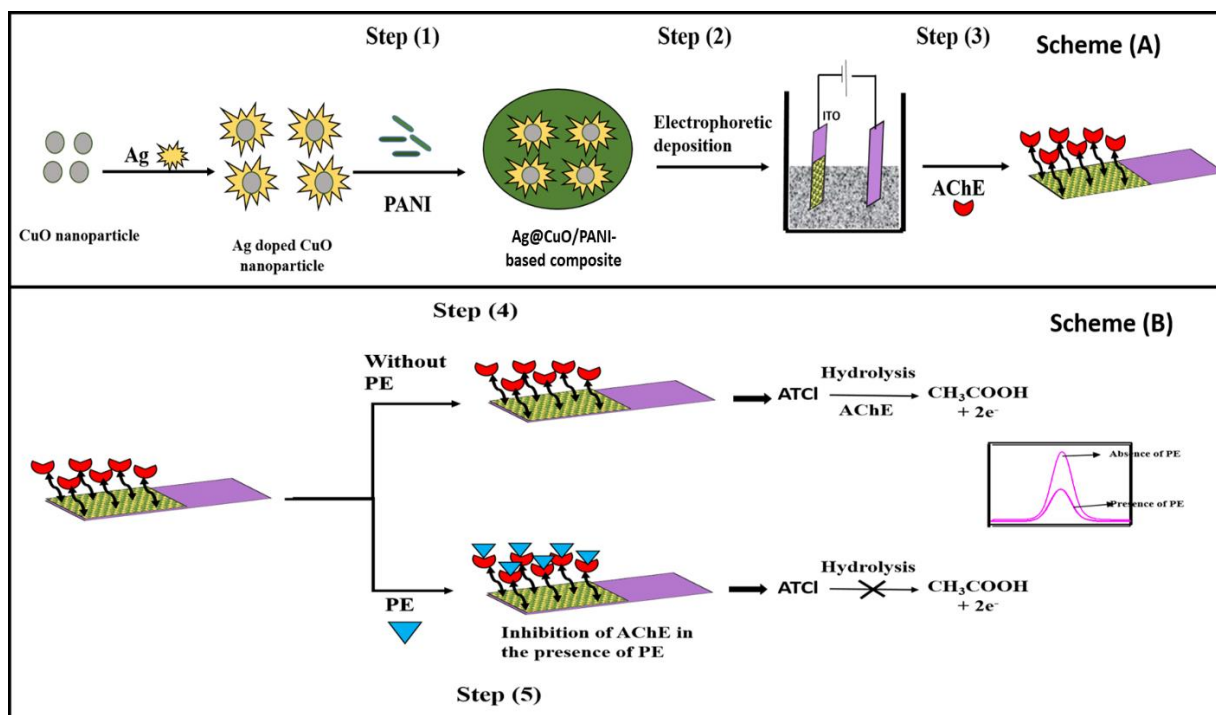


Fig. 4.1. A schematic view of (A) biosensor fabrication and (B) working mechanism of fabricated biosensor for PE detection

4.3. Results and Discussion

4.3.1. Design of Sensor

In the present work, a novel composite is synthesized by chemical oxidative polymerization method using Ag@CuO and PANI (Fig. 4.1A, step 1). The composite is further used for the OPs (paraoxon-ethyl) detection. To achieve the biosensor fabrication, the composite is deposited electrophoretically onto the ITO surface (Fig. 4.1A, step 2) followed by immobilization of AChE enzyme (Fig. 4.1A, step 3). Then, this biosensor is tested for PE detection. The AChE enzyme facilitates the hydrolysis of ATCl in the absence of paraoxon-ethyl leading to the production of electroactive thiocholine and acetic acid. Thiocholine undergo an oxidation to form dithio-bis-choline, while acetic acid diffuses to the electrode surface resulting in the protonation of the polymer, PANI. This protonation of PANI enables electron transport which generates signals (Fig. 4.1B, step 4). Conversely, the presence of pesticides block the active sites of AChE, restricting the hydrolysis of ATCl and causing a

decrease in the signal intensity [1] (Fig. 4.1B, step 5). Therefore, by monitoring the peak currents in the presence and absence of PE, the concentration of PE can be determined.

4.3.2. Structural, Morphological and Elemental Studies

The characteristic peaks of CuO appeared at angle $2\theta = 32.5^\circ, 35.5^\circ, 38.9^\circ, 49^\circ, 53.7^\circ, 58.3^\circ, 61.7^\circ, 66.2^\circ, 68.3^\circ, 72.5^\circ, 75.3^\circ$, confirm the successful formation of CuO nanoparticles (Fig. 4.2A, curve a). The additional peaks observed in curve (b) at $2\theta = 38.1^\circ, 44.3^\circ, 64.4^\circ$, and 77.6° , confirm the formation of Ag-doped CuO nanoparticles [2]. A broad peak at angle $2\theta = 25^\circ$ represents a characteristic peak of polymer, PANI [3] as shown in Fig. 4.2A, curve d. All the characteristic peaks of CuO, Ag@CuO and PANI are observed in curve (c) of Fig. 4.2 A which further confirm the Ag@CuO/PANI-based composite is synthesized successfully.

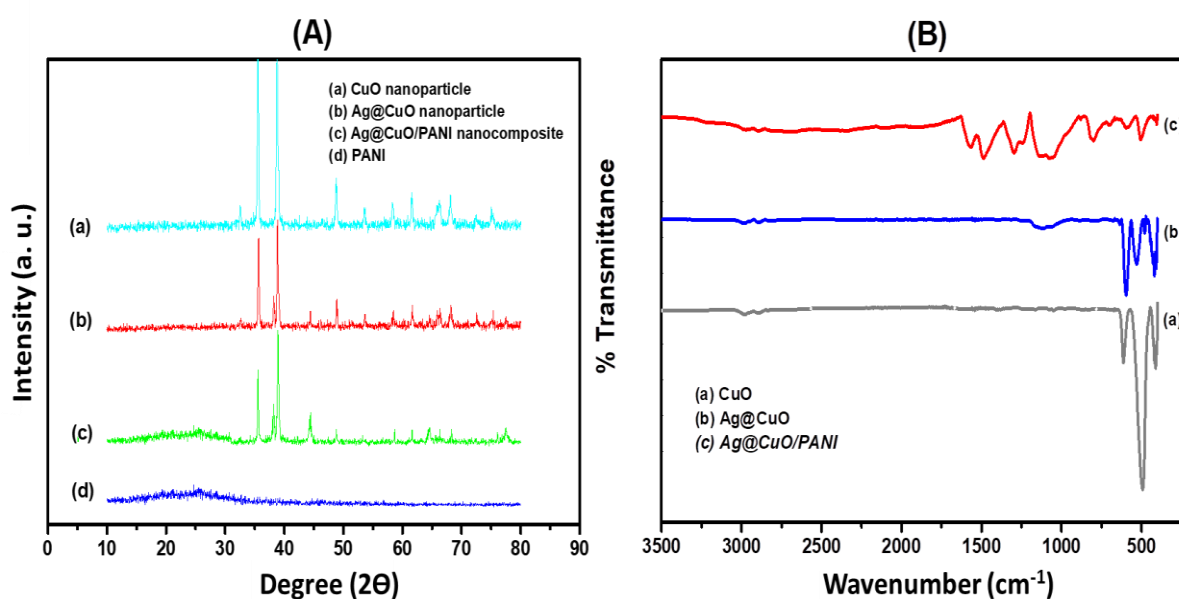


Fig. 4.2. (A) XRD spectra of (a) CuO (b) Ag@CuO (c) Ag@CuO/PANI (c) and PANI (B) FTIR spectra of CuO (a), Ag@CuO (b) and Ag@CuO/PANI (c)

The FTIR spectra of all the prepared materials have been illustrated in the Fig. 4.2B. The bands at $419, 494$ and 619 cm^{-1} in curves (a) and (b) are attributed due to the Cu-O bond vibration. While in curve (b), the bands at 540 and 1136 cm^{-1} are the characteristic bands of Ag [2, 4]. In curve (c), the bands below 1000 cm^{-1} are due to the CuO and a band at 1136 cm^{-1}

supports the presence of Ag. Moreover, a band at 1120 cm^{-1} is the characteristic band of PANI found due to the N-Q-N stretching vibration. Other bands appear at 1245 and 1295 cm^{-1} are attributed due to the C=C stretching vibrations in quinoid and benzenoid rings, respectively.

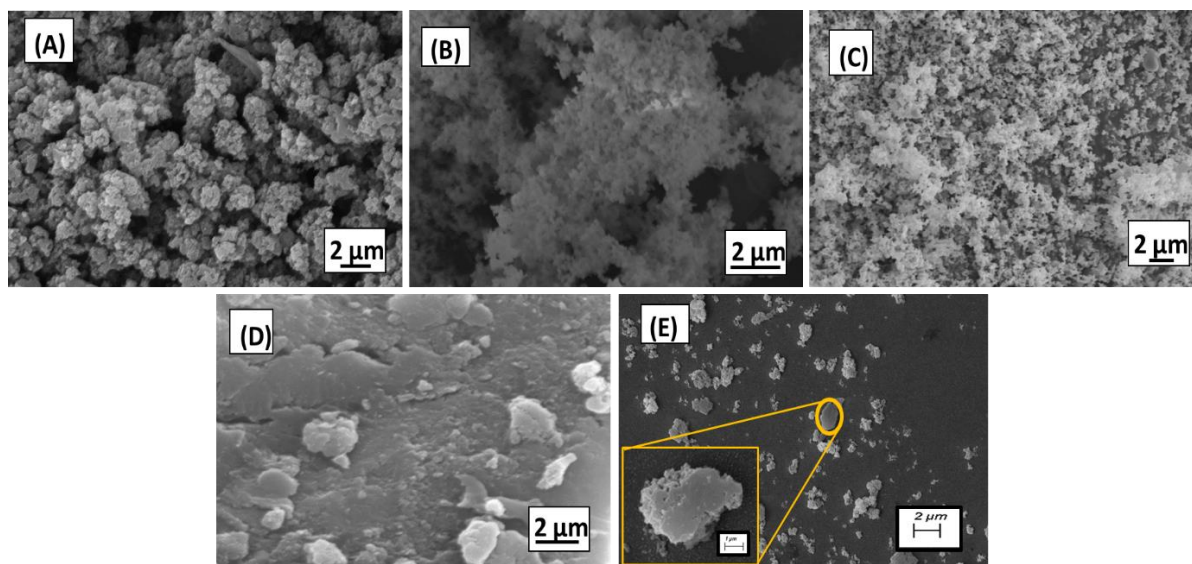


Fig. 4.3. SEM images of (A) PANI (B) CuO nanoparticles (C) Ag@CuO nanoparticles (D) Ag@CuO/PANI nanocomposite and (E) Ag@CuO/PANI/ITO

The morphological characterization of all the prepared materials is done by scanning electron microscopy (SEM) technique. The morphology of PANI illustrates the porous in nature with a large surface area (Fig. 4.3A). Small particles seen in the Fig. 4.3(B) and 4.3(C) represent the morphology of CuO and Ag@CuO nanoparticles, respectively. In Fig. 4.3(D), SEM micrograph of Ag@CuO/PANI based composite is represented. It is clear from this figure that the nanoparticles are uniformly distributed over the surface of PANI and generate a smooth path that improves the electron transfer and enhances the performance of biosensor. The Ag@CuO/PANI/ITO electrode morphology is represented in Fig. 4.3(E) and it confirms that the composite is successfully deposited onto the ITO coated glass substrate.

The SEM-EDX spectra of all the prepared materials are illustrated in Fig. 4.4. In the EDX spectra of CuO (Fig. 4.4A), the peaks attribute to Cu, O and Au which are clearly observed. The peaks of Cu, O, Au and Ag are observed in Fig. 4.4B. Additionally, the peaks

of C, N, Ag, Cu, O and Au are clearly seen in a Fig. 4.4C. All these peaks confirm the successful formation of the prepared material. It is also observed that the Au peak appears in all the EDX spectra because of the gold coating of samples during the EDX analysis.

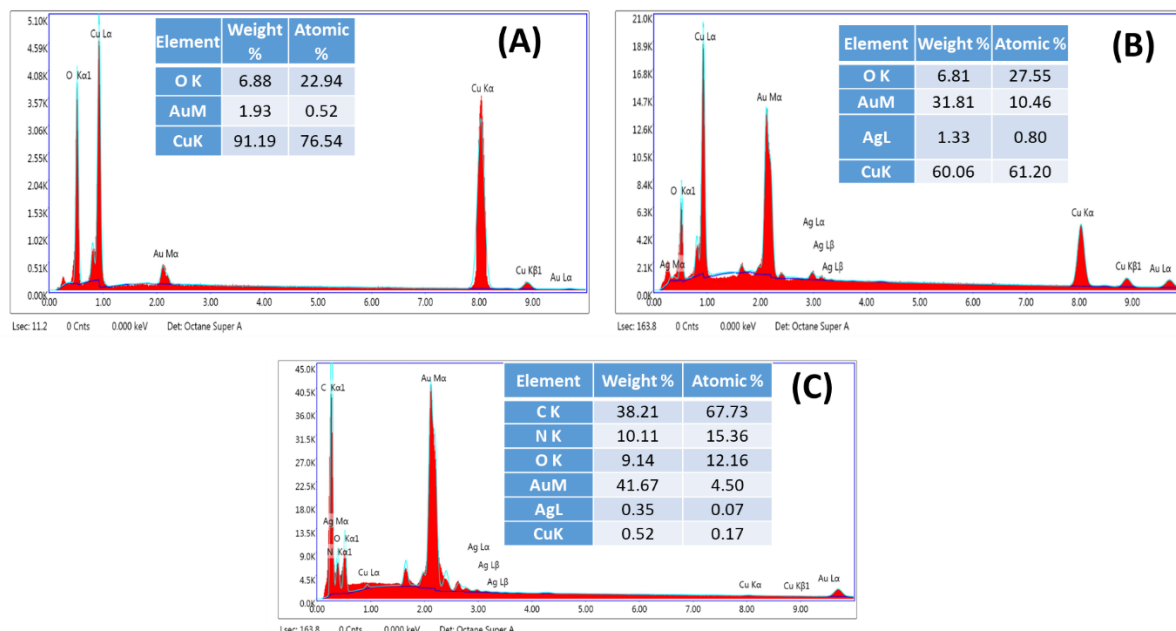


Fig. 4.4. SEM-EDAX data of (A) CuO, (B) Ag@CuO, and (C) Ag@CuO/PANI

4.3.3. Electrochemical Characterization

CV technique was used for the electrochemical characterization of all the modified electrodes. This study was performed at 50 mV/sec scan rate in 6.5 pH PBS buffer containing 0.8% NaCl and 5 mM $[\text{Fe}(\text{CN})_6]^{3-/4-}$. Cyclic voltammogram of all the modified electrodes is represented in Fig. 4.5(A). It illustrates that the Ag@CuO/PANI/ITO electrode has a higher peak current, which indicates its superior ability for electron transfer and conductivity as compared to all the other tested electrodes. On the other hand, AChE immobilized Ag@CuO/PANI/ITO modified electrode showing the poor current due to the AChE enzyme of non-conducting nature [5].

The CV studies at scan rate of 10-300 mV/sec of CuO/ITO, Ag@CuO/ITO and Ag@CuO/PANI/ITO are depicted in Fig. 4.5(B), 4.5(C) and 4.5(D), respectively. It is observed that when we increase a scan rate from 10-300 mV/sec, the anodic peak current (I_{pa}) value

shifting to a more positive side and at the same time, the cathodic peak current (I_{pc}) value shifting to a more negative side. It suggests that the peak potentials (E_{pa} and E_{pc}) and logarithmic scale of scan rate ($\log v$) are in the linear relationship (Fig. 4.5E) and it is clearly expressed by the below-mentioned equations:

$$E_{pa} [\text{Ag@CuO/PANI/ITO}] = 0.075 \text{ V } \log (v) + 0.177 \text{ V} ; R^2 = 0.9946 \quad \text{.....(4.1)}$$

$$E_{pc} [\text{Ag@CuO/PANI/ITO}] = - 0.075 \text{ V } \log (v) + 0.165 \text{ V} ; R^2 = 0.9814 \quad \text{.....(4.2)}$$

$$E_{pa} [\text{Ag@CuO/ITO}] = 0.073 \text{ V } \log (v) + 0.165 \text{ V} ; R^2 = 0.9930 \quad \text{.....(4.3)}$$

$$E_{pc} [\text{Ag@CuO/ITO}] = - 0.069 \text{ V } \log (v) + 0.176 \text{ V} ; R^2 = 0.9908 \quad \text{.....(4.4)}$$

$$E_{pa} [\text{CuO/ITO}] = 0.067 \text{ V } \log (v) + 0.155 \text{ V} ; R^2 = 0.9844 \quad \text{.....(4.5)}$$

$$E_{pc} [\text{CuO/ITO}] = - 0.061 \text{ V } \log (v) + 0.188 \text{ V} ; R^2 = 0.9908 \quad \text{.....(4.6)}$$

Slopes of these above-mentioned equations were further used for the calculation of electron transfer coefficient (α) in case of CuO/ITO, Ag@CuO/ITO and Ag@CuO/PANI/ITO electrodes and the data have been reported in Table 4.1.

Table 4.1. Kinetic parameters of all the modified electrodes

| Fabricated electrodes | Diffusion coefficient (D) (cm ² / sec) | Effective surface area (A) (cm ²) | Electron transfer coefficient (α) | i_o (A/cm ²) | K_{app} (cm/ sec) |
|-----------------------|---|---|--|----------------------------|-----------------------|
| CuO/ITO | 8.41×10^{-2} | 3.80×10^{-1} | 0.14 | 6.67×10^{-5} | 3.35×10^{-4} |
| Ag@CuO/ITO | 9.29×10^{-2} | 4.10×10^{-1} | 0.19 | 1.08×10^{-4} | 5.45×10^{-4} |
| Ag@CuO/PANI/ITO | 12.11×10^{-2} | 4.20×10^{-1} | 0.22 | 1.84×10^{-4} | 9.23×10^{-4} |

A linear relationship between the peak currents (I_{pa} and I_{pc}) and $v^{1/2}$ of PANI/ITO and CuO@PANI/ITO electrodes are illustrated in Fig. 4.5(F) which obey the following equations:

$$I_{pa} [\text{Ag@CuO/PANI/ITO}] = 91.69 \mu\text{A} / (\text{mVsec}^{-1}) \times v^{1/2} + 326.35 \mu\text{A} ; R^2 = 0.9970 \quad \text{.....(4.7)}$$

$$I_{pc} [\text{Ag@CuO/PANI/ITO}] = -55.84 \mu\text{A} / (\text{mVsec}^{-1}) \times v^{1/2} - 174.41 \mu\text{A} ; R^2 = 0.9651 \quad \text{.....(4.8)}$$

$$I_{pa} [\text{Ag@CuO/ITO}] = 75.53 \mu\text{A} / (\text{mVsec}^{-1}) \times v^{1/2} + 174.41 \mu\text{A} ; R^2 = 0.9651 \quad \text{.....(4.9)}$$

$$I_{pc} [\text{Ag@CuO/ITO}] = -50.63 \mu\text{A} / (\text{mVsec}^{-1}) \times v^{1/2} - 260.30 \mu\text{A} ; R^2 = 0.9968 \quad \text{.....(4.10)}$$

$$I_{pa} [\text{CuO/ITO}] = 59.31 \mu\text{A} / (\text{mVsec}^{-1}) \times v^{1/2} + 3.08 \mu\text{A} ; R^2 = 0.9968 \quad \text{.....(4.11)}$$

$$I_{pc} [\text{CuO/ITO}] = -32.11 \mu\text{A} / (\text{mVsec}^{-1}) \times v^{1/2} - 152.24 \mu\text{A} ; R^2 = 0.9842 \quad \text{.....(4.12)}$$

Now, for calculating the effective surface area (A) for CuO/ITO, Ag@CuO/ITO and Ag@CuO/PANI/ITO, the Randles-Sevcik equation, that is, $I_p/v^{1/2} = 2.69 \times 10^5 (n^{3/2} A D^{1/2} C)$ has been used.

Here, D is a dissociation coefficient and C the conc of $[\text{Fe}(\text{CN})_6]^{3-/4-}$. These calculated values of A and D in case of all the modified electrodes have been reported in Table 4.1. This table illustrates that the Ag@CuO/PANI/ITO electrode shows highest value of D and A because of the precise diffusion of all the redox ions on the electrode surface [6].

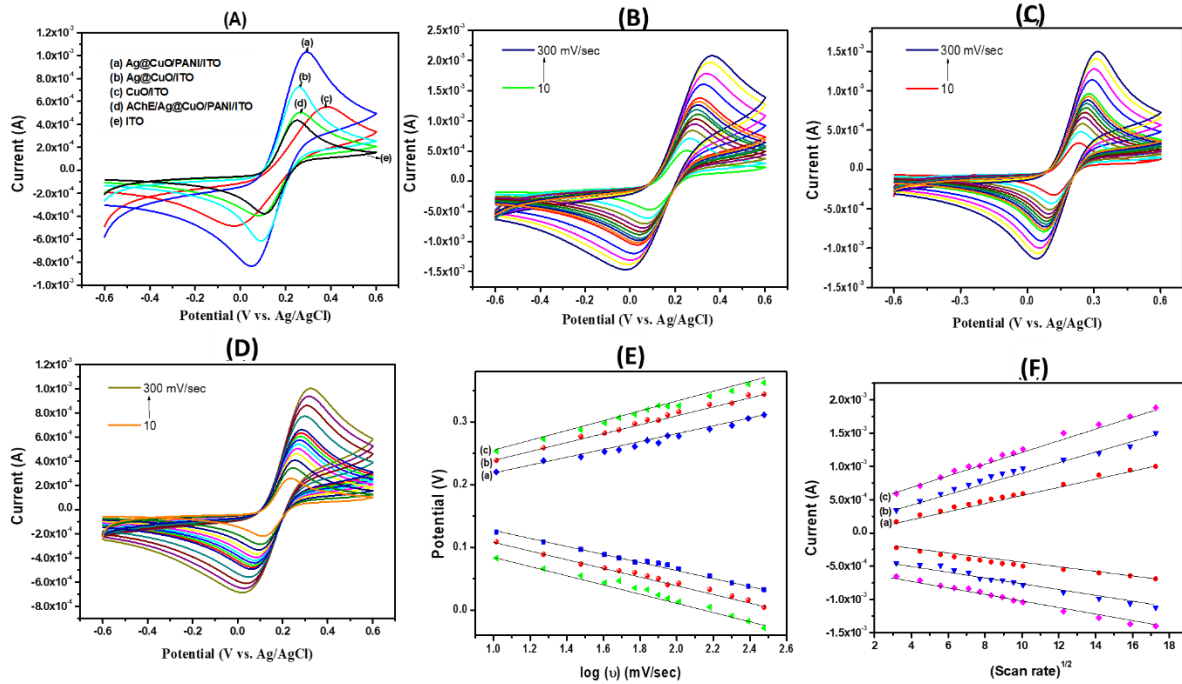


Fig. 4.5. (A) Cyclic voltammogram of Ag@CuO/PANI/ITO (a), Ag@CuO/ITO (b), CuO/ITO (c), AChE/Ag@CuO/PANI/ITO (d) and ITO (e) at a scan rate of 50 mV/sec. Cyclic voltammogram of (B) Ag@CuO/PANI/ITO (C) Ag@CuO/ITO and (D) CuO/ITO electrodes with different scan rates (10 - 300 mV/sec) (E) Graphs of potential vs. log (scan rate) in case of CuO (a), Ag@CuO (b) and Ag@CuO/PANI nanocomposite (c). (F) Graphs of current vs.

square root of scan rate in case of CuO (a), Ag@CuO (b) and Ag@CuO/PANI nanocomposite (c)

4.3.4. Optimization Studies

The pH of the electrolytic solution, incubation time and amount of AChE enzyme are optimized by using DPV technique. Fig. 4.6A demonstrates the effect of pH values ranging from 6 to 8 on the sensor's performance. It is observed here that the maximum current is achieved at 6.5 pH in the figure. Therefore, all the electrochemical studied are being performed at this pH. Additionally, the AChE/Ag@CuO/PANI/ITO electrode's incubation time is measured by changing the time between 0 to 20 min as shown in Fig. 4.6B).

These observed results demonstrate a gradual decrease in current magnitude within the initial 0 to 6 min. After 6 min, the current reaches saturation, indicating maximum binding of PE with the enzyme (AChE), achieved within 6 min. To optimize the enzyme quantity, the DPV response of the AChE/Ag@CuO/PANI/ITO electrode was examined in presence of 5pM PE and 2 mM ATCl. Fig. 4.6C illustrates that as the AChE concentration increases from 0.025 mg/mL to 0.125 mg/mL, the current response rises until it reaches to 0.1 mg/mL. Beyond this value, the current decreases due to the increased mass transfer resistance, confirming that 0.1 mg/mL is an optimal quantity for effectively catalyzing the hydrolysis of ATCl.

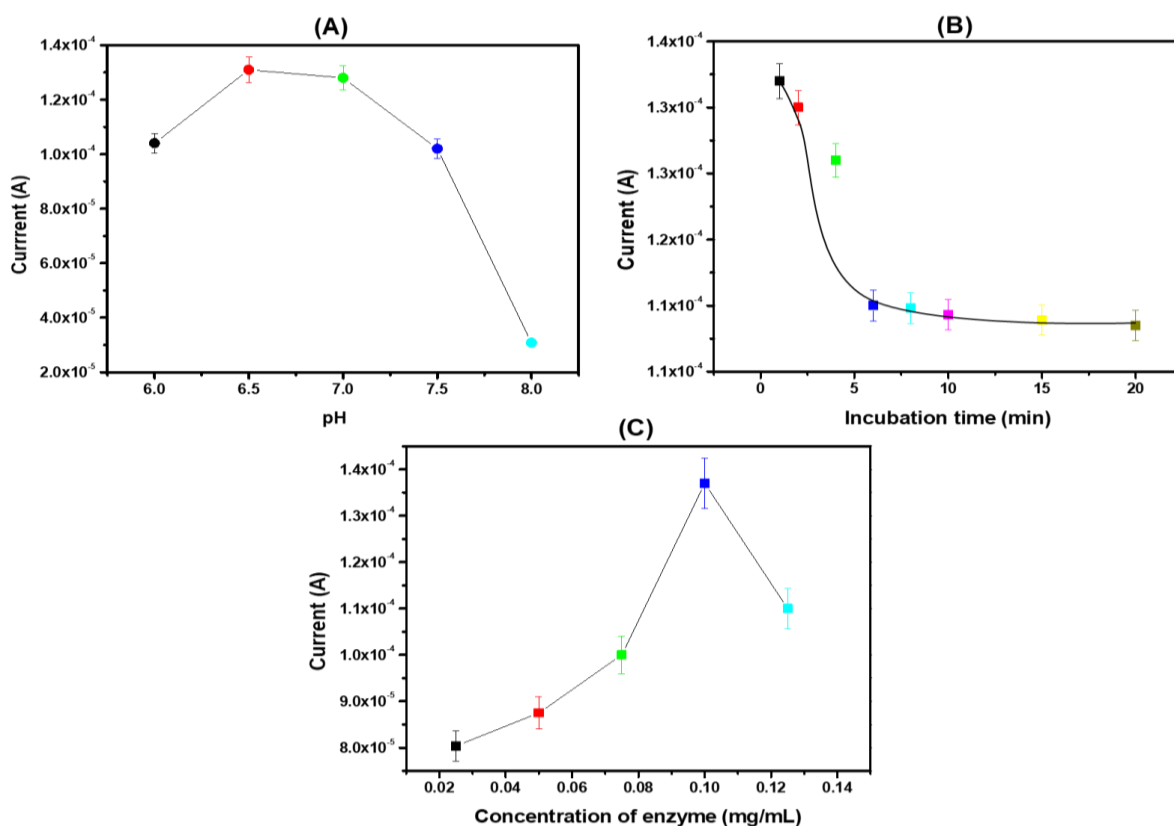


Fig. 4.6. Optimization of (A) effect of pH (6-8 pH), (B) incubation time (0-20 min) of PE (C) concentration of enzyme (0.025 to 0.125 mg/mL)

4.3.5. Electrochemical Biosensing Studies

Electrochemical studies of the AChE/Ag@CuO/PANI/ITO fabricated electrode were conducted as a function of PE conc from 5-100 pM in 6.5 PBS containing 5 mM $[\text{Fe}(\text{CN})_6]^{3-/4-}$ by using the DPV technique. It is observed that the anodic peak current decreases continuously when this developed biosensor was treated with an increasing PE conc as shown in Fig. 4.7A. Such decrease in current is observed because of the inhibition of AChE enzyme by PE. Fig. 4.7B shows the calibration curve of inhibition (ΔI) and PE conc (C_{PE}) and obeys the below-mentioned regression equation:

$$I = 125.09 \mu\text{A} - 0.227 \mu\text{A} (\text{pM})^{-1} \times C_{\text{PE}}; R^2 = 0.9894 \quad \dots (4.13)$$

AChE/Ag@CuO/PANI/ITO electrode's sensitivity (slope/surface area) is calculated and found as $0.55 \mu\text{A} (\text{pM})^{-1} (\text{cm})^{-1}$. Also, a limit of detection is calculated by using a

relationship, i.e., $3\sigma/\text{sensitivity}$ for the developed biosensor where σ is the standard deviation of the blank electrode [7]. The LOD value is found as 11.35 pM in this study. The biosensor's performance is then compared to that of recently developed biosensors designed for the PE detection. The developed biosensor outperforms over all the considered biosensors in terms of sensitivity, detection limit and linear range.

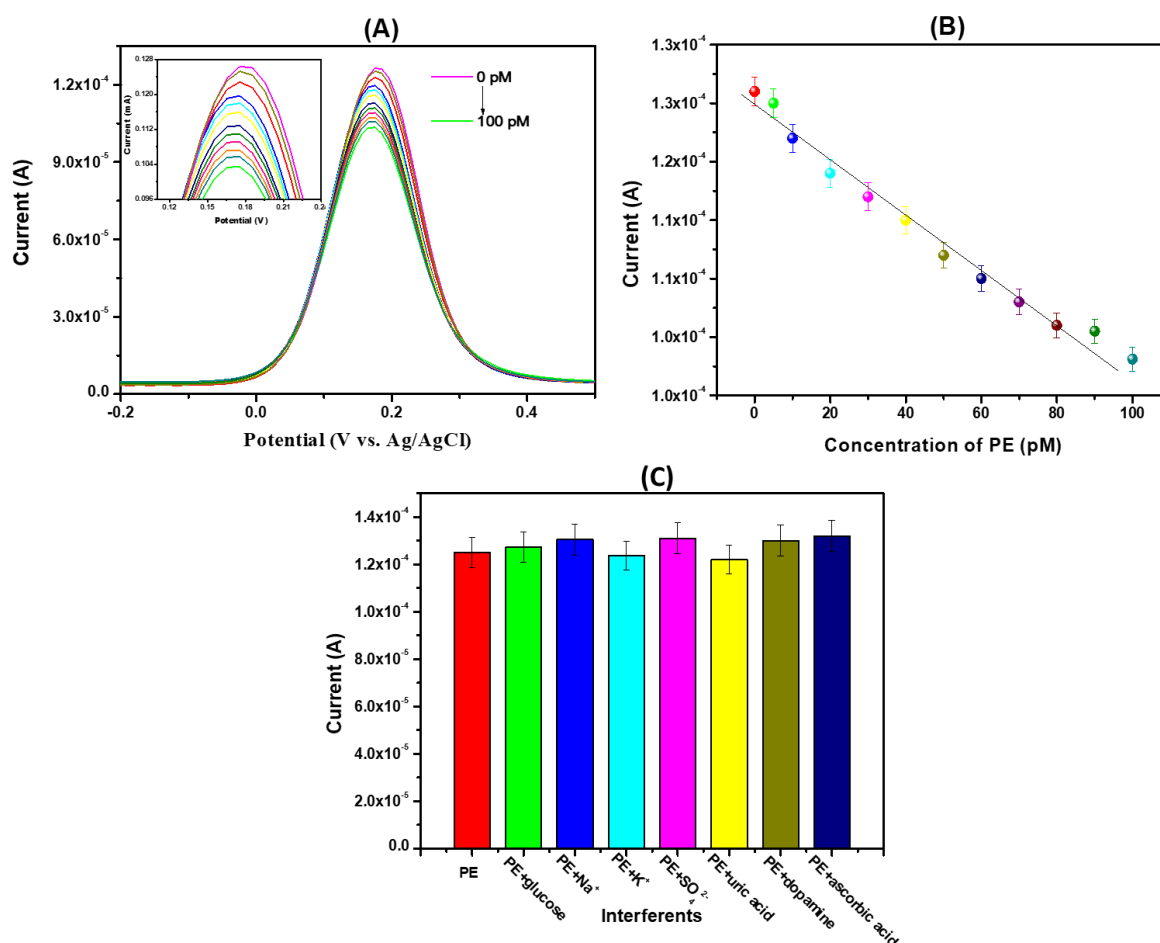


Fig. 4.7. (A) DPV response study of AChE/Ag@CuO/PANI/ITO developed electrode after incubation of various conc of PE (5-100 pM). (B) Calibration curve between current vs. PE conc (C) Interference data in presence of $1 \mu\text{M}$ Na^+ , K^+ , SO_4^{2-} ions, malathion, and uric acid with a coexistence of 5 pM PE

4.3.6. Selectivity and Real Sample Analysis

The selectivity of developed biosensor was studied by incubating AChE/Ag@CuO/PANI/ITO-based sensor with $1\mu\text{M}$ Na^+ , K^+ , SO_4^{2-} ions, ascorbic acid, dopamine, and uric acid with a coexistence of 5 pM PE. Fig. 4.7C clearly shows through a bar diagram that no current change was observed after the addition of these interfering entities which confirms the high selectivity of this biosensor for PE detection.

An applicability of proposed biosensor in real-world scenarios is checked in spiked banana, tomato and soil samples at 5, 10, 20, 30 pM. These results show the acceptable recoveries of 92-111 % and a relative standard deviation (RSD) of < 10% which suggests that the developed biosensor may be a substitute technique for PE detection. All the results are reported in the Table 4.2.

Table 4.2. PE detection in spiked soil, banana and tomato samples using AChE/Ag@CuO/PANI/ITO electrode

| Sample | Added amount (pM) | Found amount (pM) | Recovery (%) | RSD (%) |
|--------|-------------------|-------------------|--------------|---------|
| Soil | 5 | 4.70 | 94 | 4.20 |
| | 10 | 9.40 | 93 | 5.10 |
| | 20 | 18.60 | 93 | 5.50 |
| | 30 | 28.20 | 94 | 5.06 |
| Banana | 5 | 5.25 | 105 | 3.48 |
| | 10 | 10.90 | 109 | 2.94 |
| | 20 | 20.40 | 102 | 2.04 |
| | 30 | 30.90 | 103 | 2.60 |
| Tomato | 5 | 5.45 | 109 | 6.50 |
| | 10 | 7.72 | 111 | 7.72 |
| | 20 | 6.56 | 109 | 6.56 |
| | 30 | 6.02 | 109 | 6.02 |

4.3.7. Reproducibility and Stability Studies

Reproducibility of AChE/Ag@CuO/PANI/ITO electrode was checked by DPV technique in the presence of PE (5 nM) and ATCl (3 mM) using 5 electrodes. The results exhibited a RSD value of 1.74 % suggesting an excellent reproducibility of developed biosensor (Fig. 4.8A).

To check the storage stability of the developed biosensor, the AChE/Ag@CuO/PANI/ITO electrode was kept in a refrigerator set at a temperature of 4°C over a period of 20 days. The response of current remains 71.3 % after the storage of 25 days which confirms the acceptable stability of the biosensor for PE detection (Fig.4.8B).

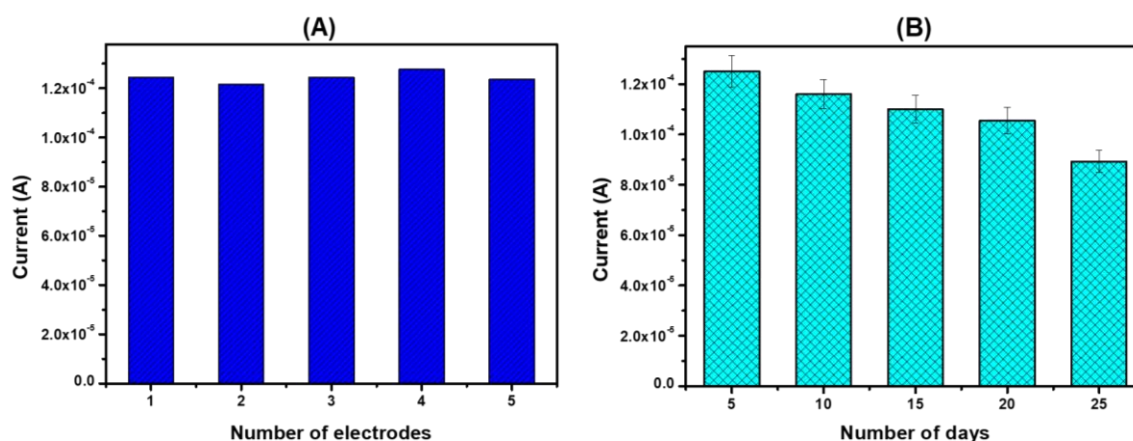


Fig. 4.8. (A) Reproducibility study of PE using different electrodes, (B) Stability study of the fabricated electrodes (AChE/Ag@CuO/PANI/ITO) over a period of 25 days

4.4. Conclusion

In this chapter, a new approach is described for the detection of PE using a synthesized Ag@CuO and PANI-based composite prepared through a chemical method. The composite significantly enhances the selectivity and sensitivity of an AChE based biosensor due to the high surface area and good catalytic property. Three hyperparameters of this biosensor are also optimized to improve its overall efficiency for PE detection. Furthermore, an accuracy and applicability of this developed biosensor in real-world scenarios were assessed using three real

samples. The results obtained from testing the biosensor with these samples confirm its effectiveness, high sensitivity ($0.55 \mu\text{A (pM)}^{-1} \text{cm}^{-2}$), low detection limit (11.35 pM), high selectivity and simplicity in on site detection of PE. This study offers a promising solution for PE detection providing an efficient and reliable method for real-world application.

.

The results of present study have been published in Sensors and Actuators B: Chemical 379, 133270 (2023)

4.5. References

1. He, L., et al., *Novel electrochemical biosensor based on core-shell nanostructured composite of hollow carbon spheres and polyaniline for sensitively detecting malathion*. Sensors Actuators B: Chemical 2018. **258**: p. 813-821.
2. Iqbal, S., et al., *Controlled synthesis of Ag-doped CuO nanoparticles as a core with poly (acrylic acid) microgel shell for efficient removal of methylene blue under visible light*. Journal of Materials Science: Materials in Electronics, 2020. **31**: p. 8423-8435.
3. de Souza, V.S., H.O. da Frota, and E.A.J.J.o.M.S. Sanches, *Polyaniline-CuO hybrid nanocomposite with enhanced electrical conductivity*. Journal of Molecular Structure, 2018. **1153**: p. 20-27.
4. Devagi, P., et al., *Actinobacterial-mediated fabrication of silver nanoparticles and their broad spectrum antibacterial activity against clinical pathogens*. Journal of Nanoscience Nanotechnology 2020. **20**(5): p. 2902-2910.
5. Nagabooshanam, S., et al., *Electro-deposited nano-webbed structures based on polyaniline/multi walled carbon nanotubes for enzymatic detection of organophosphates*. Food Chemistry, 2020. **323**: p. 126784.
6. Jalil, O., C.M. Pandey, and D. Kumar, *Highly sensitive electrochemical detection of cancer biomarker based on anti-EpCAM conjugated molybdenum disulfide grafted reduced graphene oxide nanohybrid*. Bioelectrochemistry, 2021. **138**: p. 107733.
7. Thakur, D., C.M. Pandey, and D. Kumar, *Highly sensitive enzymatic biosensor based on polyaniline-wrapped titanium dioxide nanohybrid for fish freshness detection*. Applied Biochemistry Biotechnology 2022. **194**(8): p. 3765-3778.

CHAPTER 5

CeO₂ embedded Polyaniline modified Electrochemical Biosensor for Paraoxon-Ethyl Detection

5.1. Introduction

In this chapter, the biosynthesized CeO₂ nanocrystals are incorporated into the PANI matrix by using a chemical oxidative method. The prepared composite is further used as a sensing electrode for the PE detection. It is observed that the properties of CeO₂ and PANI effectively enhance the performance of the developed biosensor. The excellent bio affinity of PANI towards the AChE enzyme also enhances the degree of immobilization. The redox nature and strong catalyzing power towards the phosphorylation reaction of CeO₂ enhance the electron kinetics. The biosensor shows high sensitivity and selectivity for PE detection. Moreover, it shows high stability due to the biocompatible nature of CeO₂ with AChE enzyme. The biosensor is also successfully applied in real-world samples.

5.2. Experimental Section

5.2.1. Synthesis of CeO₂ Nanocrystals

For synthesizing the CeO₂ nanocrystals, the *Musa sapientum* fruit was washed, dried and crushed. After that, the extraction process was done by the soaking method using water as a solvent. In this process, the 10 g dried powder of *Musa sapientum* fruit was soaked in 50 mL DI water for 24 h in a conical flask followed by shaking the solution at 500 rpm for 1h. Then, the resultant extract was filtered using Whatman filter paper. The obtained filtrate (stored at 0-4°C) was further diluted by DI water in the ratio of 1:4, i.e., 10 mL filtrate diluted by 40 mL water. Subsequently, the aqueous solution of cerium nitrate hexahydrate (2.17 g in 50 mL DI water) was added and then the resultant solution was stirred for 15 min. Further,

4M NaOH was added till the pH of solution reached at 10, then the solution was stirred for 4 h at 75°C. This solution was centrifuged at 3000 rpm for 10 min and then washed for 2 to 3 times using DI water. The white precipitate so obtained was dried at 80°C and calcined at 300°C with heating rate 4°C/min in a muffle furnace for 2 h.

5.2.2. Synthesis of CeO₂/PANI-based Composite

CeO₂@PANI-based composite has been synthesized through in-situ polymerization method in the presence of CeO₂ nanocrystal. In this process, 0.2 g of CeO₂ and 0.72 mL aniline were dispersed in 100 mL HCl (2M) through constant stirring for 2h. Subsequently, 0.5 M ammonium per sulphate (2.28 g in 20 mL DI water) was added under constant stirring. This solution was subsequently stirred for 24 h at room temperature which is leading to the formation of a composite based on CeO₂@PANI. The resultant composite was centrifuged at 4000 rpm and then washed by using a mixture of ethanol and water (1:1). The black-coloured precipitate was dried at 60°C.

5.2.3. Electrophoretic Deposition of CeO₂@PANI Composite and Fabrication of Biosensor

The deposition of prepared composite material was carried out by electrophoretic deposition technique. For this deposition process, firstly, the suspension of 0.1 mg PANI and CeO₂@PANI were prepared in a mixed solution of ethanol and water (1:10) by using the sonication. Subsequently, 12 V DC voltage is applied for 12 sec for a smooth deposition of PANI and CeO₂@PANI-based composite.

For the biosensor fabrication, 25 µL of prepared AChE solution containing the 0.1 mg/ml in 7pH PBS is drop casted onto the CeO₂@PANI modified ITO surface. Finally, the developed biosensor was kept in moist condition at 4°C for 18 h. Fig. 5.1 illustrates the fabrication of the CeO₂@PANI/ITO biosensor.

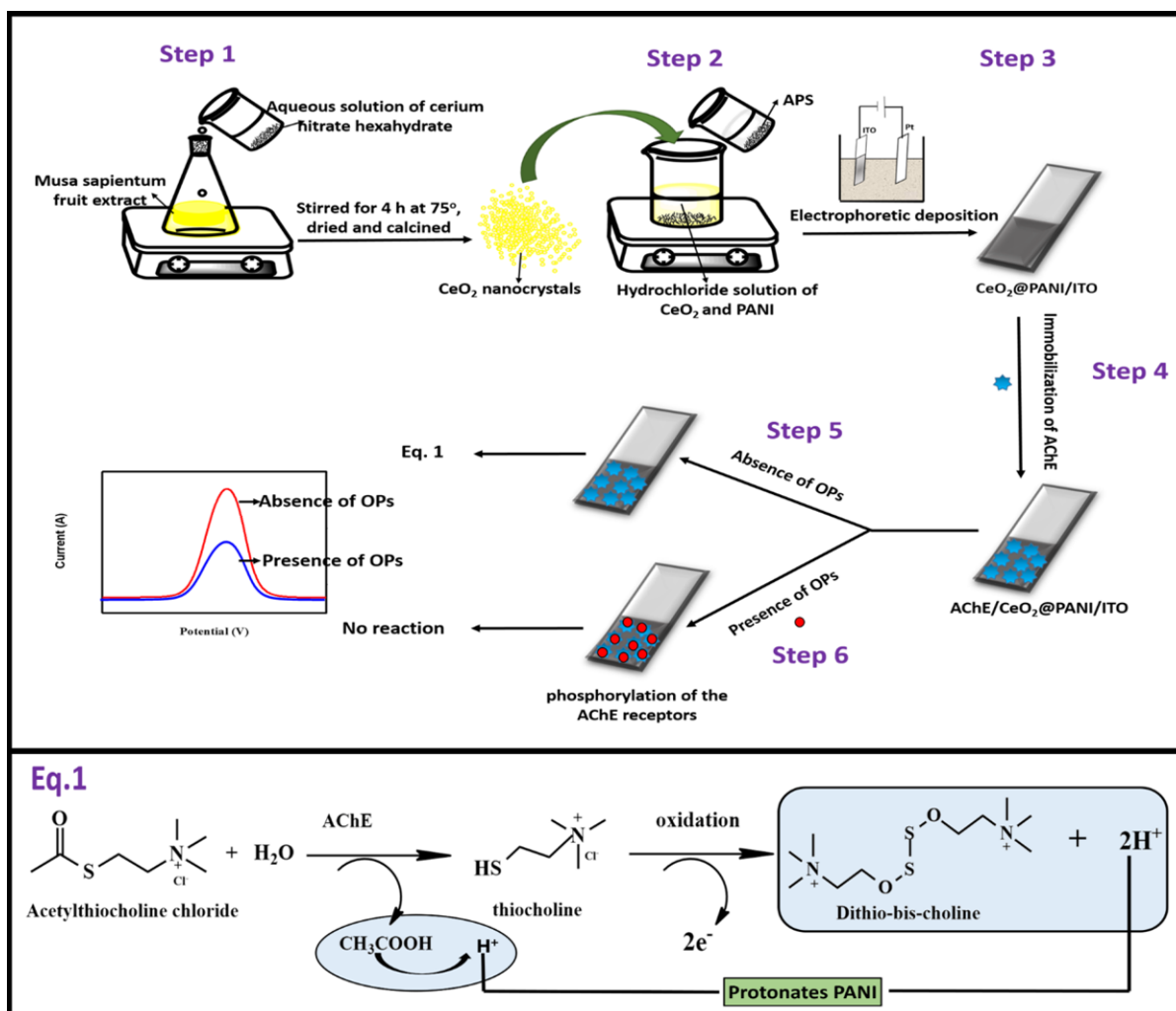


Fig. 5.1. Schematic diagram of biosensor fabrication and working mechanism for PE detection

5.3. Results and Discussion

5.3.1. Design of Sensor

In the proposed biosensor, CeO₂ and PANI was utilized as a sensing platform due to their specific characteristics for pesticide determination. For the fabrication of AChE/CeO₂@PANI/ITO biosensor, firstly, biosynthesis of CeO₂ nanocrystals was carried out by using *Musa sapientum* fruit extract (Fig. 5.1, step 1). Then, the prepared nanocrystals were incorporated into the PANI matrix (Fig. 5.1, step 2). The composite was further deposited by electrophoretic deposition technique onto the ITO coated substrate (Fig. 5.1, step 3) and then

AChE enzyme has been immobilized onto the surface of developed electrode (Fig. 5.1, step 4). Finally, the OPs detection was carried out by monitoring the current obtained in the presence and absence of OPs. In the absence of OPs, the AChE enzyme behaves like a catalyst for ATCl hydrolysis. In this hydrolysis reaction, the electroactive products such as thiocholine and acetic acid were formed as the main products. The thiocholine gets oxidized into dithio-bis-choline and releases two electrons. Simultaneously, an acetic acid also releases protons (H^+) on the electrode surface. These released protons protonate the PANI and produce a signal (Fig. 5.1, step 5). While the presence of OPs causes phosphorylation of the AChE receptors and inhibits its catalyzing property which finally decreases the peak current [1] (Fig. 5.1, step 6).

5.3.2. Structural, Morphological and Elemental Studies

The structural characterization of all the prepared materials was done by XRD and FTIR spectroscopy. Fig. 5.2(A) illustrates the XRD pattern of PANI (curve a), CeO_2 (curve b) and $CeO_2@PANI$ (curve c) nanocomposite. In curve (a), the broad peak at $2\theta = 25^\circ$ confirms the formation of PANI and illustrates its amorphous nature [2]. In curve (b), the diffraction peaks located at 29° , 33.5° , 47.8° , 56.8° , 70.1° , 76.9° , and 79.5° confirm the successful synthesis of CeO_2 [3]. While in curve (c), all the peaks of PANI and CeO_2 are present which confirm that the CeO_2 nanoparticles are successfully incorporated into the matrix of PANI.

The FTIR spectra of CeO_2 (curve a), PANI (curve b) and $CeO_2@PANI$ (curve c) are shown in Fig. 5.2(B). In curve (a), large absorption bands appear at 422 and 712 cm^{-1} which correspond to the Ce-O bond vibrations. The bands at 1059 and 1331 cm^{-1} appear due to the vibrational modes of Ce-O-Ce bonds. The band appears at 1621 cm^{-1} is due to the bending vibrations of absorbed H_2O [4]. In curve (b), the absorption band appears at 1119 cm^{-1} is characteristic band of PANI (N-Quinoid-N, stretching vibration). The bands appear at 1222

and 1297 cm^{-1} correspond to the C-N stretching vibrations in the ring. Also, the absorption bands located at 1476 and 1565 cm^{-1} are due to the C=C stretching vibrations in the benzenoid and quinoid rings, respectively. The bands confirm that curve (b) represents the FTIR spectra of PANI. The FTIR spectra of CeO_2 @PANI composite (curve c) is almost similar to the FTIR spectra of PANI. The characteristic vibrational bands of CeO_2 are not distinguished in FTIR spectra of CeO_2 @PANI composite due to very intensive bands of PANI. It can only be noticed in curve (c) that the intensity of the bands (characteristic band of PANI and C-N stretching vibrations) decreases and some shifting of the band appear (the band shifts from 1119 to 1167 cm^{-1}). All these changes appear due to the interaction of nitrogen (present in PANI) and the oxide of CeO_2 which further confirms that the CeO_2 was successfully incorporated in the matrix of PANI [5].

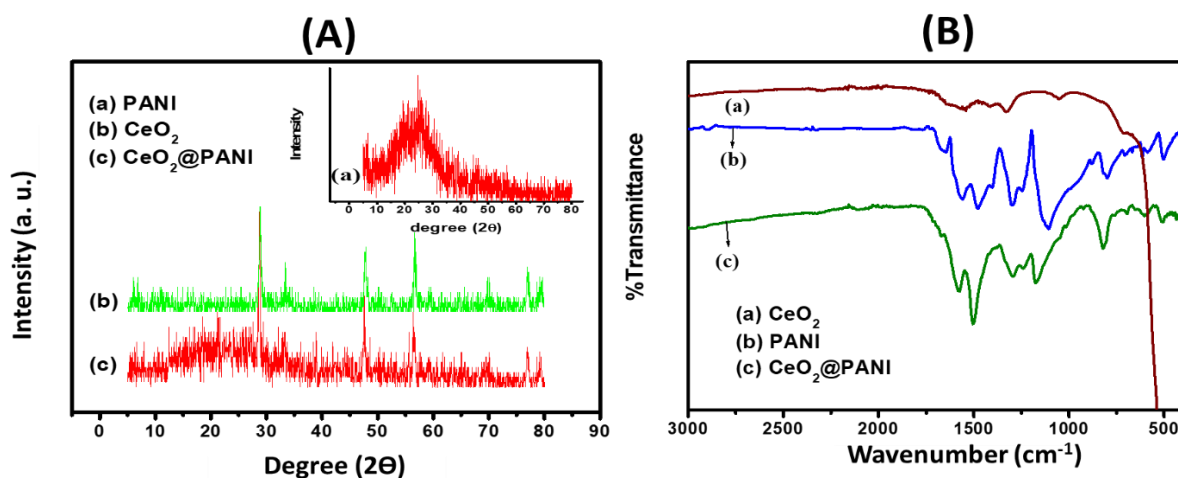


Fig. 5.2. (A) XRD curves of (a) PANI (b) CeO_2 (c) CeO_2 @PANI (B) FTIR spectra of (a) CeO_2 (b) PANI and (c) CeO_2 @PANI

The morphological characterization was done by the SEM and TEM techniques. Fig. 5.3(A) and 5.3(B) illustrates the SEM and TEM micrographs of CeO_2 nanocrystals. It is clear from the Fig. 5.3(B) that the diameter of CeO_2 nanocrystals is found in the range between 10 to 50 nm . The SEM and TEM micrographs of the CeO_2 @PANI composite are depicted in the

Fig. 5.3(C) and 5.3(D), respectively. It is clear from these figures that the CeO_2 nanocrystals are uniformly spread over the matrix of PANI which ensures that the composite material has optimal properties like enhanced catalytic activity, surface area, and stability.

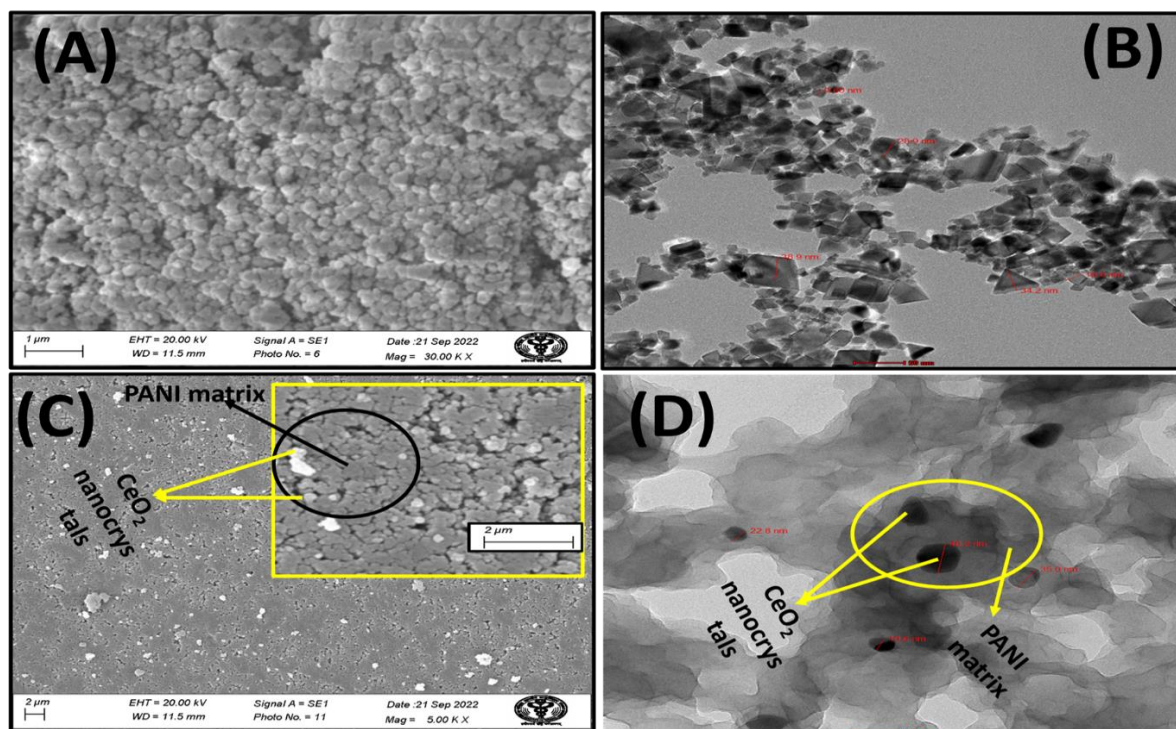


Fig. 5.3. (A) SEM micrograph of CeO_2 nanocrystals (B) TEM micrograph of CeO_2 nanocrystals (C) SEM micrograph of CeO_2 @PANI composite (D) TEM micrograph of CeO_2 @PANI composite

The energy dispersive X-ray (EDAX) spectra of CeO_2 nanocrystal is shown in Fig. 5.4(A). This figure clearly displays all the peaks associated with Ce and O which confirms that the CeO_2 was successfully synthesized. Moreover, in the EDAX spectra of the composite (Fig. 5.4B), the peaks of carbon (C), nitrogen (N), oxygen (O) and cerium (Ce) were observed which confirms the formation of the CeO_2 @PANI composite. In both EDAX spectra (Fig. 5.4A and 5.4B), an additional peak of Au was observed due to the sample's coating with gold for EDAX analysis.

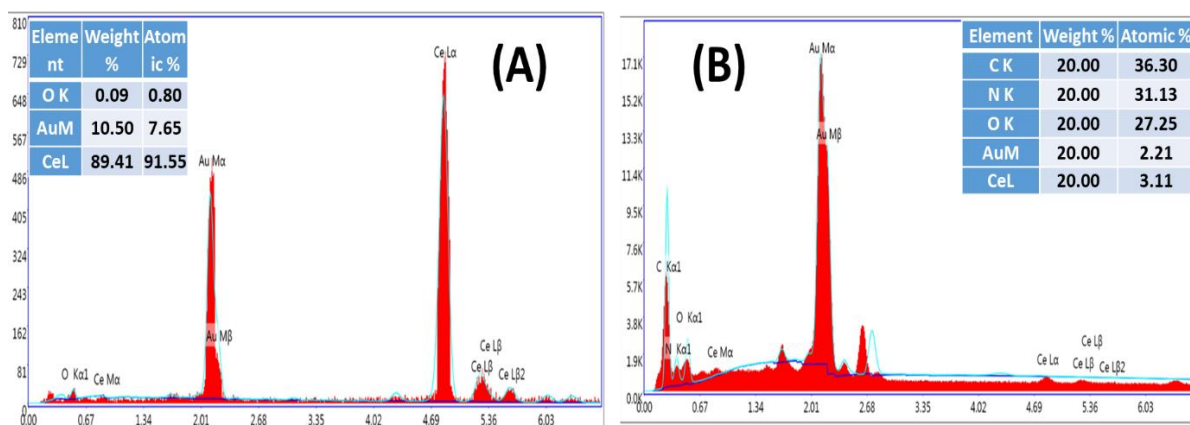


Fig. 5.4. SEM-EDAX analysis of (A) CeO₂ and (B) CeO₂@PANI-based composite

5.3.3. Electrochemical Characterization

Electrochemical studies of all the developed electrodes were done by the cyclic voltammetry (CV) technique in a phosphate buffer (0.2 M PBS) at pH 7.4 as used in the previous chapter. Fig. 5.5(A) illustrates the peak currents of CeO₂@PANI/ITO, AChE/CeO₂@PANI/ITO, PANI/ITO and ITO electrodes at 50 mV/sec scan rate which can be seen in curves (a), (b), (c) and (d), respectively. This figure clearly illustrates that the CeO₂@PANI/ITO electrode shows the highest peak current which signifies its high conducting nature among all the developed electrodes. The conductivity of AChE enzyme immobilized biosensor is found to decrease (curve b, 0.48 mA) due to a non-conducting behaviour of immobilized protein [6].

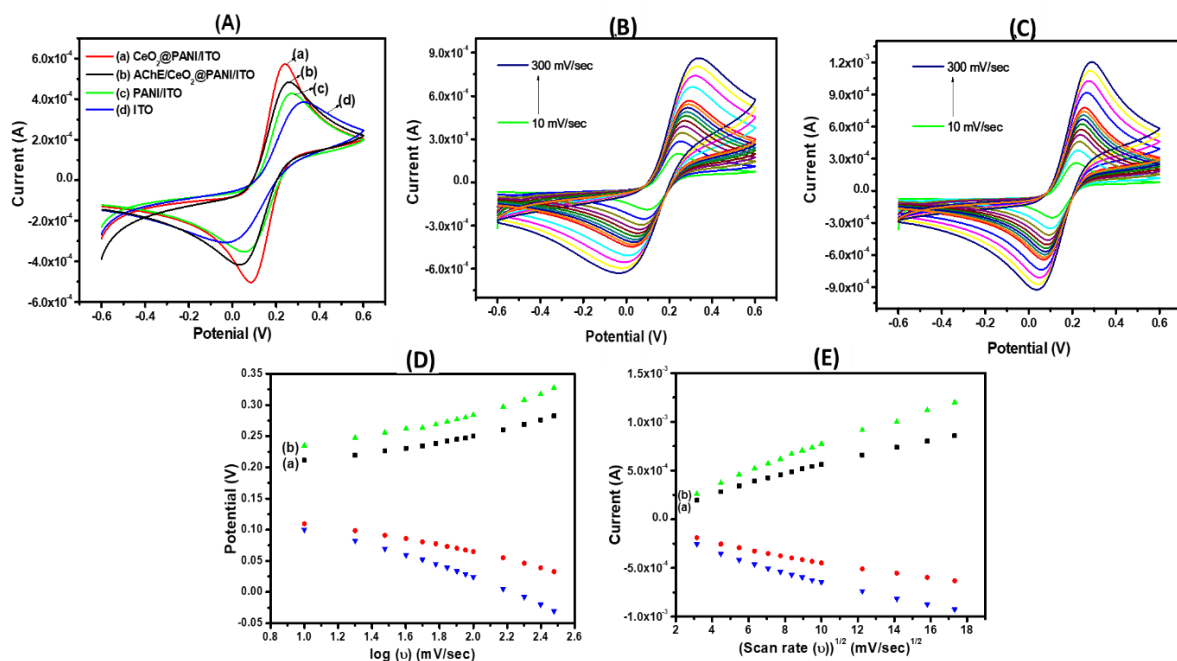


Fig. 5.5. (A) Cyclic voltammogram of CeO₂@PANI/ITO (a), AChE/CeO₂@PANI/ITO (b), PANI/ITO (c) and ITO (d) at scan rate 50 mV/sec. CV curves of (B) PANI/ITO (C) CeO₂@PANI/ITO at various scan rates (10 - 300 mV/sec) (D) Plots of current vs. square root of scan rate in case of PANI (a) and CeO₂@PANI (b) (E) Plots of potential vs. log (scan rate) for CeO₂@PANI/ITO (a) and PANI/ITO (b)

Fig. 5.5(B) and 5.5(C) illustrate the CV studies at a scan rate varying in the range of 10-300 mV/sec of PANI/ITO and CeO₂@PANI/ITO electrodes. These graphs illustrate that as the value of scan rate increases from 10 to 300 mV/sec, an oxidation and reduction peak currents shift to more positive and more negative values, respectively. This shifting suggests a linear relationship between the peak potentials and log of scan rates having cathodic and anodic slopes of $2.303RT/\alpha nF$ and $2.303RT/(1-\alpha)nF$, respectively as shown in Fig. 5.5D. These slopes are obtained by using the following equations and also used for calculating the electron transfer coefficient (α).

$$E_{pa} [\text{CeO}_2\text{@PANI/ITO}] = 0.0599 \text{ (V)} \times \log (\nu) \text{ (mVsec}^{-1}\text{)} + 0.1543 \text{ (V)} ; R^2 = 0.9670 \dots (5.1)$$

$$E_{pc} [\text{CeO}_2@\text{PANI}/\text{ITO}] = -0.0591 (\text{V}) \times \log (v) (\text{mVsec}^{-1}) + 0.1677 (\text{V}) ; R^2 = 0.9824 \dots (5.2)$$

$$E_{pa} [\text{PANI}/\text{ITO}] = 0.0619 (\text{V}) \times \log (v) (\text{mVsec}^{-1}) + 0.1635 (\text{V}) ; R^2 = 0.9580 \dots (5.3)$$

$$E_{pc} [\text{PANI}/\text{ITO}] = -0.090 (\text{V}) \times \log (v) (\text{mVsec}^{-1}) + 0.2011 (\text{V}) ; R^2 = 0.9828 \dots (5.4)$$

The calculated value of α for PANI/ITO and CeO₂@PANI/ITO developed electrodes are summarized in Table 5.1.

Fig. 5.5(E) represents a linear relationship between the peak current and square root of scan rate of PANI/ITO and CeO₂@PANI/ITO developed electrodes. It clearly indicates that the process of electron transfer through these electrodes is found as a surface-controlled process and it obeys the below mentioned equations [7]:

$$I_{pa} [\text{CeO}_2@\text{PANI}/\text{ITO}] = 64.8 \mu\text{A} / (\text{mVsec}^{-1}) \times v^{1/2} + 104.3 (\mu\text{A}) ; R^2 = 0.9932 \dots (5.5)$$

$$I_{pc} [\text{CeO}_2@\text{PANI}/\text{ITO}] = -45.7 \mu\text{A} / (\text{mVsec}^{-1}) \times v^{1/2} - 165.9 (\mu\text{A}) ; R^2 = 0.9846 \dots (5.6)$$

$$I_{pa} [\text{PANI}/\text{ITO}] = 45.61 \mu\text{A} / (\text{mVsec}^{-1}) \times v^{1/2} + 93.03 (\mu\text{A}) ; R^2 = 0.9916 \dots (5.7)$$

$$I_{pc} [\text{PANI}] = -30.2 \mu\text{A} / (\text{mVsec}^{-1}) \times v^{1/2} - 130.1 (\mu\text{A}) ; R^2 = 0.9842 \dots (5.8)$$

Based on these equations (Eq. 5.5 to 5.9) and the Randle Sevcik equation as mentioned below (Eq. 5.9), the values of diffusion constant (D) and effective surface area (A) were calculated [8]. The calculated values of D and A are summarized in Table 5.1.

$$I_p = 0.45 \text{ nAFC} (n\nu\text{FD}/\text{RT})^{1/2} \text{ or } I_p = 2.69 \times 10^5 n^{3/2} D^{1/2} C v^{1/2} \text{ A} \dots (5.9)$$

Here, n = number of transferred electrons for the redox process, C = conc of [Fe(CN)₆]^{3-/4-} in mol/cm³, F is the Faraday constant in C/mol, D = diffusion coefficient in cm²/sec, v = scan rate in V/ sec and R = gas constant in C K⁻¹ mol⁻¹.

The peak current studies of all the electrodes were further used to calculate the surface coverage (Γ) using the equation $I_p = n^2 F^2 A \Gamma v / 4RT$. The values of Γ for PANI/ITO and CeO₂@PANI/ITO electrodes are also reported in Table 5.1.

Table 5.1. Kinetic parameters of PANI/ITO and CeO₂@PANI /ITO electrodes

| Modified electrodes | Diffusion coefficient (D) (cm ² /sec) | Effective surface area (A) (cm ²) | Electron transfer coefficient (α) | Surface coverage (Γ) (mol/cm ²) |
|-----------------------------|--|---|--|--|
| PANI/ITO | 1×10^{-2} | 4.18×10^{-1} | 0.65 | 2.14 |
| CeO ₂ @PANI /ITO | 1.32×10^{-2} | 4.22×10^{-1} | 0.99 | 2.88 |

5.3.4. Optimization Studies

For optimal bioelectrode response for OPs detection, various parameters like pH of electrolytic solution and the incubation time of pesticide have been investigated by using the differential pulse voltammetry measurement. Fig. 5.6(A) illustrates the effect of pH (6-8) on the activity of enzyme in the developed biosensor. This figure clearly shows that the highest current is obtained at pH 7. Thus, this optimum pH value has been used in subsequent biosensing studies.

The incubation time of OPs on the fabricated electrode surface has been examined by changing the time between 0 to 10 min as shown in Fig. 5.6B. This can be seen in the figure that the response of current saturates within 6 min which indicates that the maximum binding of OPs has been achieved with the AChE enzyme during this time period.

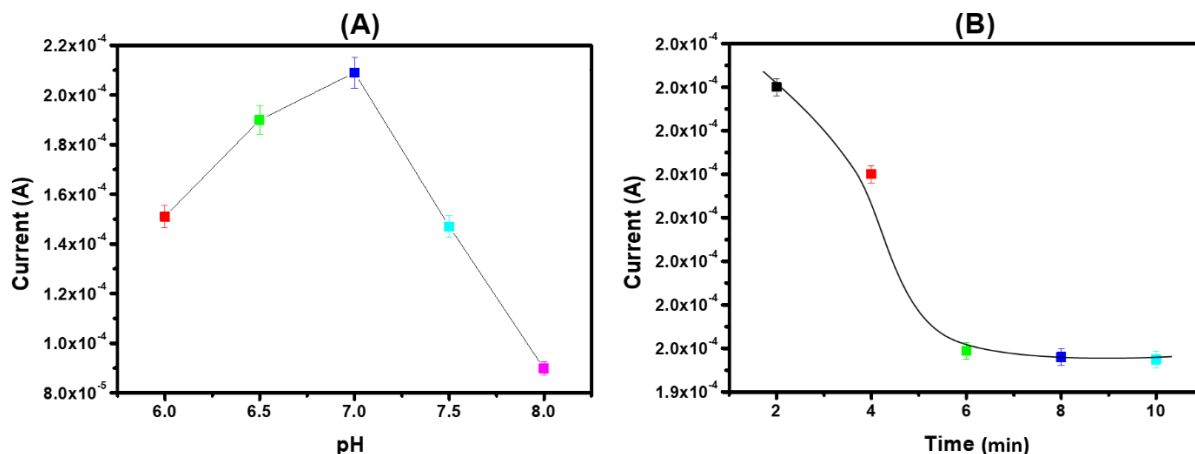


Fig. 5.6. Optimization of (A) effect of pH (6-8 pH), (B) incubation time (0-10 min) of PE

5.3.5. Electrochemical Biosensing Studies

The performance of AChE/CeO₂@PANI/ITO biosensor towards the PE detection was examined by the differential pulse voltammetry which is shown in Fig. 5.7A. The Fig. 5.7A clearly illustrates that a peak current decrease gradually as the concentration of OPs increases. Such a decrease in peak current is due to the phosphorylation of AChE receptors by OPs which leads to the formation of an enzyme-inhibitor complex and reduces the availability of enzyme for catalyzing the ATCl hydrolysis. A plot of current vs. OPs concentration for PE is given in Fig. 5.7(B). It is clearly seen in the figure that a calibration plot follow the linearity which is defined by a regression equation given as below:

$$I = 177.46 \mu\text{A} - 0.27 \mu\text{A/pM} \times C_{\text{PE}} \quad \dots(5.10)$$

The regression equation was further used to calculate the sensitivity (S) (slope/effective surface area) and detection limit (LOD) ($3\sigma / S$) of the fabricated sensor. Here, the standard deviation of blank electrode is represented by a symbol σ [9]. The sensitivity and LOD values for PE detection were found to be $0.59 \mu\text{A (pM)}^{-1} \text{cm}^{-2}$ and 5.55 pM, respectively.

5.3.6. Selectivity and Real sample studies

Selectivity of AChE/CeO₂@PANI/ITO-based biosensor was studied by using a DPV technique in the presence of some interferents like uric acid (UA), ascorbic acid (AA), glucose

and metal ions (Na^+ , K^+ , Cu^{2+}) and anion (SO_4^{2-}). For this study, 10 pM of mentioned interferents were mixed with 10 pM of PE. The bar diagram confirms that there were no significant changes in peak currents when the developed biosensor was subjected to interferent analytes which reveals the good selectivity for PE detection (Fig. 5.7C).

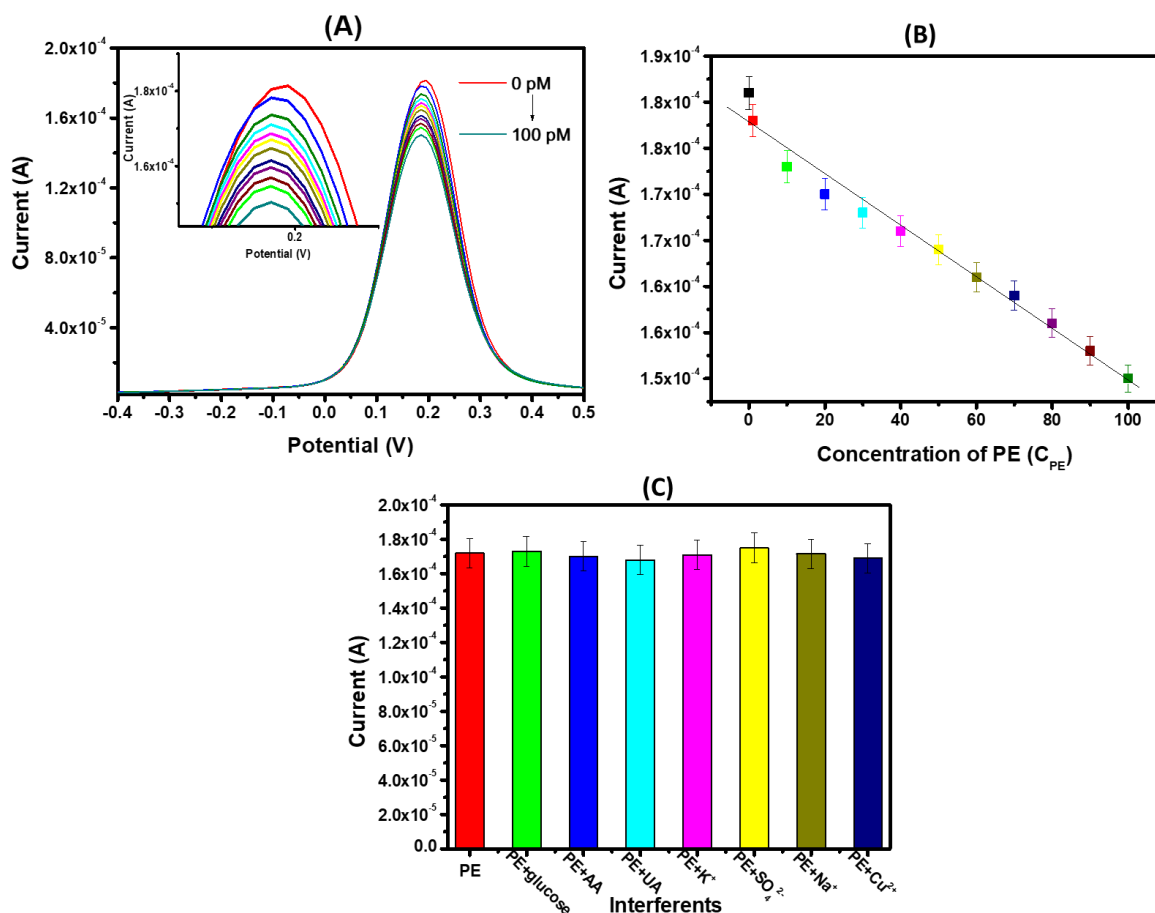


Fig. 5.7. (A) DPV response study of AChE/CeO₂@PANI/ITO developed electrode after incubation of various conc (1-100 pM) of PE (B) Calibration graph of current vs. conc (C) Interference data in presence of 10 pM glucose, ascorbic acid, uric acid, K⁺, SO₄²⁻ ions, Na⁺, Cu²⁺ with the coexistence of 10 pM PE

The real sample analysis for carrot and soil was conducted to validate the accuracy and real-world applicability of the developed biosensor. All the results have been presented in the following Table (Table 5.2). These results also confirm the satisfactory recovery (100.5-107 %) and good accuracy (RSD<5%) of developed biosensor.

Table 5.2. Detection of PE in Spiked Soil and Carrot Samples using AChE/CeO₂@PANI/ITO Electrode

| Real samples | Added amount (pM) | Found amount (pM) | Recovery (%) | RSD (%) |
|--------------|-------------------|-------------------|--------------|---------|
| Carrot | 10 | 10.2 | 102 | 2.0 |
| | 20 | 20.6 | 103 | 2.5 |
| | 30 | 30.9 | 103 | 2.1 |
| | 40 | 41.6 | 104 | 3.0 |
| Soil | 10 | 10.1 | 101 | 0.8 |
| | 20 | 20.2 | 101 | 0.9 |
| | 30 | 30.2 | 101 | 0.8 |
| | 40 | 40.4 | 101 | 1.4 |

5.3.7. Reproducibility and Stability Studies

Reproducibility of developed biosensor was also measured by conducting a series of repetitive DPV analyses in presence of 10 pM PE (Fig. 5.8A). The relative standard deviation (RSD) of 1.23 % was calculated using five different AChE/CeO₂@PANI/ITO electrodes which confirm its excellent reproducibility.

The stability of AChE/CeO₂@PANI/ITO electrodes was also checked using DPV technique when the electrode was stored at 4°C. After 35 days, a current response remains 94.2 % of its initial peak current value that demonstrates its good stability as shown in Fig. 5.8B.

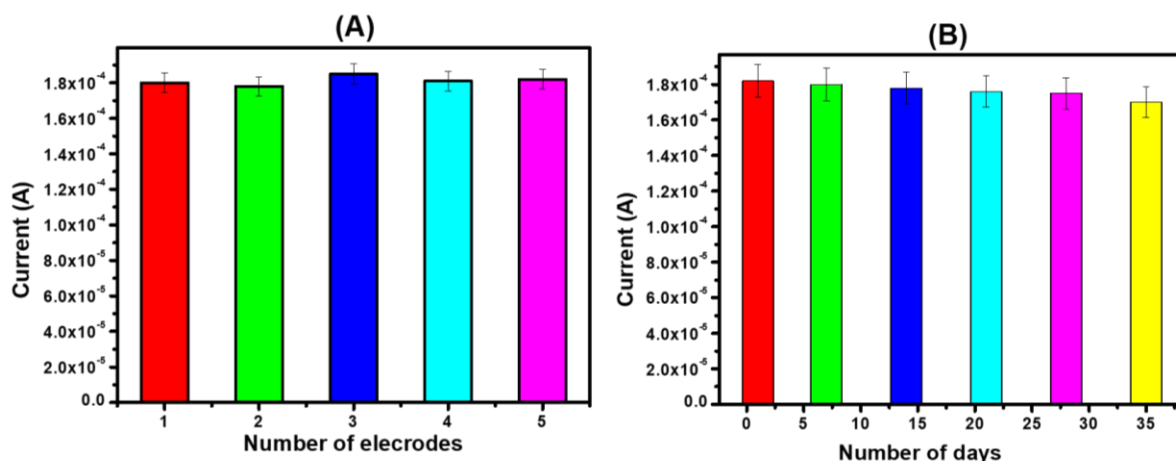


Fig. 5.8. (A) Reproducibility study of PE using different electrodes (B) Stability study of the fabricated electrodes (AChE/CeO₂@PANI/ITO) over a period of 40 days

5.4. Conclusion

In this work, the biosynthesized CeO₂ nanocrystal was successfully incorporated into the matrix of PANI. The prepared CeO₂ and PANI-based composite was explored as a sensing electrode for multiple OPs detection. For better performance, the biosensor was optimized using two parameters. It shows an excellent sensitivity of $0.59 \mu\text{A (pM)}^{-1} (\text{cm})^{-2}$ and a low detection limit (LOD) of 5.55 pM for three OPs detection. Moreover, it shows the good reproducibility, selectivity and permissible stability. This fabricated biosensor shows the outstanding results in all metrics over the reported nonenzymatic and enzymatic biosensors. It can be concluded that this work provides an effective platform for multiple OPs detection.

5.5. References

1. He, L., et al., *Novel electrochemical biosensor based on core-shell nanostructured composite of hollow carbon spheres and polyaniline for sensitively detecting malathion*. Sensors Actuators B: Chemical 2018. **258**: p. 813-821.
2. de Souza, V.S., H.O. da Frota, and E.A.J.J.o.M.S. Sanches, *Polyaniline-CuO hybrid nanocomposite with enhanced electrical conductivity*. Journal of Molecular Structure, 2018. **1153**: p. 20-27.
3. Jayakumar, G., A.A. Irudayaraj, and A.D. Raj, *Investigation on the synthesis and photocatalytic activity of activated carbon–cerium oxide (AC–CeO₂) nanocomposite*. Applied Physics A, 2019. **125**(11): p. 1-9.
4. Javad Farhangi, M., et al., *MOF-mediated synthesis of CuO/CeO₂ composite nanoparticles: Characterization and estimation of the cellular toxicity against breast cancer cell line (MCF-7)*. Journal of Functional Biomaterials, 2021. **12**(4): p. 53.
5. Kuzmanović, B., et al., *The influence of oxygen vacancy concentration in nanodispersed non-stoichiometric CeO₂- δ oxides on the physico-chemical properties of conducting polyaniline/CeO₂ composites*. Electrochimica Acta, 2019. **306**: p. 506-515.
6. Nagabooshanam, S., et al., *Electro-deposited nano-webbed structures based on polyaniline/multi walled carbon nanotubes for enzymatic detection of organophosphates*. Food Chemistry, 2020. **323**: p. 126784.
7. Paneru, S. and D. Kumar, *A Novel Electrochemical Biosensor Based on Polyaniline-Embedded Copper Oxide Nanoparticles for High-Sensitive Paraoxon-Ethyl (PE) Detection*. Applied Biochemistry Biotechnology 2023: **195** p. 1-18.

8. Jalil, O., C.M. Pandey, and D. Kumar, *Highly sensitive electrochemical detection of cancer biomarker based on anti-EpCAM conjugated molybdenum disulfide grafted reduced graphene oxide nanohybrid*. *Bioelectrochemistry*, 2021. **138**: p. 107733.
9. Thakur, D., C.M. Pandey, and D. Kumar, *Highly sensitive enzymatic biosensor based on polyaniline-wrapped titanium dioxide nanohybrid for fish freshness detection*. *Applied Biochemistry Biotechnology* 2022. **194**(8): p. 3765-3778.

CHAPTER 6

CuO and PEDOT:PSS grafted Whatman paper based Biosensor for PE Detection

6.1. Introduction

This chapter describes the fabrication of a biodegradable and cost-effective biosensor based on CuO and PEDOT:PSS grafted paper as a sensing electrode for paraoxon-ethyl detection. The CuO and PEDOT:PSS were deposited onto the surface of Whatman paper by a simple dip-coating method. The workability, stability and conductivity of the fabricated electrode is enhanced by the treatment of ethylene glycol (EG). The fabricated biosensor shows the sensitivity as high as 9.12 $\mu\text{A/nM}$ and a low LOD value as 0.42 nM. It is also applied for the PE detection in two real samples. All the results confirm that the developed biosensor may be a promising substitute to the available sensing platforms.

6.2. Experimental Section

6.2.1. Synthesis of CuO Nanoparticles

The co-precipitation method was utilized for the preparation of CuO nanoparticles. In this method, firstly, 1.5 g of $\text{CuSO}_4 \cdot 5\text{H}_2\text{O}$ is dissolved in 50 mL DI water with a constant stirring for a duration of 30 min. Thereafter, 0.12 g of sodium lauryl sulfate was added with continuous stirring at a temperature of 90°C. Further, 0.4 M NaOH was added till the pH becomes 14. The obtained solution was stirred further for 6 h. Finally, a black-coloured precipitate so obtained was centrifuged and then washed with deionized water followed by ethanol. It was dried overnight at 50°C and then calcined by heating in the absence of air at 800°C for 4 h [1].

6.2.2. Fabrication of PEDOT: PSS/WP and CuO@PEDOT: PSS/WP and EG-treated CuO@PEDOT: PSS/WP Conducting Papers

To fabricate the PEDOT: PSS and CuO@PEDOT: PSS-based conducting papers, a series of steps were followed. Firstly, the Whatman paper (WP) was stabilized by treating it with a solution of surfactant (tween-20) in DI water. Thereafter, it was subjected to ultrasonication in the ethanol for 15 min to ensure a proper cleaning and subsequently kept at 60°C for the purpose drying. The prepared paper electrodes were then immersed in the aqueous dispersion of PEDOT: PSS and CuO@PEDOT: PSS for a duration of 1 h. This step allowed the deposition of PEDOT:PSS onto the surface of the paper. To improve the flexibility, mechanical strength and conductivity of the paper substrate, this dipping process was repeated thrice. Each repetition contributed to the accumulation of additional layers of PEDOT:PSS and CuO@PEDOT:PSS on the paper substrate. Subsequently, the conducting paper substrate was treated by using ethylene glycol for a period of 5 min. This treatment aimed to further increase the conductivity of the paper. After the ethylene glycol treatment, the conducting paper was dried at a higher temperature of 100°C which helped to remove any residual solvent and ensure the stability of the fabricated conducting paper [2].

6.2.3. Biosensor Fabrication

In the biosensor fabrication, 20 μ L solution of enzyme (at 0.1 mg/mL concentration) was carefully applied onto the surface of developed electrode. Once the enzyme solution was applied, the biosensor has been incubated at a temperature of 4°C for a duration of 12 h in a humid chamber. This incubation time allowed the enzyme to bind to the surface of the electrode and form a stable and functional biosensing interface. A schematic diagram of biosensor fabrication is presented in the Fig. 6.1.

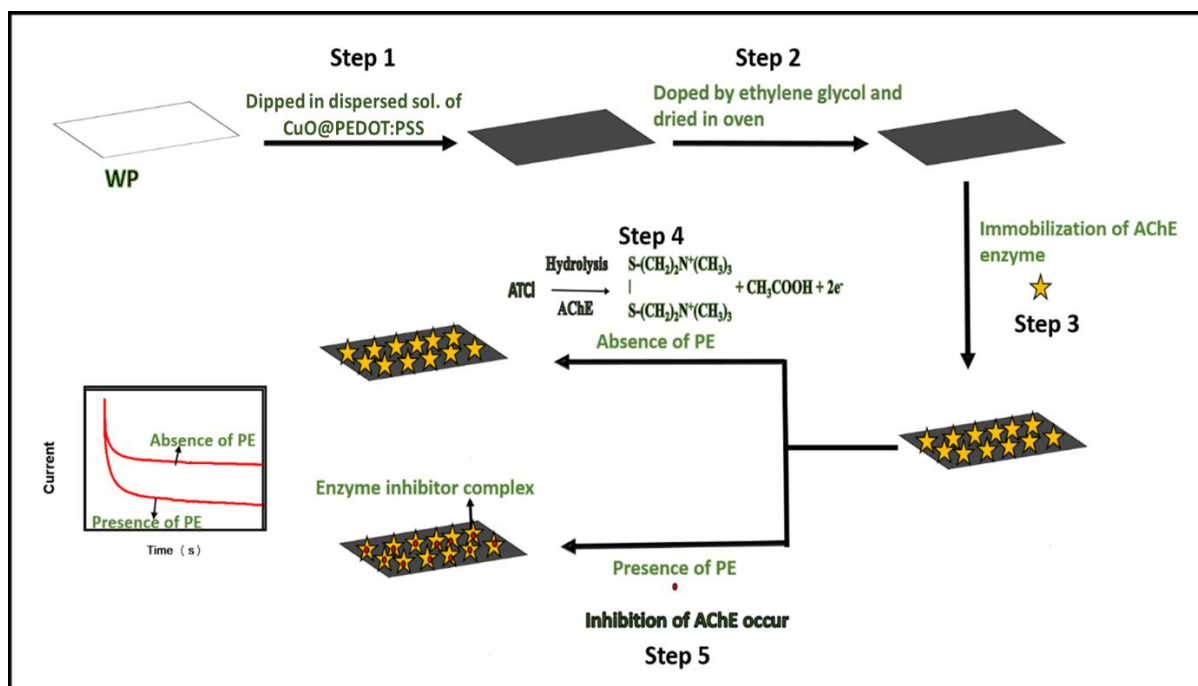


Fig. 6.1. Fabrication and mechanism of CuO@PEDOT: PSS-grafted paper based biosensor for OPs detection

6.3. Results and Discussion

6.3.1. Design of Sensor

In this chapter, a CuO@PEDOT:PSS sensing platform based biosensor has been developed and used for paraoxon-ethyl detection. To fabricate the biosensor, the following steps were considered. Initially, a Whatman paper (WP) was dipped in an aq. dispersion containing CuO@PEDOT: PSS and then it was dried in the oven as shown in Fig. 6.1, step 1. Next, the CuO@PEDOT:PSS/WP electrode was treated with EG and then dried (Fig. 6.1, step 2). Further, the AChE enzyme was covalently immobilized onto the surface of prepared electrode as shown in Fig. 6.1, step 3. Finally, this fabricated biosensor was incubated with ATCl and PE for further analysis. In the absence of PE, the ATCl hydrolyses and produces two electrons which generate a peak current as seen in Fig. 6.1, step 4 [3]. While, the PE blocks the

catalytic activity of AChE enzyme resulting in a decrease of peak current as shown in Fig. 6.1, step 5.

6.3.2. Structural and Morphological Characterization of Prepared Materials and Fabricated Electrodes

Fig. 6.2(A) illustrates the X-ray diffraction pattern of PEDOT: PSS-coated-WP, CuO nanocrystals and CuO@PEDOT: PSS-coated-WP in the curve (a), (b) and (c), respectively. The curve (a) shows the peaks at 16° and 23.2° are due to the presence of PEDOT:PSS and identify their successful coating on the surface of WP [4]. The curve (b) shows the characteristic peaks positioned at 35.8° , 39° , 46° , 48° , 61° , 66.4° , and 68° which confirm that CuO was successfully synthesized [5]. The sharp peaks at 35.8° and 39° confirm the high crystalline nature of CuO. Finally, in curve (c), only three peaks of CuO were observed at 46° , 66.4° and 82° . It is due to the poor crystalline nature of CuO in the presence of PEDOT: PSS.

The FTIR spectra of both PEDOT: PSS/WP and CuO@PEDOT: PSS/WP have been given in Fig. 6.2(B) curve a and b, respectively. In curve (a), the characteristic bands at 656 and 1054 cm^{-1} are attributed due to the stretching vibrations of C-S and C-O in the thiophene ring of PEDOT. The characteristic bands at 1106 and 1162 cm^{-1} correspond to the SO_3^- asymmetric stretching vibrations in PSS. The characteristic bands at 1516 and 1637 cm^{-1} are found due to the C-C and C=C stretching vibrations, respectively. These bands confirm a successful coating of PEDOT:PSS onto the surface of WP. The characteristic vibrational bands of CuO are not distinguished in FTIR spectra of CuO@PEDOT:PSS/WP (curve c) due to the very intensive characteristic bands of PEDOT: PSS [6, 7].

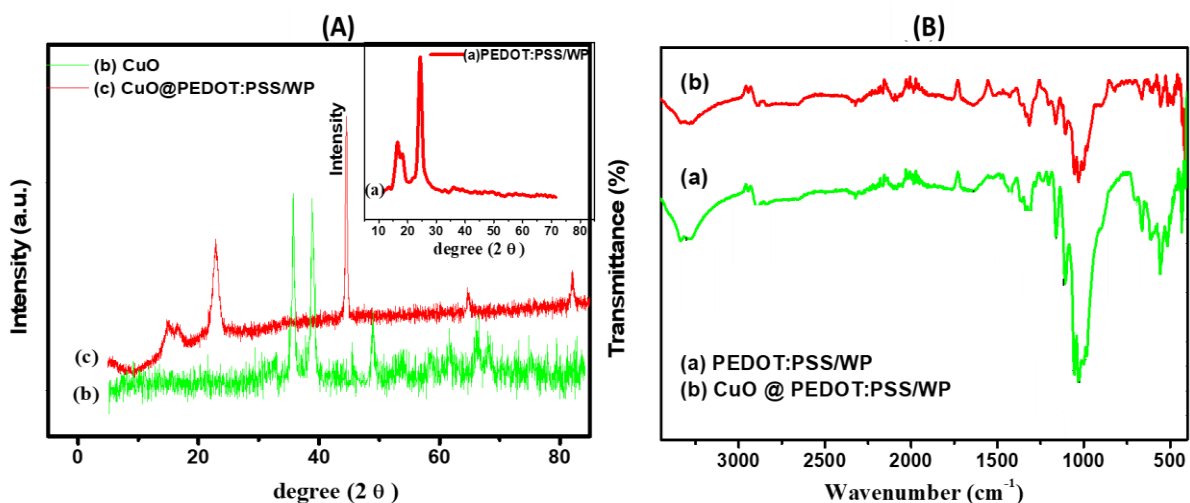


Fig. 6.2. (A) XRD pattern of PEDOT: PSS/ITO (a) CuO (b) and CuO@PEDOT: PSS/WP (c) (B) FTIR spectra of PEDOT: PSS/WP (a) and CuO@PEDOT: PSS/WP (b)

For morphological characterizations, the scanning electron microscopy and transmission electron microscopy techniques were used. The SEM image of a bare WP is illustrated in Fig. 6.3(A). In this figure, the fiber-like structure of cellulose is observed. Further, the SEM micrograph of PEDOT: PSS/WP is illustrated in Fig. 6.3(B). This figure clearly illustrates the uniform distribution of PEDOT: PSS on the surface of WP. In Fig. 6.3(C), CuO nanocrystals are clearly observed in PEDOT: PSS matrix which confirm that the CuO@PEDOT: PSS is successfully coated onto the WP surface. Also, the SEM micrograph of ethylene glycol-treated CuO@PEDOT: PSS/WP electrode is illustrated in Fig. 6.3(D).

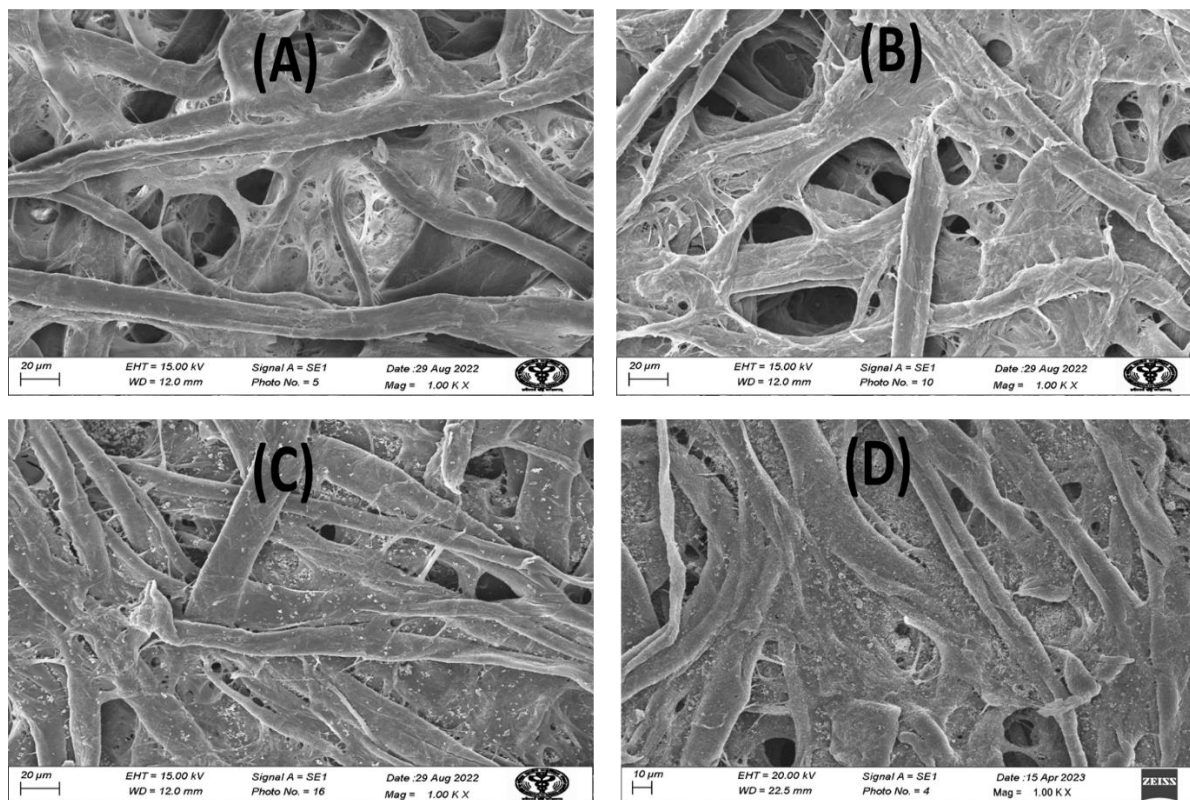


Fig. 6.3. SEM micrographs of (A) WP, (B) PEDOT: PSS/WP, (C) CuO@PEDOT: PSS/WP (D) Ethylene glycol treated CuO@PEDOT: PSS/WP electrodes

6.3.3. Electrical Conductivity Study of all Fabricated Electrodes

The electrical conductivity study of PEDOT: PSS/WP, NMP-treated PEDOT: PSS/WP, NMA-treated PEDOT: PSS/WP, DMF-treated PEDOT: PSS/WP, glycerol-treated PEDOT: PSS/WP, EG-treated PEDOT: PSS/WP and EG-treated CuO@ PEDOT: PSS/WP was performed by using a four probe method. Among all these electrodes, EG-treated CuO@ PEDOT: PSS/WP shows the maximum conductivity (Table 6.1). Therefore, this electrode was further used for all subsequent studies in the present work.

Table 6.1. Electrical conductivities of various electrodes

| S. No. | Samples/Electrodes | Conductivity (S/cm) |
|--------|---|----------------------|
| 1 | PEDOT:PSS coated WP (PEDOT:PSS/WP) | 8.7×10^{-4} |
| 2 | 1-methyl-2-pyrrolidone (NMP) treated PEDOT:PSS/WP | 6.0×10^{-3} |
| 3 | N,N-dimethyl acetamide (NMA) treated PEDOT:PSS/WP | 7.8×10^{-3} |
| 4 | Dimethylformamide (DMF) treated PEDOT:PSS/WP | 9.3×10^{-3} |
| 5 | Glycerol treated PEDOT:PSS/WP | 1.1×10^{-2} |
| 6 | EG treated PEDOT:PSS/WP | 1.4×10^{-2} |
| 7 | EG-treated CuO@PEDOT:PSS/WP | 6.0×10^{-2} |

6.3.4. Electrochemical Characterization

The electrochemical characterization of all the fabricated electrodes was done by chronoamperometry. In Fig. 6.4 (A), the maximum current is obtained for ethylene glycol-treated CuO@ PEDOT: PSS/WP electrode (represented in curve a), showing the maximum conductivity value among all other electrodes. However, the presence of AChE enzyme decreases the conductivity of ethylene glycol-treated CuO@ PEDOT: PSS/WP electrode due to the non-conductive or resistive nature of the enzyme [8] as shown in curve c.

6.3.5. Electrochemical Biosensing Studies

The biosensor's performance was examined as a function of increasing concentration in the range of 10-80 nM of PE by using chronoamperometry in PBS at pH 7, containing 2 mM acetyl thiocholine chloride (ATCI) and 5 mM $[\text{Fe}(\text{CN})_6]^{3-/4-}$. Fig. 6.4(B) demonstrated that the peak current decreases when we increase the concentration of PE. Here, PE leads to the phosphorylation of AChE receptors, resulting in a decrease in the hydrolysis rate of ATCI

and ultimately leading to a reduction in the peak current. Fig. 6.4(C) represents the calibration plot of current (I) vs. PE concentration (C_{PE}) and defined by following mentioned equation:

$$\Delta I = -9.12 \mu A/nM \log C_{PE} + 1060 \mu A; R^2 = 0.9751 \quad \dots\dots\dots (6.1)$$

Using the above equation, the LOD and sensitivity for this biosensor is reported as 0.42 nM and 9.12 $\mu A/nM$, respectively [9].

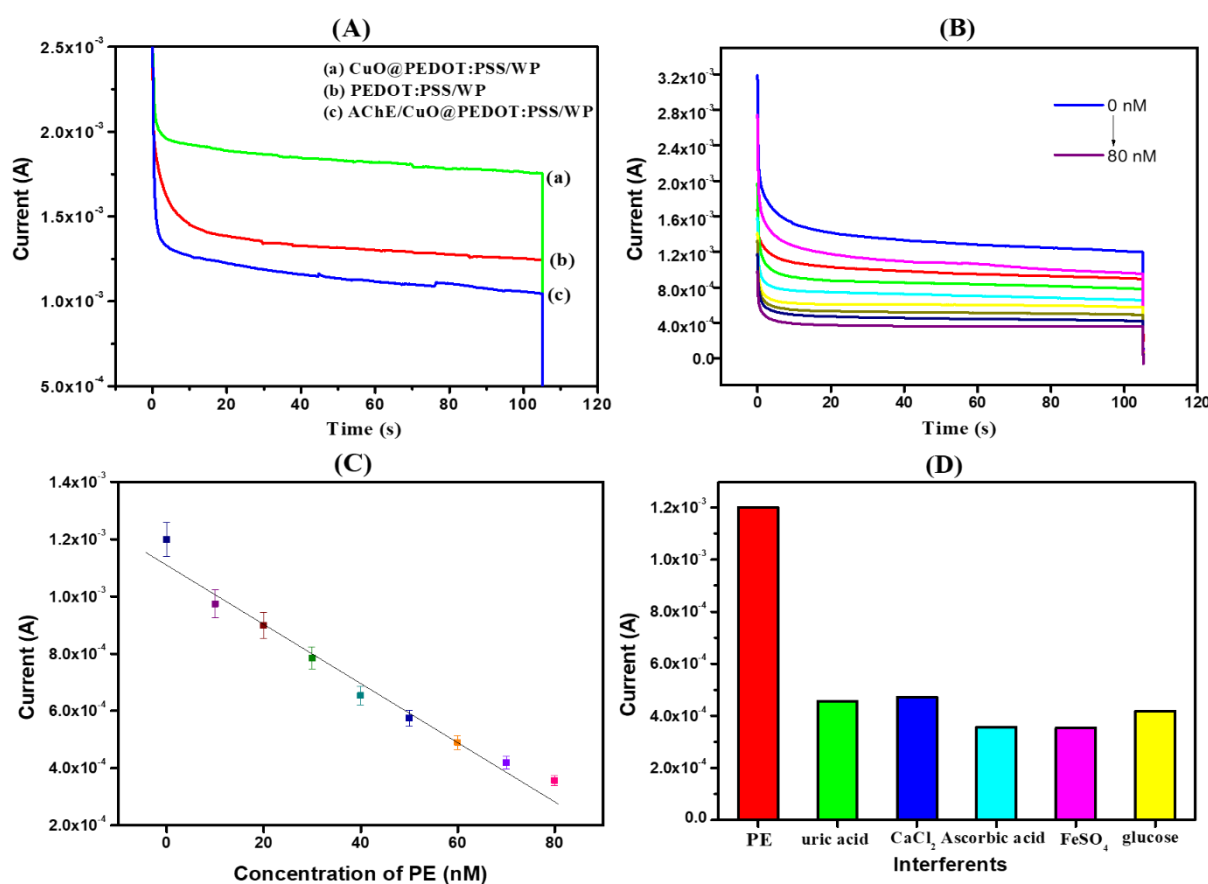


Fig. 6.4. (A) Chronoamperometry curves of (a) CuO@PEDOT: PSS/WP, (b) PEDOT: PSS/WP and (c) AChE/CuO@PEDOT: PSS/WP electrodes (B) An electrochemical response study of AChE/CuO@PEDOT: PSS/WP electrode after incubation of various conc (10-80 nM) of PE (C) Calibration graph of current vs. PE conc (D) Interference data of AChE/CuO@PEDOT: PSS/WP electrode in 10 nM uric acid, $CaCl_2$, $FeSO_4$, ascorbic acid and glucose.

6.3.6. Selectivity and Real Sample Analysis

The selectivity of AChE/CuO@PEDOT: PSS/WP-based biosensor has been studied in presence of 10 nM of interfering species like uric acid (UA), ascorbic acid (AA), CaCl₂, FeSO₄ and glucose. The results so obtained from the experiments clearly demonstrate that the highest current was obtained for the target analyte. On the other hand, the current generated by other interfering species was significantly low as compared to the current produced by PE (Fig. 6.4D). This observation reveals the satisfactory selectivity of developed biosensor for the detection of PE.

The precision and applicability of proposed biosensor were assessed by conducting the measurements on two real samples, namely, pulse and rice. The concentration of the target analyte was determined by using the proposed biosensor. These results have been given in the Table 6.2. These data values clearly indicate the satisfactory recovery rate for PE detection, ranged from 93-104% with RSD < 10%.

Table 6.2. Detection of PE in Spiked Rice and Pulse samples by using the AChE/CuO@PEDOT: PSS/WP biosensor

| Sample | Added amount (nM) | Found amount (nM) | Recovery (%) | RSD (%) |
|--------|-------------------|-------------------|--------------|---------|
| Rice | 5 | 4.58 | 91.66 | 6.15 |
| | 10 | 9.04 | 90.38 | 6.46 |
| Pulse | 5 | 5.34 | 106.8 | 5.34 |
| | 10 | 10.56 | 105.6 | 3.86 |

6.3.7. Reproducibility and Stability Studies

To check the reproducibility of developed biosensor, the chronoamperometry response of four different electrodes was analyzed (Fig. 6.5A). The results indicate that the electrode's peak current does not differ significantly with a low relative standard deviation (RSD) of 2.73%, indicating an excellent reproducibility.

Finally, to evaluate the stability of proposed biosensor when stored at 4°C, a chronoamperometry response was analyzed each 7 days upto a total of 28 days. After 28 days, the current response remained 87.6 % of its initial value which indicates the good stability of developed biosensor (Fig. 6.5B).

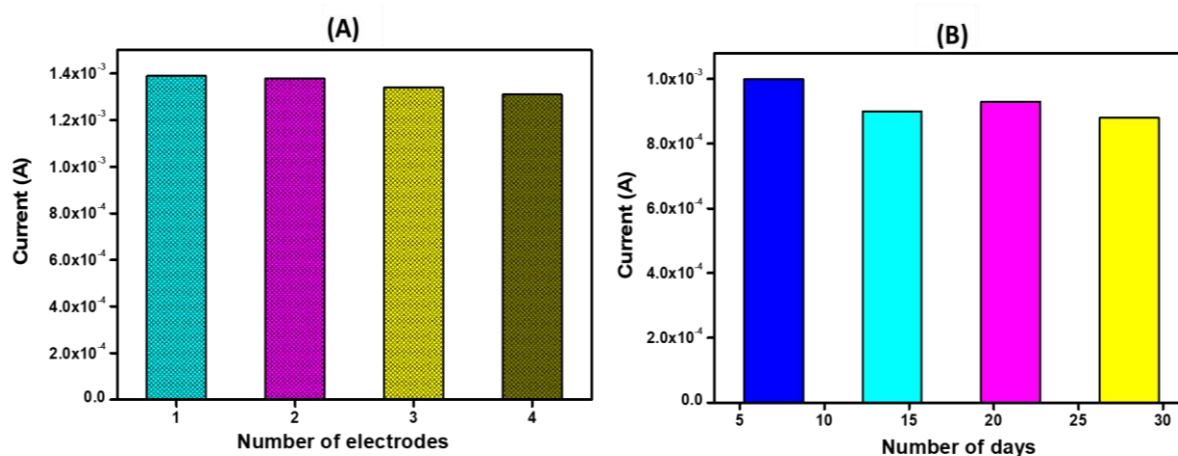


Fig. 6.5. (A) Reproducibility studies of the developed biosensor for PE detection using different electrodes (B) Stability studies of AChE/CuO@PEDOT: PSS/WP biosensor over a period of 28 days

6.4. Conclusion

This chapter presents the fabrication of a biodegradable, cost-effective and an efficient biosensor for PE detection. This biosensor utilizes a sensing platform composed of CuO and

PEDOT: PSS-modified conducting paper. An integration of CuO and PEDOT: PSS offers the several advantages. It facilitates the optimal environment for enzyme immobilization, which improves electron transfer rate. As a result, the electrochemical performance is significantly enhanced. The biosensor exhibits a high sensitivity value of $9.12 \mu\text{A/nM}$, indicating its ability to detect even minute concentrations of PE. Furthermore, it achieves a LOD of 0.42 nM , emphasizing its sensitivity in accurately quantifying PE levels. Two two real samples were analyzed to assess the accuracy and applicability of the proposed biosensor. The results obtained from these samples demonstrate promising outcomes, indicating the biosensor's effectiveness for PE detection in practical scenarios.

The results of present study have been published in “Journal of Applied Electrochemistry” 2023

6.5. References

1. Iqbal, S., et al., *Controlled synthesis of Ag-doped CuO nanoparticles as a core with poly (acrylic acid) microgel shell for efficient removal of methylene blue under visible light*. Journal of Materials Science: Materials in Electronics 2020. **31**: p. 8423-8435.
2. Kumar, S., et al. *Conducting paper based sensor for cancer biomarker detection*. in *Journal of Physics: Conference Series*. 2016. IOP Publishing.
3. He, L., et al., *Novel electrochemical biosensor based on core-shell nanostructured composite of hollow carbon spheres and polyaniline for sensitively detecting malathion*. Sensors Actuators B: Chemical 2018. **258**: p. 813-821.
4. Yoo, D., J. Kim, and J.H.J.N.R. Kim, *Direct synthesis of highly conductive poly (3, 4-ethylenedioxythiophene): poly (4-styrenesulfonate)(PEDOT: PSS)/graphene composites and their applications in energy harvesting systems*. Nano Research, 2014. **7**: p. 717-730.
5. Xie, Y., et al., *A CuO-CeO₂ composite prepared by calcination of a bimetallic metal-organic framework for use in an enzyme-free electrochemical inhibition assay for malathion*. Microchimica Acta, 2019. **186**: p. 1-9.
6. Kumar, S., et al., *Reduced graphene oxide modified smart conducting paper for cancer biosensor*. Biosensors Bioelectronics 2015. **73**: p. 114-122.
7. Paul, G., et al., *PEDOT: PSS-grafted graphene oxide-titanium dioxide nanohybrid-based conducting paper for glucose detection*. Polymers for Advanced Technologies 2021. **32**(4): p. 1774-1782.

8. Nagabooshanam, S., et al., *Electro-deposited nano-webbed structures based on polyaniline/multi walled carbon nanotubes for enzymatic detection of organophosphates*. Food Chemistry, 2020. **323**: p. 126784.
9. Thakur, D., C.M. Pandey, and D. Kumar, *Highly sensitive enzymatic biosensor based on polyaniline-wrapped titanium dioxide nanohybrid for fish freshness detection*. Applied Biochemistry Biotechnology 2022. **194**(8): p. 3765-3778.

CHAPTER 7

CeO₂ and PEDOT: PSS grafted Whatman paper-based Biosensor for PE Detection

7.1. Introduction

In this chapter, a novel, cost-effective, and environmental-friendly AChE-based electrochemical biosensor was developed and utilized for paraoxon-ethyl detection. This CeO₂ and PESOT: PSS modified paper electrode was fabricated by a simple dip-coating method. The synergistic effect of CeO₂ and PEDOT: PSS enhance the performance of AChE-based biosensor with respect to its sensitivity and selectivity. The electrical conductivity and stability of fabricated electrode are further improved with the treatment of ethylene glycol (EG). All the electrochemical results validate that the developed biosensor shows high sensitivity of 52.10 $\mu\text{A/nM}$, LOD of 0.12 nM and high stability. The accuracy and applicability of the proposed biosensor were also checked with two real samples. All the findings confirm that the fabricated paper electrode has the potential to emerge as a highly promising alternative to the traditional electrodes.

7.2. Experimental Section

7.2.1. Biosynthesis of CeO₂ Nanocrystals

The CeO₂ nanocrystals were synthesized by banana fruit extract. The fruit was washed, dried and crushed before undergoing the extraction process by using water as a solvent. In this process, 10 g of dried banana powder was soaked in 50 mL of distilled water for 24 h. The solution was centrifuged for 1 h at 500 rpm followed by filtration with Whatman paper. After obtaining the filtrate, it was diluted with DI water in a ratio of 1:4 (10 mL of filtrate

diluted with 40 mL of DI water) then an aqueous solution of cerium nitrate hexahydrate (2.17 g in 50 mL DI water) was added. Further, this solution was stirred for a duration of 4 h at a temperature of 75°C. Subsequently, the solution was subjected to centrifugation and then washed many times with DI water. A white precipitate so obtained was subjected to drying at a temperature of 80°C and calcined in a muffle furnace at 300°C with a heating rate of 4°C/min.

7.2.2. Fabrication of PEDOT: PSS/WP, CeO₂@PEDOT: PSS/WP, and ethylene glycol-treated CeO₂@PEDOT: PSS/WP Conducting Papers

The Whatman paper was utilized for the fabrication of conducting papers. Initially, WP was stabilized by immersing it into the solution of tween-20 surfactant and then subjecting it to sonication for 15 min. Then, the WP was dried in the oven at a temperature of 100°C and further utilized for the fabrication process.

The stabilized WP was immersed into the suspension of PEDOT: PSS (2mL in 10 mL water) for 1 h followed by drying in an oven at a temperature of 100°C to fabricate the PEDOT: PSS-coated WP. To obtain better flexibility and conductivity of conducting paper, this process was repeated four times. The colour change from white to blue validated the successful coating of the polymer onto WP.

The CeO₂@PEDOT: PSS-coated WP fabrication was carried out by dissolving 5 mg CeO₂ nanocrystals into the solution (aqueous) of PEDOT: PSS through magnetic stirring for 4 h. Further, the stabilized WP was immersed into the resultant solution of CeO₂ and PEDOT: PSS for 1 h followed by drying in an oven at 100°C. This procedure was repeated four times to fabricate the CeO₂@PEDOT: PSS-coated WP. For more stability and conductivity, the prepared electrode was subjected to a 37.5% ethylene glycol (EG) and then dried in an oven at 100°C [1].

7.2.3. Biosensor Fabrication

The fabrication of biosensor (AChE/EG-treated CeO_2 @PEDOT: PSS/WP) was achieved by drop-casting of 30 μL AChE enzyme (0.1 mg/mL) onto the surface of fabricated conducting paper (EG-treated CeO_2 @PEDOT: PSS/WP). Then, the fabricated biosensor was kept overnight in the incubation chamber at a temperature of 4°C . The biosensor was further washed with phosphate buffer saline (PBS) before conducting the electrochemical analysis. A schematic representation of the proposed biosensor has been illustrated in the below Fig. 7.1.

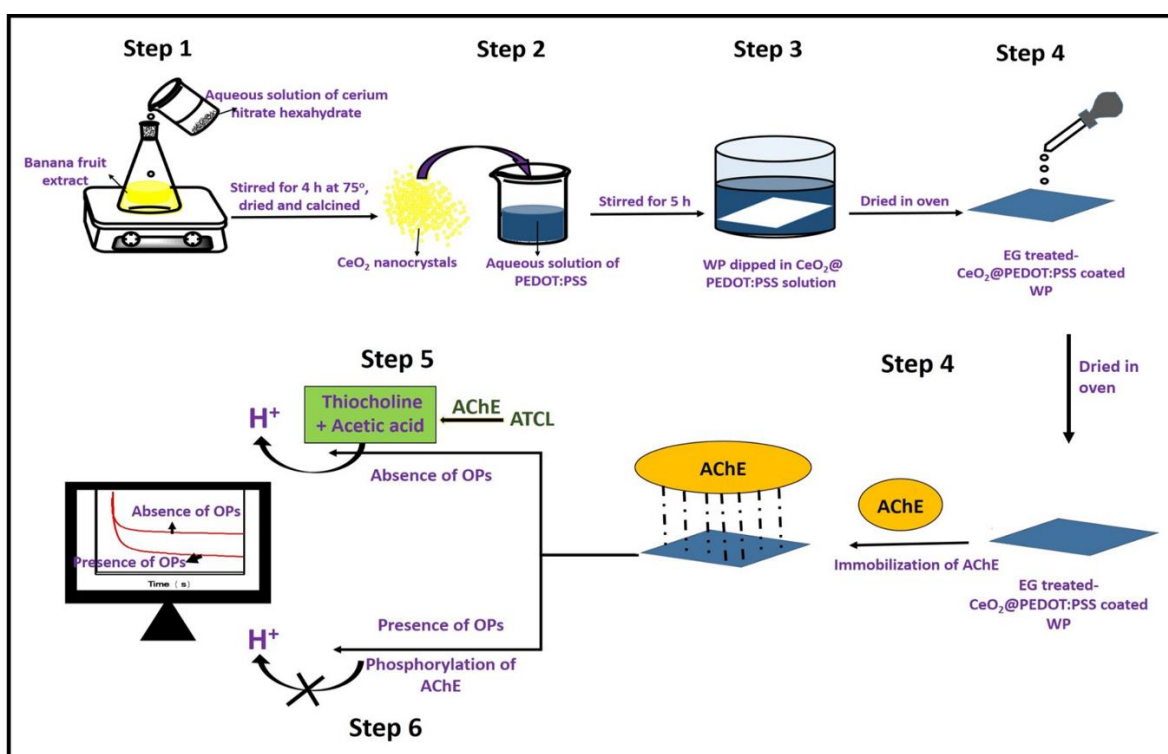


Fig. 7.1. A schematic view of biosensor fabrication and its working mechanism for PE detection

7.3. Results and Discussion

7.3.1. Design of Sensor

In this proposed work, a paper electrode-based electrochemical biosensor was developed for PE detection using CeO₂-incorporated PEDOT:PSS as a sensing platform. The biosensor (AChE/EG-treated CeO₂@PEDOT:PSS) was fabricated by synthesizing the CeO₂ nanocrystal using banana extract (Fig. 7.1, step1) and depositing the CeO₂@PEDOT:PSS onto the WP by dip-coating method (Fig. 7.1, step2). The electrode was further treated with a solvent like EG to improve its flexibility and conductivity (Fig. 7.1, step3). Then, the AChE enzyme was immobilized over the surface of the fabricated paper electrode (EG-treated CeO₂@PEDOT:PSS/WP) (Fig. 7.1, step 4). The developed biosensor was further utilized for OPs detection. The detection of OPs was accomplished by monitoring the current generated in the presence and absence of OPs. When OPs were not present, the AChE enzyme functioned as a catalyst in the hydrolysis of ATCl. This hydrolysis reaction results in the formation of acetic acid and thiocholine as primary products. The thiocholine then undergoes oxidation to form dithio-bis-choline which releases two protons. Additionally, the acetic acid also releases protons (H⁺) at the electrode surface. The released protons then protonate the PEDOT, resulting in the production of a signal (Fig. 7.1, step 5). On the other hand, the presence of OPs leads to the phosphorylation of AChE enzyme that inhibits its catalytic activity towards hydrolysis of ATCl, thereby leading to a decrease in the peak current intensity [2] (Fig. 7.1, step 6).

7.3.2. Structural, Morphological and Elemental Characterization of Prepared Materials and Fabricated Electrodes

XRD and FTIR spectroscopy techniques have been used for the structural analysis of all the fabricated electrodes and materials. Fig. 7.2(A) illustrates the X-ray diffraction pattern

of PEDOT: PSS-coated-WP, CeO₂ nanocrystals and CeO₂ @PEDOT: PSS-coated-WP in curve (a), (b) and (c), respectively. The peaks located at 16° and 23.2° are the characteristic peaks of PEDOT: PSS and identify their successful coating on the surface of WP [3] as shown in curve (b). The characteristic peaks positioned at 29°, 33.5°, 48°, 56.8°, 70°, 77°, and 79.3° confirm that CeO₂ was successfully synthesized [4] as seen in curve (b). Finally, in curve (c), all the characteristic peaks of both PEDOT:PSS and CeO₂ are present, indicating both materials were successfully deposited onto the surface of WP.

The FTIR data of CeO₂ (curve a), PEDOT: PSS/WP (curve b) and CeO₂ @PEDOT: PSS/WP are illustrated in Fig. 7.2(B). In curve (a), the band appears at 712 cm⁻¹, corresponds to the Ce-O bond vibrations. While, the bands located at 1059 and 1331 cm⁻¹ are attributed due to the vibrational modes of Ce-O-Ce bonds. The band appears at 1609 cm⁻¹ is attributed due to the bending vibrations of absorbed H₂O [5] [6]. All these bands confirm the successful formation of CeO₂. In curve (b), the bands at 656 and 1054 cm⁻¹ are attributed due to the stretching vibrations of C-S and C-O in a thiophene ring of PEDOT. The bands appear at 1106 and 1162 cm⁻¹ correspond to the SO₃⁻ asymmetric stretching vibrations in PSS. The bands at 1516 and 1637 cm⁻¹ are due to the C-C and C=C stretching vibrations, respectively. These bands confirm a successful coating of PEDOT:PSS onto the surface of WP. The characteristic vibrational bands of CeO₂ are not distinguished in FTIR spectra of CeO₂@PEDOT:PSS/WP due to the presence of very intensive bands of PEDOT:PSS [7, 8].

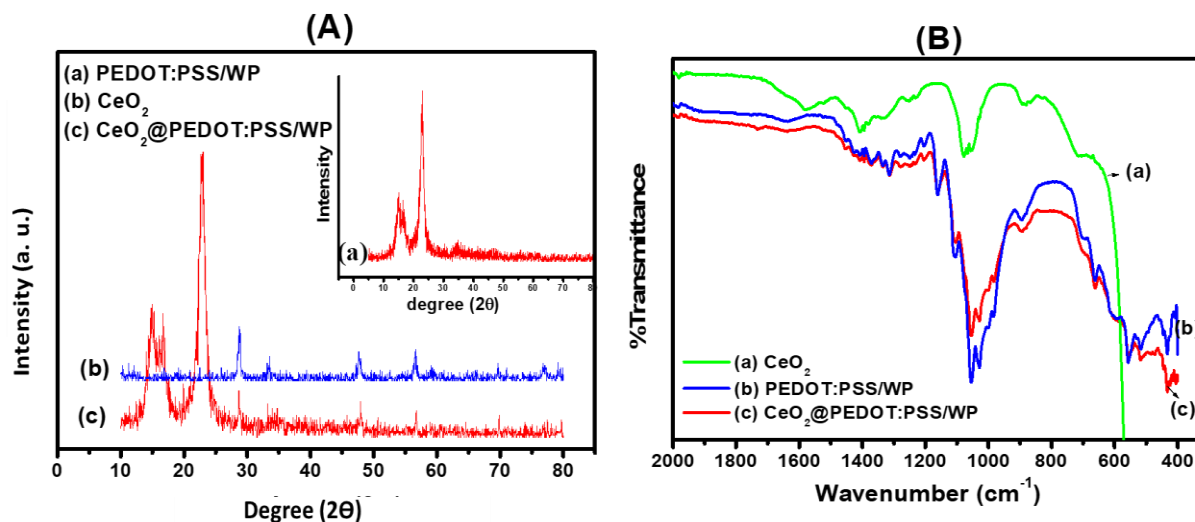


Fig. 7.2. (A) XRD pattern of (a) PEDOT: PSS/WP (b) CeO₂ and (c) CeO₂@PEDOT: PSS/WP
(B) FTIR plots of (a) CeO₂, (b) PEDOT: PSS/WP and (c) CeO₂@PEDOT: PSS/WP

For morphological characterizations, SEM and TEM techniques were used. Fig. 7.3(A) and 7.3(B) represent the SEM and TEM images of CeO₂ nanocrystals. The TEM image of CeO₂ confirms that the size of nanocrystals is less than 50 nm. The SEM image of bare WP is illustrated in Fig. 7.3(C). In this figure, the fiber-like structure of cellulose is observed. Further, a SEM image of PEDOT: PSS/WP is illustrated in Fig. 7.3(D). This figure clearly illustrates the PEDOT: PSS uniform distribution over the surface of WP. In Fig. 7.3(E), CeO₂ nanocrystals are clearly observed in PEDOT: PSS matrix which confirm that the CeO₂@PEDOT: PSS is successfully coated onto the WP surface. The SEM micrograph of ethylene glycol-treated CeO₂@PEDOT: PSS/WP electrode has been illustrated in Fig. 7.3(F).

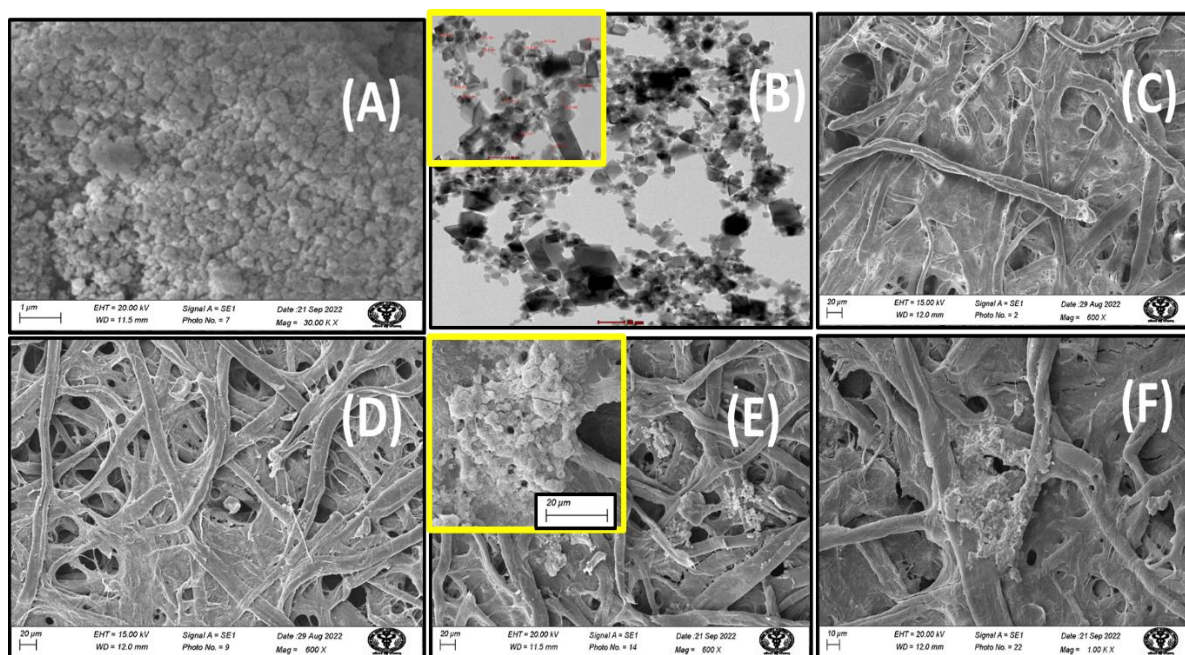


Fig. 7.3. (A) SEM micrograph of CeO_2 nanocrystals (B) TEM micrograph of CeO_2 nanocrystals (C) SEM micrograph of WP (D) SEM micrograph of PEDOT: PSS/WP electrode (E) SEM micrograph of CeO_2 @PEDOT: PSS/WP electrode (F) SEM micrograph of ethylene glycol-treated CeO_2 @PEDOT: PSS/WP electrode

Fig. 7.4(A) and 7.4(B) illustrate the EDAX (energy dispersive X-ray) spectra of CeO_2 nanocrystals and CeO_2 @PEDOT: PSS/WP electrode, respectively. The presence of all peaks related to Ce and O in Fig. 7.4(A) confirm the successful formation of CeO_2 nanocrystal, while all peaks related to C, S, Ce, and O in Fig. 7.4(B) confirm the successful design of CeO_2 @PEDOT: PSS/WP electrode. The appearance of an additional peak in both figures is attributed due to the gold coating applied to the samples for SEM-EDAX analysis.

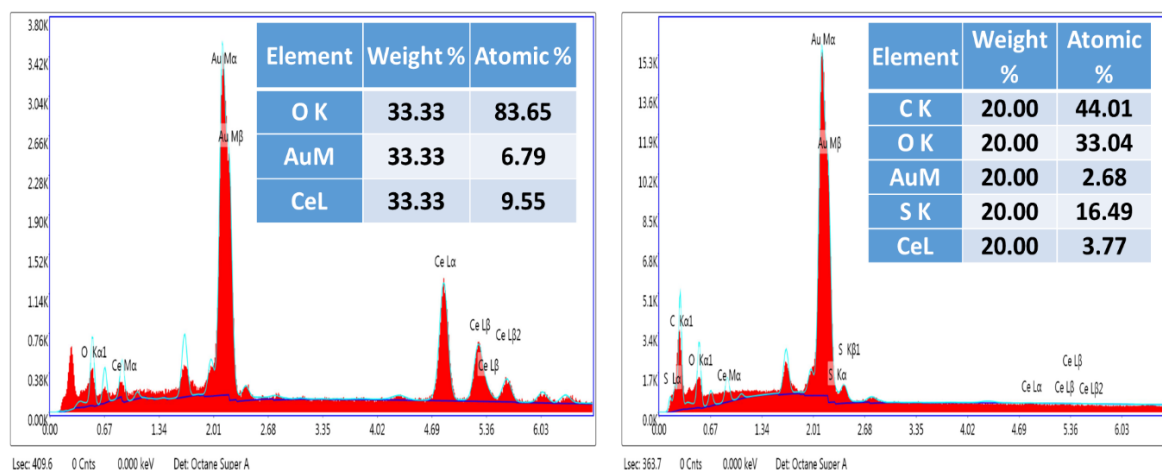


Fig. 7.4. SEM-EDAX analysis of (A) CeO₂ and (B) CeO₂@PEDOT:PSS/WP electrode

7.3.3. Electrical Conductivity Study of all Fabricated Electrodes

The electrical conductivity of all the modified electrodes was studied by the Four-Probe technique. The WP coated with PEDOT:PSS shows a conductivity of 5.2×10^{-3} S/cm (Table 7.1). Further, the CeO₂ incorporated PEDOT:PSS/WP leads to an enhanced conductivity of 3.4×10^{-2} S/cm. Additionally, to improve the stability and conductivity, CeO₂@ PEDOT:PSS/WP electrode was treated with different concentrations of ethylene glycol including 50, 37.5, 25, and 12.5 % (V/V). The electrical conductivity data presented in Table 7.1 confirm that the treatment of 37.5% ethylene glycol highly improves the electrode conductivity. Therefore, 37.5% ethylene glycol was used for all the subsequent studies. The ethylene glycol decreases the coulombic interactions between PEDOT and PSS molecules, causes the polymer chain reorientation and improves the non-covalent interaction between cellulose molecule and PEDOT leading to the higher conductivities.

Table 7.1. Electrical conductivity studies of all modified electrodes

| S. No. | Modified electrodes | Conductivity (S/cm) |
|--------|--|----------------------|
| 1. | PEDOT:PSS-coated-WP (PEDOT:PSS/WP) | 5.2×10^{-3} |
| 2. | CeO ₂ @ PEDOT:PSS/WP | 3.4×10^{-2} |
| 3. | 50% EG-treated-CeO ₂ @ PEDOT:PSS/WP | 3.8×10^{-2} |
| 4. | 37.5% EG-treated-CeO ₂ @ PEDOT:PSS/WP | 1.4×10^{-1} |
| 5. | 25% EG-treated-CeO ₂ @ PEDOT:PSS/WP | 6.5×10^{-2} |
| 6. | 12.5% EG-treated-CeO ₂ @ PEDOT:PSS/WP | 4.5×10^{-2} |

7.3.4. Electrochemical Characterization

The chronoamperometry studies of PEDOT: PSS/WP, CeO₂@ PEDOT: PSS/WP, AChE/EG treated-CeO₂@PEDOT: PSS/WP and EG treated-CeO₂@ PEDOT: PSS/WP electrodes have been illustrated in Fig. 7.5(A) curve a, b, c and d, respectively. The highest electrochemical current value for ethylene glycol treated-CeO₂@PEDOT: PSS/WP electrode (1.0 mA) represents its highest conductivity as compared to PEDOT: PSS/WP (0.56 mA) and CeO₂@PEDOT: PSS/WP (0.70 mA) electrodes. An AChE enzyme immobilization onto the surface of EG treated-CeO₂@PEDOT: PSS/WP electrode further causes the depletion of the electrochemical current. This decrease in current is attributed to the enzyme's non-conducting nature which confirms that the enzyme was effectively immobilized [9].

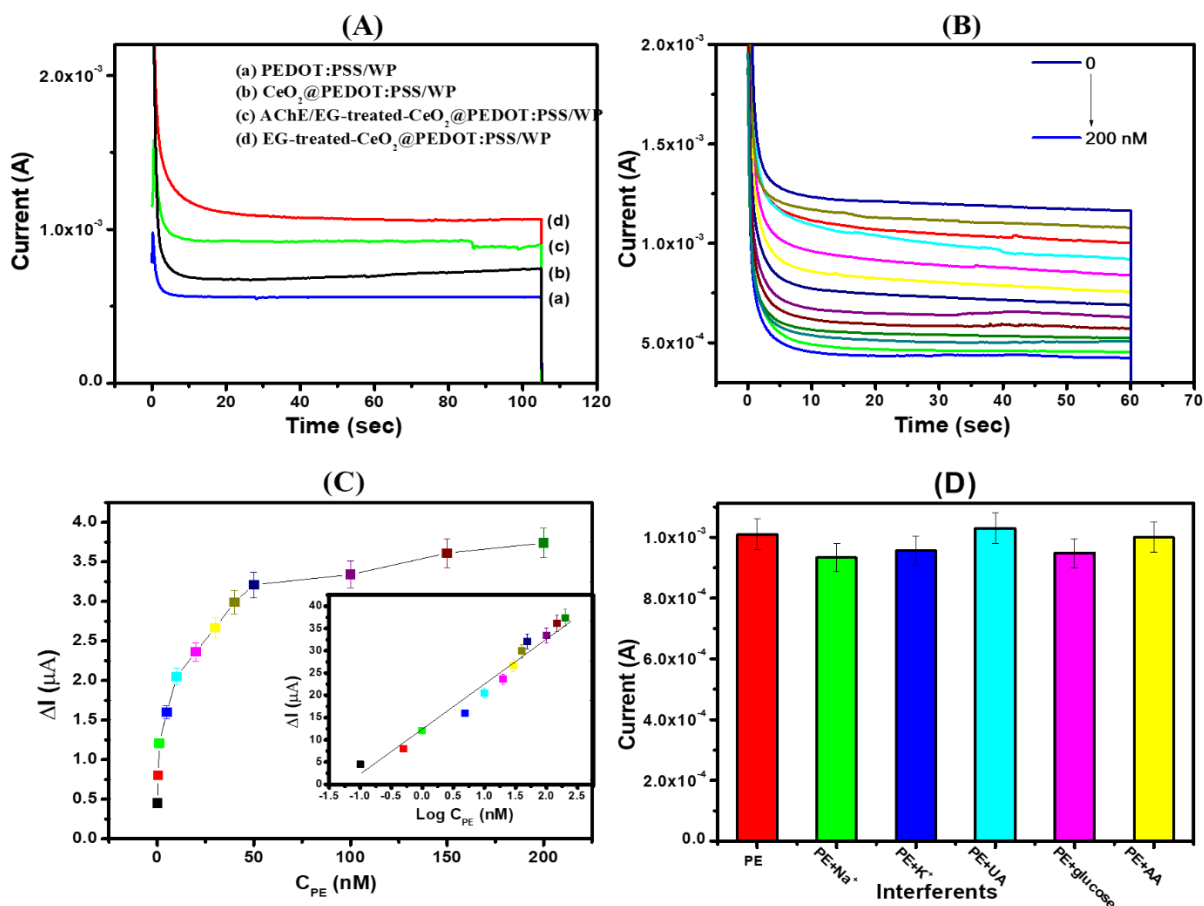


Fig.7.5. (A) Chronoamperometry plot obtained for (a) PEDOT: PSS/WP, (b) CeO_2 @PEDOT: PSS/WP, (c) AChE/EG-treated- CeO_2 @PEDOT: PSS/WP and (d) EG-treated- CeO_2 @PEDOT: PSS/WP (B) Chronoamperometry response study of AChE/EG-treated- CeO_2 @PEDOT: PSS/WP electrode after incubation of various concentrations (0, 0.1, 0.5, 1, 5, 10, 20, 30, 40, 50, 100, 150, and 200 nM) of PE. (C) Calibration graph of inhibition (ΔI) vs. PE concentration (C_{PE}). Inset of (C) shows a linear curve of ΔI vs. $\log(C_{\text{PE}})$ (D) Interference study of AChE/EG-treated- CeO_2 @PEDOT: PSS/WP electrode in the presence of Na^+ , K^+ , uric acid (UA), glucose, and ascorbic acid (AA).

7.3.5. Optimization Studies

In order to achieve the best bioelectrode response for PE detection, different parameters including the incubation time of pesticide and pH of the electrolytic solution were

analyzed by using chronoamperometry technique. Firstly, the duration of PE incubation on the fabricated working electrode (AChE/EG treated-CeO₂@PEDOT: PSS/WP) surface was investigated by varying the time between 1 to 6 min as depicted in Fig. 7.6(A). This figure illustrates that the current response reached to the saturation after 3 min signifying that the maximum amount of PE has been bound to the AChE enzyme during this period.

The effect of pH on the enzyme activity in developed biosensor is also depicted in Fig. 7.6(B). It is evident from the figure that the enzyme achieves its highest activity at pH 7 resulting in the highest current. Therefore, this optimal pH value was utilized in all the subsequent biosensing experiments.

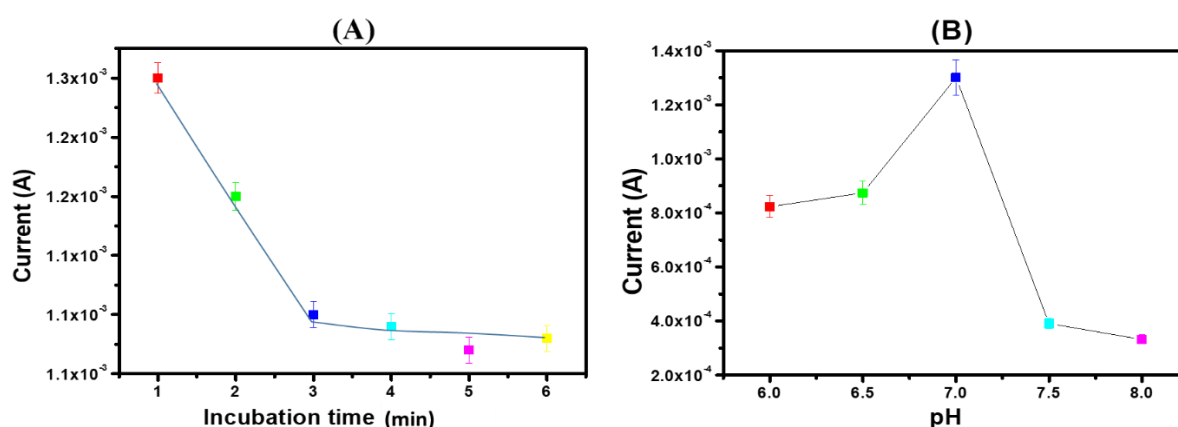


Fig. 7.6. Optimization of (A) incubation time (0-6 min) of PE (B) effect of pH (6-8 pH)

7.3.6. Electrochemical Biosensing Studies

The biosensor's (AChE/EG treated-CeO₂@PEDOT: PSS/WP) performance has been examined as a function of increasing concentration of PE (0.1-200 nM) by using chronoamperometry technique at 7 pH PBS containing 3 mM acetyl thiocholine chloride (ATCl) and 5 mM [Fe(CN)₆]^{3-/4-}. It is revealed from the Fig. 7.5(B) that the peak current decreases when the PE concentration increases. This PE leads to the phosphorylation of AChE receptors resulting in a decrease in the hydrolysis rate of ATCl and ultimately leading to a

reduction in the peak current. A calibration plot of inhibition (ΔI) vs. PE conc (C_{PE}) is given in Fig. 7.5(C). The inset of Fig. 7.5(C) reveals that there is a linear relationship between ΔI and the logarithm of PE conc which is defined by the following regression equation:

$$\Delta I = 52.10 \mu A/nM \log C_{PE} + 11.97 \mu A; R = 0.9856 \quad \dots\dots\dots (7.1)$$

The sensitivity of AChE/EG-doped-CeO₂@PEDOT: PSS/WP biosensing platform is calculated as 52.10 $\mu A/nM$ and this value is obtained by using the slope of the regression equation as mentioned above (Eq. 7.1). Furthermore, the limit of detection (LOD) for the proposed biosensor is determined to be 0.12 nM by using the following equation [10]:

$$LOD = 3\sigma / S \quad \dots\dots\dots (7.2)$$

7.3.7. Selectivity and Real Sample Studies

To study the selectivity of AChE/EG treated-CeO₂@PEDOT: PSS/WP-based biosensor for PE detection, an interference investigation was performed in presence of various interfering species including Na⁺, K⁺, uric acid (UA), glucose and ascorbic acid (AA). To conduct this study, a mixture of 10 pM of specified interferents and 10 pM of PE was prepared. The bar diagram (Fig. 7.5D) demonstrated that the current response remains relatively unchanged with the addition of the interfering species indicating an excellent selectivity of this developed biosensor (AChE/EG-doped-CeO₂@PEDOT: PSS/WP) for PE detection.

An applicability and precision of this proposed biosensing platform were evaluated by measuring the conc of PE in two real samples such as soil and carrot. These results are presented in Table 7.2 which clearly demonstrate the excellent performance of biosensor with satisfactory recovery rates ranging from 93-104 % and a good level of accuracy (as indicated by the related standard deviation (RSD) of less than 5%). These findings suggest that the biosensor is a reliable and an effective tool for detecting and quantifying the pesticides in food and environmental samples.

Table 7.2. Detection of PE in Spiked Soil and Carrot Samples using AChE/CeO₂@PEDOT: PSS/WP Electrode

| Sample | Added amount (nM) | Found amount (nM) | Recovery (%) | RSD (%) |
|--------|-------------------|-------------------|--------------|---------|
| Soil | 0.1 | 0.09 | 93 | 4.41 |
| | 0.5 | 0.49 | 97 | 2.12 |
| | 1 | 0.98 | 98 | 0.74 |
| | 5 | 4.91 | 98 | 1.12 |
| | 10 | 9.45 | 94 | 4.06 |
| Carrot | 0.1 | 0.09 | 94 | 3.78 |
| | 0.5 | 0.51 | 103 | 2.71 |
| | 1 | 1.07 | 107 | 5.07 |
| | 5 | 5.21 | 104 | 2.90 |
| | 10 | 9.87 | 98 | 0.73 |

7.3.8. Reproducibility and Stability Studies

Reproducibility of this developed biosensor was analyzed by measuring the chronoamperometry response of five different electrodes as shown in Fig. 7.7A. The results indicate that the electrode's peak current does not differ significantly with a low relative standard deviation (RSD) of 1.44% which supports an excellent reproducibility.

Finally, stability of this proposed biosensor stored at 4°C was analyzed by measuring the chronoamperometry response every 5 days period for a total of 25 days. This current response remained 92.6 % of its initial value even after 25 days which indicates the good stability of developed biosensor as depicted in Fig. 7.7B.

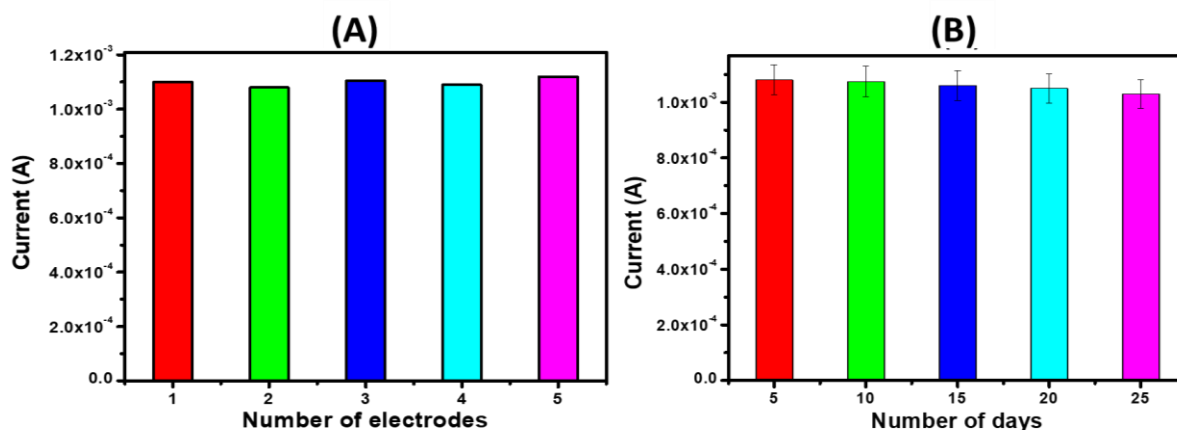


Fig. 7.7. (A) Reproducibility studies of the developed biosensor for PE detection using different electrodes (B) Stability studies of the developed electrode (AChE/CeO₂@PEDOT: PSS/WP) over a period of 28 days

7.4. Conclusion

In this chapter, a CeO₂@PEDOT: PSS-based paper electrode was fabricated by dip-coating method and then subjected to ethylene glycol for more stability and conductivity. The fabricated electrode was further used to develop an AChE-based electrochemical biosensor for the PE detection. In order to improve the performance of the fabricated biosensor, an optimized process was conducted focused on two key parameters: pH and incubation time. This biosensor shows the high sensitivity ($52.10 \mu\text{A/nM}$), selectivity, LOD (0.12 nM) and high stability. The practicality of this proposed biosensor in the real-world situations were also examined and these results offer a reliable, cost-effective and sensitive method for OPs detection.

7.5. References

1. Kumar, S., et al. *Conducting paper based sensor for cancer biomarker detection*. in *Journal of Physics: Conference Series*. 2016. IOP Publishing.
2. He, L., et al., *Novel electrochemical biosensor based on core-shell nanostructured composite of hollow carbon spheres and polyaniline for sensitively detecting malathion*. *Sensors Actuators B: Chemical* 2018. **258**: p. 813-821.
3. Yoo, D., J. Kim, and J.H.J.N.R. Kim, *Direct synthesis of highly conductive poly (3, 4-ethylenedioxythiophene): poly (4-styrenesulfonate)(PEDOT: PSS)/graphene composites and their applications in energy harvesting systems*. *Nano Research*, 2014. **7**: p. 717-730.
4. Jayakumar, G., A.A. Irudayaraj, and A.D. Raj, *Investigation on the synthesis and photocatalytic activity of activated carbon–cerium oxide (AC–CeO₂) nanocomposite*. *Applied Physics A*, 2019. **125**(11): p. 1-9.
5. Javad Farhangi, M., et al., *MOF-mediated synthesis of CuO/CeO₂ composite nanoparticles: Characterization and estimation of the cellular toxicity against breast cancer cell line (MCF-7)*. *Journal of Functional Biomaterials*, 2021. **12**(4): p. 53.
6. Kuzmanović, B., et al., *The influence of oxygen vacancy concentration in nanodispersed non-stoichiometric CeO₂- δ oxides on the physico-chemical properties of conducting polyaniline/CeO₂ composites*. *Electrochimica Acta*, 2019. **306**: p. 506-515.
7. Kumar, S., et al., *Reduced graphene oxide modified smart conducting paper for cancer biosensor*. *Biosensors Bioelectronics* 2015. **73**: p. 114-122.
8. Paul, G., et al., *PEDOT: PSS-grafted graphene oxide-titanium dioxide nanohybrid-based conducting paper for glucose detection*. *Polymers for Advanced Technologies* 2021. **32**(4): p. 1774-1782.

9. Nagabooshanam, S., et al., *Electro-deposited nano-webbed structures based on polyaniline/multi walled carbon nanotubes for enzymatic detection of organophosphates*. Food Chemistry, 2020. **323**: p. 126784.
10. Thakur, D., C.M. Pandey, and D. Kumar, *Highly sensitive enzymatic biosensor based on polyaniline-wrapped titanium dioxide nanohybrid for fish freshness detection*. Applied Biochemistry Biotechnology 2022. **194**(8): p. 3765-3778.

CHAPTER 8

Summary and Future Prospects

8.1. Summary

The conclusion of this thesis work and further research scope is reported in this chapter. Various novel and effective sensing platforms using CuO-incorporated PANI, Ag@CuO-incorporated and CeO₂-incorporated PANI-based composites are being fabricated and then utilized for paraoxon-ethyl detection. The uniform distribution of CuO, Ag@CuO and CeO₂ nanoparticles onto the PANI matrix enhances the bio-affinity towards the AChE enzyme, surface area and conductivity of nanocomposite. The process of biosensor fabrication involves the electrophoretic deposition of nanocomposite onto the electrode surface followed by an immobilization of the AChE enzyme onto the surface of resulting electrode. The fabricated biosensors show the excellent stability, reproducibility and selectivity. The sensitivity for CuO@PANI/ITO, Ag@CuO/PANI/ITO and CeO₂@PANI/ITO biosensors is found to be 49.86, 0.23×10^3 and $0.59 \times 10^3 \mu\text{A (nM)}^{-1}$, respectively. Moreover, the limit of detection for CuO@PANI/ITO, Ag@CuO/PANI/ITO and CeO₂@PANI/ITO is found to be 0.096, 0.011 and 0.005, respectively for PE detection.

The prepared CuO and CeO₂ nanoparticles are also incorporated in PEDOT:PSS and then utilized for the fabrication of paper-based electrochemical sensors for PE detection. In this study, CeO₂ and PESOT:PSS modified paper electrodes are fabricated by a simple dip-coating method. The electrical conductivity and stability of the fabricated electrodes were further improved by ethylene glycol treatment. The electrochemical results validate that the biosensors show a good selectivity, stability and reproducibility. The sensitivity for CuO@PEDOT:PSS/WP and CeO₂@PEDOT:PSS/WP biosensors is found to be 9.12 and 52.10

$\mu\text{A (nM)}^{-1}$, respectively. Additionally, the limit of detection for CuO@PEDOT:PSS/WP and CeO₂@PEDOT:PSS/WP is found to be 0.42 and 0.12, respectively for PE detection.

From all these results, we can conclude that the CeO₂-based biosensors show the important and effective results in comparison to CuO which is due to high biocompatibility of CeO₂ towards AChE enzyme. The CuO shows some adverse effects on biocompatibility which influence their interaction with AChE enzyme. The applicability of developed biosensors is validated with real samples like fruit, vegetables, soil, rice and pulse etc. which shows the promising results for PE detection. Thus, the developed biosensors have a potential to be used for an effective detection of PE.

8.2. Future Scope

It may be possible to explore the use of these nanocomposites in conjunction with other sensing technologies such as optical and electrochemical sensors to develop new hybrid sensing platforms for pesticide detection. This could allow a development of highly sensitive and selective sensors with an improved performance characteristics.

Publications

- 1.** Paneru S, Kumar D. Ag-doped-CuO nanoparticles supported polyaniline (PANI) based novel electrochemical sensor for sensitive detection of paraoxon-ethyl in three real samples. *Sensors and Actuators B: Chemical*. 2023 Mar 15;379:133270, Impact factor = 9.2
- 2.** Paneru S, Kumar D. A Novel Electrochemical Biosensor Based on Polyaniline-Embedded Copper Oxide Nanoparticles for High-Sensitive Paraoxon-Ethyl (PE) Detection. *Applied Biochemistry and Biotechnology*. 2023 Jan 26:1-8, Impact factor = 3.09
- 3.** Paneru S, Sweety, Kumar D. CuO@ PEDOT: PSS-grafted paper-based electrochemical biosensor for paraoxon-ethyl detection. *Journal of Applied Electrochemistry*. 2023 May 9. Impact factor = 2.92
- 4.** Paneru S, Kumar D. Biosynthesized CeO₂ nanocrystals incorporated PANI-based high-sensitive electrochemical biosensor for multiple OPs detection in two real samples. (Communicated)
- 5.** Paneru S, Kumar D. CeO₂ and PEDOT:PSS modified conducting paper for OPs detection. (Communicated)

Poster presentation in Conferences

- 1.** Presented a poster in virtual International Conference on Surface Chemistry held on SUCH-2020, 27th - 11th-12th February-2022 in the Department of Chemistry Annamalai university (a state university-accredited with a grade by NAAC) Annamalai Nagar-608002, Tamil Nadu, India.
- 2.** Presented a poster in International virtual Conference on Nanotechnology: Opportunities & Challenges (ICNOC–2022), organized by Department of Applied Sciences & Humanities, Faculty of Engineering & Technology, Jamia Millia Islamia, New Delhi, India on November 28-30, 2022.
- 3.** Presented a poster in 7th International Conference on Nanoscience and Nanotechnology (ICONN-2023) organized by Department of Physics and Nanotechnology, SRM IST, Tamil Nadu, India during March 27- 29, 2023.



Contents lists available at ScienceDirect

Sensors and Actuators: B. Chemical

journal homepage: www.elsevier.com/locate/snb

Ag-doped-CuO nanoparticles supported polyaniline (PANI) based novel electrochemical sensor for sensitive detection of paraoxon-ethyl in three real samples

Saroj Paneru, Devendra Kumar^{1,*}

Department of Applied Chemistry, Delhi Technological University, Delhi 110042, India

ARTICLE INFO

Keywords:
Ag@CuO
Polyaniline
Electrochemical biosensor
OPs detection
Acetylcholinesterase

ABSTRACT

In this paper, a novel nanocomposite is chemically synthesized by reinforcing Ag-doped CuO (Ag@CuO) nanoparticles into the matrix of polyaniline (PANI). This nanocomposite is used as a sensing platform for paraoxon-ethyl (PE) detection. The homogeneous distribution of Ag@CuO nanoparticles onto the PANI matrix provides a smooth and dense surface area, further accelerating the transmission of electrons. The synergistic effect of Ag@CuO and PANI matrix is responsible for the outstanding conductivity, biocompatibility, and catalytic power of the proposed biosensor. For the biosensor fabrication, the nanocomposite is electrophoretically deposited onto the surface of the ITO glass substrate and then the acetylcholinesterase (AChE) enzyme is immobilized onto the fabricated electrode surface by using glutaraldehyde as a crosslinking agent. Under all optimized detection conditions, the proposed biosensor (AChE/Ag@CuO/PANI/ITO) shows a broad linear range from 5 to 100 pM with a low detection limit (LOD) of 11.35 pM. All the electrochemical results confirm the high sensitivity ($0.5536 \mu\text{A} (\text{pM})^{-1} \text{cm}^{-2}$), high selectivity, good reproducibility, and acceptable stability of the proposed biosensor. Moreover, the proposed biosensor is successfully applied for paraoxon-ethyl (PE) detection in three real samples.

1. Introduction

The high insecticidal properties and potency of organophosphate pesticides (OPs) make them popular for agricultural productivity and pest control. Although OPs have enormous benefits in the farming industries but their excessive and careless uses cause serious health issues worldwide [1,2]. Moreover, their inhibition activity towards the acetylcholinesterase (AChE) enzyme produces neurotoxicity in animals and humans, which further causes different severe diseases like Alzheimer's, Parkinson's, cognitive disorders, etc. [3,4]. Thus, it opens an opportunity to develop efficient techniques for optimal detection of OPs which enhance agricultural productivity and reduce the associated health risk simultaneously.

Reviews of existing literature reveal that there are few chromatography techniques, such as gas chromatography [5], gas chromatography associated with mass spectroscopy [6], and liquid chromatography-tandem mass spectrometry [7] which perform significantly well. However, their complex off-site procedures, overpriced

instrumentation, and the requirement of skillful handling make them more vulnerable in terms of practical uses. To overcome these issues, biosensors came into existence as they are cheap, fast, and having simple on-site operating procedures. Recently, AChE inhibition-based biosensors have been widely explored for the detection of OPs owing to their high selectivity and quick response [8]. Their mechanism is based on the enzyme's inhibition rate in the presence of OPs [9,10]. The sensitivity of AChE enzyme-based biosensors heavily relies on two factors: (i) How to prevent the leakage of the enzyme from the electrode surface? (ii) How to enhance the electron transfer rate between enzyme and electrode surface? To consider these two important factors, various transducers have been explored by researchers so far [11–14].

In recent years, metal oxides have been gaining a lot of popularity in the fabrication of effective transducers due to their outstanding properties like high stability, non-toxic nature and high catalytic power. Among all metal oxides, copper oxide (CuO) shows a high affinity with sulfur-containing compounds and accelerates the hydrolysis of acetyl thiocholine chloride (ATCI), further improving the AChE-based

* Corresponding author.

E-mail address: dkumar@dce.ac.in (D. Kumar).¹ ORCID No. orcid.org/0000-0001-9118-2070



A Novel Electrochemical Biosensor Based on Polyaniline-Embedded Copper Oxide Nanoparticles for High-Sensitive Paraoxon-Ethyl (PE) Detection

Saroj Paneru¹ · Devendra Kumar¹

Accepted: 10 January 2023

© The Author(s), under exclusive licence to Springer Science+Business Media, LLC, part of Springer Nature 2023

Abstract

This paper proposes a fabrication of a hyper-sensitive amperometric biosensor for paraoxon-ethyl (PE) detection. In this developed biosensor, polyaniline (PANI) and copper oxide (CuO)-based nanocomposite is used as a sensing platform. The homogeneous distribution of CuO onto the PANI matrix enhances the surface area and conductivity of the nanocomposite. Additionally, the PANI produces a compatible environment for enzyme immobilization, which further enhances the rate of electron transfer. For biosensor fabrication, the nanocomposite is deposited electrophoretically onto the ITO glass substrate and immobilization of acetylcholinesterase (AChE) enzyme is conducted onto the fabricated electrode surface. The results validate good reproducibility, good stability, and high selectivity of the fabricated biosensor (AChE/PANI@CuO/ITO). The inhibition rate of paraoxon-ethyl (PE) is recorded in the concentration range of 1–200 nM with a low limit of detection of 0.096 nM or 96 pM. The sensitivity of the developed biosensor is found to be 49.86 $\mu\text{A}(\text{nM})^{-1}$. The developed biosensor is further successfully accomplished for the detection of PE in real samples like rice and pulse.

Keywords Polyaniline (PANI) · Copper oxide (CuO) · Electrochemical biosensor · Organophosphate pesticides (OPs) · Acetyl cholinesterase (AChE)

Introduction

To increase productivity in the agricultural field and reduce insecticides, organophosphate pesticides (OPs) have been widely used in recent years. Although these pesticides have enormous uses in crop production, their residues in soil, water, fruits, and vegetables cause several health issues for mankind [1, 2]. The excess amount of OPs in the human body inhibits the activity of the acetylcholinesterase (AChE) enzyme, which further prevents the

✉ Devendra Kumar
dkumar@dce.ac.in

Saroj Paneru
saroj4843@gmail.com

¹ Department of Applied Chemistry, Delhi Technological University, Delhi 110042, India



CuO@PEDOT:PSS-grafted paper-based electrochemical biosensor for paraoxon-ethyl detection

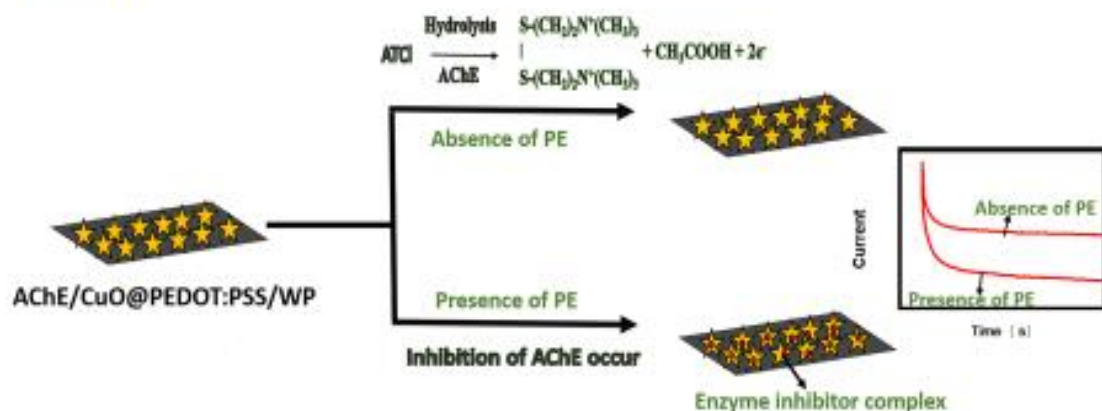
Saroj Paneru¹ · Sweety¹ · Devendra Kumar¹

Received: 16 December 2022 / Accepted: 25 April 2023
© The Author(s), under exclusive licence to Springer Nature B.V. 2023

Abstract

A highly sensitive, flexible, cheap, and biodegradable biosensor has been fabricated to detect paraoxon-ethyl (PE) more effectively. In this work, copper oxide (CuO) and poly(3,4-ethylenedioxythiophene):poly(4-styrenesulfonate) (PEDOT:PSS)-modified Whatman paper (WP)-based electrode are fabricated and then characterized by using different techniques. For the fabrication of CuO@PEDOT:PSS/WP electrode, firstly, the PEDOT:PSS/WP was optimized by various solvents such as ethylene glycol (EG), 1-methyl-2-pyrrolidone (NMP), dimethylformamide (DMF), N,N-dimethyl acetamide (DMA), and glycerol to enhance the conductivity. The EG-treated PEDOT:PSS/WP electrode shows maximum conductivity ($1.4 \times 10^{-2} \text{ S cm}^{-1}$) among all solvents. Further, the incorporation of CuO enhances the electrochemical performance of proposed biosensor. All electrochemical results validate that the proposed biosensor (AChE/CuO@PEDOT:PSS/WP) shows high sensitivity and low detection limit of $9.1279 \mu\text{A/nM}$ and 0.42 nM , respectively. The proposed paper electrode can be a highly promising alternative to conventional electrodes that are known to have limited applications due to their high cost and limited flexibility. The accuracy of the proposed biosensor was successfully checked in two real samples, which makes it more applicable for PE detection in real-world scenarios.

Graphical abstract



Keywords PEDOT:PSS · Copper oxide (CuO) · Electrochemical biosensor · Organophosphate pesticides (OPs) · Acetyl cholinesterase (AChE)

✉ Devendra Kumar
dkumar@dce.ac.in

Extended author information available on the last page of the article

Published online: 09 May 2023